Determination of oxygen reduction reaction (ORR) catalyst activity in gas diffusion electrode half-cells

TECHNISCHE
UNIVERSITÄT
DARMSTADT

at the Department of Chemistry
of the Technische Universität Darmstadt

submitted in fulfilment of the requirements for the
degree of Doctor of Engineering
(Dr.-Ing.)

Doctoral thesis
by
Nicolai Schmitt

First reviewer: Prof. Dr.-Ing. Bastian J. M. Etzold

Second reviewer: Prof. Dr. Jan Philipp Hofmann

Third reviewer: Prof. Dr. Karl J. J. Mayrhofer

Darmstadt 2023

Date of submission: 29th August 2023

Day of the oral examination: 10th October 2023

Schmitt, Nicolai: Determination of oxygen reduction reaction (ORR) catalyst activity in gas diffusion electrode half-cells

Darmstadt, Technische Universität Darmstadt
Year of publication of doctoral thesis on TUprints: 2023
URN: urn:nbn:de:tuda-tuprints-247510
Day of the oral examination: 10th October 2023

Published under CC-BY-NC-ND 4.0 International
https://creativecommons.org/licenses/by-nc-nd/4.0/

Acknowledgements

This thesis would not have been possible without help and support of several people.

First of all, I would like to thank my doctoral supervisor Bastian Etzold for giving me the opportunity to work on this interesting topic in collaboration with industry in an optimal research environment. Thank you for the freedom and opportunities you gave me and for everything I was able to learn from you!

Thank you to Prof. Dr. Jan Philipp Hofmann and Prof. Dr. Karl J. J. Mayrhofer for assessment of my work.

In general, I thank all members of our group, especially the varying members of our office, for the enjoyable working atmosphere, new friendships and private gatherings. A special thank you to all colleagues participating the active lunch breaks, that have become tradition.

A special thank you goes to Michael George, who introduced me to electrochemistry during my studies and greatly supervised me during my master thesis, which later allowed me to take this PhD position.

Thanks to Alfons Drochner, Jan Gläsel and Marianne Blascak for the help in daily PhD life and the support during my work.

Thank you to everyone helping with instrumental analytics. Thank you to Dr. Felix Reinauer, Pedram Babaei and Ingeborg Gärtner for ICP-OES analysis. Thanks to Ariane Rösler and Muhammad Olvianas for the help with elemental analysis. Thank you to Patrick Schmatz for the help with physisorption analysis. Thanks to Phillip Reif for XRD analysis. Thank you to Miriam Geissler, Melina Römer and Hendryk Steldinger for SEM investigation.

Thank you to our industry collaborator Volkswagen AG, especially to Gerold Hübner, Jonathan E. Mueller, Lasse Schmidt and Sebastian Kirsch. Thank you for funding, scientific discussion and especially for the openness towards publication of the results within our collaboration.

Also I would like to thank Konrad Ehelebe, Anders W. Jensen, Gustav Sievers, Armin Hrnjić and all further people for the open collaboration and the discussions we had on comparison of the different GDE setups.

I thank my students Nils Näser, Michael Trabold, Felix Biermann, Mareike Schmidt, Julia Hoffmann and Joshua Mercadal Gener for the contribution to this work. It was great to supervise all of you!

Thank you to all coworkers of our electronic and mechanical workshop for the support with experimental setups and the great work.

A special thank you goes to my parents and my whole family, who always supports me and made all of this possible to me. You are great! Finally, I would like to thank you, Melina, for making life a little bit more beautiful for me every single day!

This dissertation is a cumulative thesis based on the following first-author publications, which are all included within this thesis:

[1] Schmitt, N., Schmidt, M., Hübner, G., & Etzold, B. J.
Oxygen reduction reaction measurements on platinum electrocatalysts in gas diffusion electrode half-cells: Influence of electrode preparation, measurement protocols and common pitfalls.
Journal of Power Sources **2022**, 539, 231530.
DOI: https://doi.org/10.1016/j.jpowsour.2022.231530

[2] Schmitt, N., Schmidt, M., Mueller, J. E., Schmidt, L., & Etzold, B. J.
How to maximize geometric current density in testing of fuel cell catalysts by using gas diffusion electrode half-cell setups.
Electrochemistry Communications **2022**, 141, 107362.
DOI: https://doi.org/10.1016/j.elecom.2022.107362

[3] N. Schmitt, M. Schmidt, J. E. Mueller, L. Schmidt, M. Trabold, K. Jeschonek, B.J.M. Etzold
Which insights can gas diffusion electrode half-cell experiments give into activity trends and transport phenomena of membrane electrode assemblies?
Energy Adv., Advance article.
DOI: https://doi.org/10.1039/D3YA00055A

Abstract

In order to face one of the biggest challenges of our time, climate change and its consequences, along with the limited availability of fossil fuels, the transition towards renewable energies is inevitable. Following the current global political strategies, a key player in energy transition will be hydrogen. Hydrogen can directly be used as an emission free-fuel or as a long-term energy storage. Key technologies for hydrogen as energy storage solution therefore are water electrolysis, which allows production of green hydrogen by the use of renewable electricity, and fuel cells, which can reconvert the chemical energy stored in hydrogen to produce electricity when required. Along the different types of fuel cell technologies, especially polymer electrolyte membrane fuel cells (PEMFC) are promising, as they exhibit high power density and electrical efficiency, and allow quick start-up and shut-down due to their low operating temperature. For a wide-spread commercialization of the PEMFC technique, one hurdle is the sluggish kinetics at the cathodic catalyst layer along with the required high overpotentials to drive the oxygen reduction reaction (ORR). Therefore, development of improved ORR catalyst is a main focus of ongoing PEMFC research.

In this regard, a major issue is the limited transferability of ORR catalyst activity data collected in lab-scale rotating disk electrode (RDE) testing to real membrane electrode assemblies (MEA). In order to overcome this limitation, this work focuses on the introduction of a novel technique for ORR catalyst evaluation, namely the gas diffusion electrode (GDE) half-cell approach. Thereby, the mass transport limitations observed in RDE testing with the catalyst coated on a bulky electrode surface and immersed in liquid electrolyte is circumvented by using a porous gas diffusion media as electrode material, allowing to directly distribute the reactant gas to the catalyst surface. Requirements to the GDE approach are to enable the study of realistic catalyst layers in fuel cell relevant current and potential regimes, while keeping advantages of the RDE technique, such as simplicity, fastness and good reproducibility. In the present work, therefore a setup using a commercially available half-cell is established. In the first step best practice advices are developed for electrode preparation and measurement of the electrochemical performance. Also pitfalls in GDE evaluation, such as electrolyte heating and falsified iR correction are identified and solutions to avoid these are presented. In the next step, the GDE setup is further developed to avoid limitations in the maximum current density that can be reached, thus allowing to study the full current range of real MEAs. Therefore, different measures are proposed and the effect of those on the maximum achievable current density is investigated individually.

Lastly, the established GDE half-cell approach is compared to real MEA testing with the use of two model catalysts analyzed by using both techniques. Thereby, it can be shown that the differing interphase of the catalyst in GDE testing (catalyst in contact with liquid acidic electrolyte) compared to the MEA (catalyst in contact with solid ionomer membrane) can result in different trends observed with both techniques. In case of differences in catalytic activity being linked to oxygen mass transport, GDE

evaluation could very well give trends for catalytic activity in a MEA and is superior compared to RDE testing in this regard. However, trends in catalytic activity being linked to proton transport could less be described within the GDE half-cell.

In sum, the setup presented in this work combines advantages of the RDE technique such as simplicity, fastness, comparability and reproducibility of the results, as well as minimum material consumption along with the possibility to test realistic catalyst layers in the full potential and current range of real PEMFCs. On one hand the presented results show that GDE testing with the catalyst layer in contact with liquid electrolyte gives reliable insides in oxygen mass transport properties of realistic catalyst layers at fuel cell relevant potentials and current densities. On the other hand, due to the different catalyst environment in GDE testing in the configuration used in this work, resulting in partial flooding of the catalyst layer by the electrolyte, no full and reliable description of all transport phenomena in real fuel cells (e.g. dry operating conditions, proton accessibility and the complex interaction with the ionomer) is possible. Therefore, future research will have to figure out, whether solid ionomer membranes, utilized in real MEAs, can be introduced in GDE half-cells between catalyst layer and liquid electrolyte, while keeping the advantages of GDE testing such as technical simplicity and faster evaluation compared to MEA testing. Based on these findings, this work helps to guide future application of the GDE technique in PEMFC catalyst research.

Zusammenfassung

Der Klimawandel mit all seinen Folgen, sowie die begrenzte Verfügbarkeit von fossilen Brennstoffen ist eine der größten Herausforderungen unserer Zeit. Um diese Hürde zu überwinden, ist ein Umstieg auf erneuerbare Energiequellen unausweichlich. Den aktuellen weltweiten politischen Strategien folgend, wird hierbei grüner Wasserstoff eine entscheidende Rolle einnehmen. Dieser kann entweder direkt als Brennstoff eingesetzt werden, der bei Verbrennung keine Emissionen freisetzt, oder kann als langfristiger Energiespeicher genutzt werden. Um Wasserstoff als Energiespeicher nutzen zu können, werden zwei Schlüsseltechnologien benötigt: Wasserelektrolyse, die es ermöglicht aus erneuerbarem Strom Wasserstoff herzustellen, sowie Brennstoffzellen, mit denen der Wasserstoff bei Bedarf rückverstromt werden kann. Hinsichtlich der Brennstoffzellentechnologie erweist sich insbesondere die Polymerelektrolytmembranbrennstoffzelle (engl. polymer electrolyte membrane fuel cell, PEMFC) als vielversprechend. Die PEMFC besitzt eine hohe Leistungsdichte und eine hohe elektrische Effizienz. Durch die niedrige Betriebstemperatur kann sie schnell gestartet und abgeschaltet werden und ist dadurch sehr flexibel einsetzbar. Eine verbleibende Hürde für eine weitreichende Kommerzialisierung der Brennstoffzelle ist der hoher Preis der eingesetzten Platin Katalysatoren zusammen mit der trägen Kinetik der kathodischen Sauerstoffreduktionsreaktion (engl. oxygen reduction reaction, ORR). Daher liegt ein Fokus der aktuellen Forschung und Entwicklung an PEMFCs auf der Entwicklung von effizienteren und aktiveren Katalysatoren für die ORR.

Problematisch hierbei ist, dass vielversprechende Katalysatoraktivitäten, die unter idealisierten Laborbedingungen mit Hilfe der rotierenden Scheibenelektrode (engl. rotating disk electrode, RDE) gemessen werden, kaum auf reale Katalysatorschichten in Membran-Elektroden Einheiten (engl. membrane electrode assembly, MEA) übertragen werden können. Als Lösung für dieses Problem der limitierten Aussagekraft von Standard-Laboruntersuchungen der ORR Aktivität, wird daher in dieser Arbeit ein Gasdiffusionselektroden (engl. gas diffusion electrode, GDE) Halbzellenaufbau präsentiert. Im Gegensatz zu RDE Messungen, in denen der Katalysator auf eine feste Elektrode aufgetragen und in einen flüssigen Elektrolyten getaucht wird, verwendet dieser Ansatz eine poröse Gasdiffusionsschicht, wie sie auch in der MEA eingesetzt wird, als Elektrodensubstrat. Auf diesem Wege kann gasförmiger Sauerstoff direkt an die Katalysatorschicht transportiert werden und Stofftransportlimitierungen werden vermieden. Die Anforderungen an den GDE Aufbau sind hierbei die Vorteile der RDE wie Einfachheit, kurze Messdauer und Reproduzierbarkeit der Messergebnisse mit der Möglichkeit zu vereinen, den kompletten Strom und Potentialbereich einer MEA abzudecken. Hierfür wird in der vorliegenden Arbeit ein Aufbau unter Verwendung einer kommerziellen Halbzelle präsentiert. Im ersten Schritt werden für die GDE Charakterisierung Methoden für die Elektrodenpräparation und geeignete Messprotokolle vorgeschlagen. Außerdem werden kritische Faktoren in der GDE Analyse, wie eine Erhitzung des Elektrolyten während der Messung und eine verfälschte iR Korrektur identifiziert, und entsprechende

Handlungsvorschläge gegeben, um das Auftreten dieser Probleme zu verhindern. Ein wichtiger Schritt dieser Arbeit ist außerdem die Entwicklung der Methode zu höheren geometrischen Stromdichten, um den gesamten Strombereich einer PEMFC abdecken zu können. Hierfür werden verschiedene Maßnahmen präsentiert, um den möglichen Strommessbereich während der GDE Charakterisierung zu maximieren. Außerdem wird individuell und unabhängig voneinander gezeigt, welchen Effekt die einzelnen Maßnahmen auf den maximal erreichbaren Strom haben. Auf dieser Basis können abschließend in dieser Arbeit zwei Modellkatalysatoren vergleichend in der GDE und in der MEA hinsichtlich ihrer ORR Aktivität charakterisiert werden. Dabei kann gezeigt werden, dass die verschiedene Umgebung des Katalysators in beiden Methoden zu unterschiedlichen Trends in der katalytischen Aktivität führen kann. Während bei der GDE Charakterisierung in dieser Arbeit der Katalysator in direktem Kontakt zum flüssig sauren Elektrolyten ist, der die Protonen für die Reaktion bereitstellt, ist der Katalysator in der MEA in Kontakt zu einer festen Ionomermembran. Einerseits kann gezeigt werden, dass trotz dieser unterschiedlichen Katalysatorumgebung Trends in der katalytischen Aktivität, die auf Unterschiede im Sauerstofftransport zurückzuführen sind, in der GDE richtig für die MEA wiedergegeben werden können. Die GDE zeigt sich hierbei insbesondere überlegen gegenüber der RDE, die Trends in der katalytischen Aktivität im Hochstrombereich nicht untersuchen kann. Allerdings können auf der anderen Seite Trends, die auf den Protonentransport und unterschiedliche Protonenzugänglichkeit zurückzuführen sind in der GDE nicht richtig für die MEA wiedergegeben werden.

Zusammenfassend vereint der GDE Aufbau, der in dieser Arbeit präsentiert wird, Vorteile der RDE Charakterisierung wie Einfachheit, kurze Messdauer und Reproduzierbarkeit der Messergebnisse sowie minimaler Materialverbrauch mit der Möglichkeit realistische Katalysatorschichten unter Strömen und Potentialen der industriellen Brennstoffzellenanwendung zu vermessen. Hervorzuheben ist hierbei insbesondere, dass GDE Testung mit der Katalysatorschicht in direktem Kontakt mit dem Flüssigelektrolyten verlässliche Aussagen über das Sauerstofftransportverhalten im Hochstrombereich ermöglicht. Allerdings zeigt diese Arbeit auch auf, dass elektrochemische Halbzellen mit dem Katalysator in direktem Kontakt mit dem wässrigen Elektrolyten nicht alle Phänomene und Prozesse, die in einer realen MEA ablaufen, richtig wiederspiegeln können. Durch den direkten Kontakt von Katalysatorschicht mit dem flüssigen Elektrolyten, der in einer partiellen Flutung der Katalysatorschicht resultiert, können Faktoren wie trockene Betriebsbedingungen, sowie die Protonenzugänglichkeit und der Einfluss des Ionomer auf diese weniger gut beschrieben werden. Hierfür ist es Aufgabe der zukünftigen Forschung zu untersuchen, ob feste Ionomermembranen, wie sie auch in MEAs verwendet werden, bei der GDE Testung zwischen Katalysatorschicht und Elektrolyt eingebracht werden können, ohne Vorteile wie technische Einfachheit und schnelle Charakterisierung zu verlieren. Basierend auf diesen Ergebnissen kann die vorliegende Arbeit Unterstützung bei der zukünftigen Anwendung von GDE Halbzellen in der Katalysatorentwicklung für die PEMFC leisten.

List of content

1. Introduction and motivation

The climate change and its consequences are one of the biggest challenges of our time. Climate change can be seen as a globally, inter-governmental threat with negative effects in numerous fields including economic, environmental, socio-economic and socio-political disciplines [1,2]. The problem with earth climate was amplified manifold with the start of the industrial revolution. Starting from this point, rising standards of life, financial welfare and increasing consumption were realized by burning fossil resources, resulting in emission of greenhouse gases (GHG, mainly CO_2 and also CH_4 and N_2O) and a rising concentration of CO_2 in the atmosphere [3,4]. The accompanying global rise in temperature (+1.09 °C between 2011-2020 compared to 1850-1900 [5]) has already led to a dramatic increase in weather extremes such as storms, floods, drought and a rising sea-level (increase by 0.2 m between 1901 and 2018 [5]). As a result of this, a long list of severe consequences can be formulated, including endangerment of ecosystems and biodiversity, risk of fresh water and food shortage, as well as numerous impacts on human health [1,2]. The human influence is expected to be *"very likely"* the main driver of global warming and its consequences [5].

In order to limit global warming and its consequences to an endurable level, in 2015, 196 parties signed the Paris Agreement as a legally binding international treaty on climate change within the UN Climate Change Conference. The overarching goal of the Paris Agreement is to hold *"the increase in the global average temperature to well below 2°C above pre-industrial levels"* and pursue efforts *"to limit the temperature increase to 1.5°C above pre-industrial levels" [6].*

In order to achieve this goal, it will be inescapable to reduce the GHG emissions to net zero in the near future (see Figure 1A) [5].

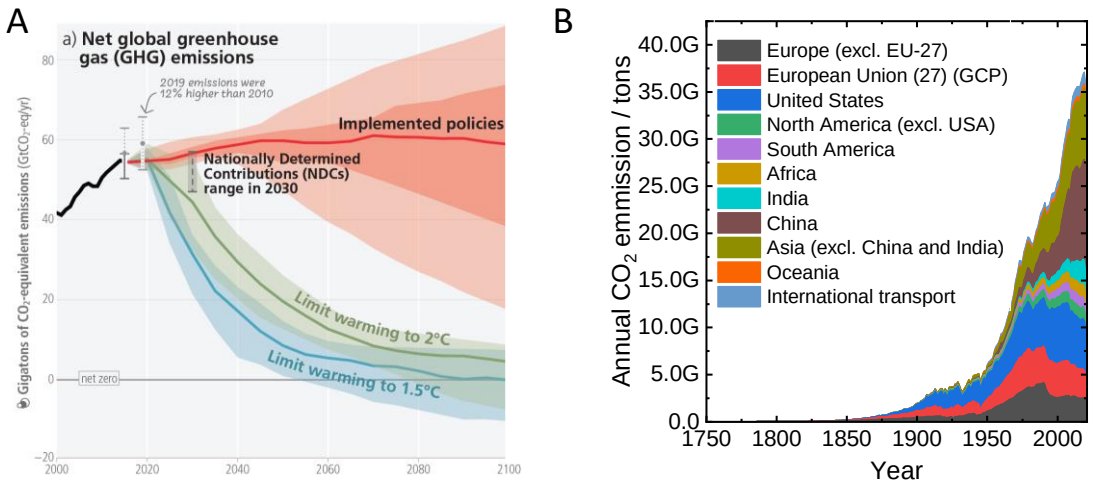

Figure 1: A: Modelled pathways of required CO_2 reductions in order to limit global warming to 2 or 1.5 °C, respectively. Reprinted from the SYNTHESIS REPORT OF THE IPCC SIXTH ASSESSMENT REPORT (AR6) in consideration of the IPCC Copyright Policy [2]. B: Annual CO2 emissions by world region from 1900-2021. Data from Roser et al. [7] (CC-BY 4.0).

However, as can be seen from Figure 1B, the global emissions of CO_2 still keep strongly increasing, and, while in America and Europe efforts to reduce CO_2 emissions have been implemented, especially in emerging markets such as Asia and India a dramatic increase in GHG emissions is still going on [7]. Thus, it is obvious that the current trend represents a big risk for failure of the goals formulated within the Paris Agreement and measures to reduce GHG emissions need to be implemented immediately.

In this regard, a global challenge will be the energy transition towards renewable and carbon free energy sources [8]. As indicated by the current global political strategies, a key player in energy transition will be hydrogen [9]. Hydrogen represents a carbon free fuel, hence, there are no CO_2 emissions when hydrogen is utilized to produce heat or electricity. The technical promise of hydrogen is that it could be used on one hand for direct, emission free combustion for heat production in critical sectors such as cement farms and iron and steel production and to replace fossil fuels in these areas. On the other hand, hydrogen technology offers a strategy for storage of electricity and to face the concern of seasonal issues with the electricity production from renewable sources such as wind and solar power [9,10]. A decisive factor for the carbon footprint of a future hydrogen economy represents the process utilized to produce the hydrogen. Therefore, in literature a color coding was introduced to describe the cleanness level of hydrogen: Grey hydrogen is produced by steam reforming of fossil fuels, such as natural gas, and is accompanied by the emission of 10 tons of CO_2 for production of one ton of H_2 [11]. Blue hydrogen is also produced by fossil fuels, but combined with technologies for carbon capture and storage to reduce GHG emissions. Green hydrogen is produced by utilization of water electrolysis using 100 % renewable energy such as wind and solar power. Further types include brown hydrogen (produced from gasification of coal-based fuel) and turquoise hydrogen (produced from the thermal decomposition of natural gas) [12]. In 2021, 47 % of the global hydrogen production could be assigned to grey hydrogen, while green hydrogen held only a minimum share of 4 % [13]. Thus, in order to achieve the goals of the Paris agreement, a massive ramp up of green hydrogen production will be necessary. A possible scenario for the role of hydrogen in renewable energy industry is given in Figure 2. Accordingly, hydrogen is produced by pyrolysis of biomass or by the use of electrolyzers powered with renewable electricity and thus complements short-term energy storage devices such as batteries as a long-term energy storage solution. The produced hydrogen can thereafter be converted together with CO_2, extracted from the air or stemming from exhaust streams, into fossil fuels and serve as carbon-based feedstock for the chemical industry. Also it can be reconverted back into electricity or used to power transport vehicles by the use of fuel cells, which therefore, besides electrolysis, might play a key role in energy transition [9,14]. Fuel cells convert hydrogen back to electricity with only heat and water being released as side products. Due to their high efficiency compared with low emissions, they have recently received major interest. Among the different types of fuel cells, especially polymer electrolyte fuel cells (PEMFC) are promising since they exhibit high power density and electrical efficiency and allow quick start-up and shut-down due to

their low operating temperature (<100 °C). These characteristics allow to use PEMFCs in the transportation sector, where they are already commercialized to power road transport (personal vehicles, trucks, busses) and also trains and airplanes. Besides this, they are also of interest as backup-power for buildings, portable power for small electric devices and for production of domestic heat and electricity [15–19].

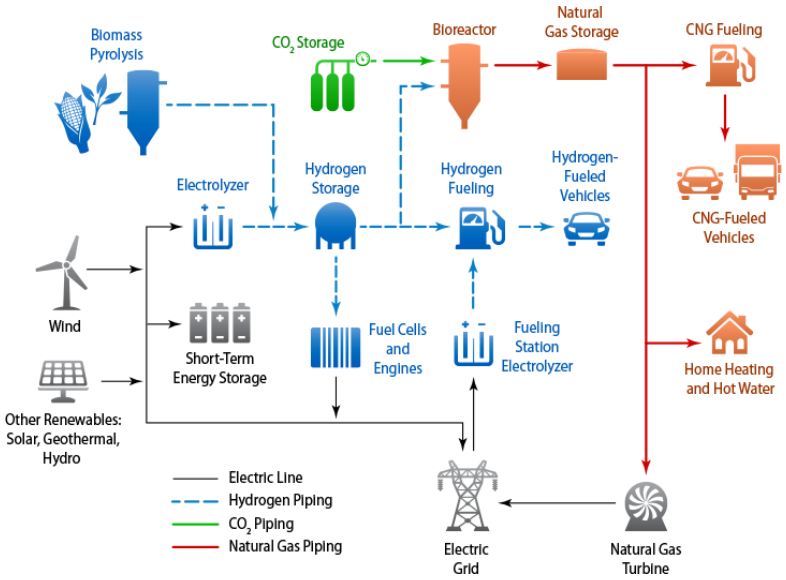

Figure 2: Role of hydrogen in a renewable energy scenario. Reprinted with permission from NREL [14].

Optimization of PEMFCs focusses on reduction of costs by minimizing the platin group metal (PGM) amount or by completely avoiding PGMs and by maximizing power density. The main focus to increase the energy efficiency, which is still low compared to batteries, therefore is to develop improved catalysts for the cathodic oxygen reduction reaction (ORR), which is slow and requires higher overpotential compared to the anodic hydrogen oxidation reaction (HOR) [20,21].

In order to achieve this goal, it is essential to have reliable techniques for catalyst activity determination already at an early stage of catalyst development, where oftentimes only milligram amount of material is available. A major issue in this regard is that recently many high performing ORR catalysts were presented on laboratory scale by using the wide spread rotating disk electrode (RDE) technique for activity determination. However, only few of these promising materials could be successfully embedded in real catalyst layers in membrane electrode assemblies (MEA), operating under application conditions [22–24].

This work is embedded in this context of reliable testing of ORR catalysts and catalyst layers on a laboratory scale. Therefore, in the next chapter, the available standard techniques for ORR catalyst evaluation, namely MEA and RDE testing, will be introduced and based on this, the necessity for new methods for ORR catalyst layer evaluation will be elaborated. Thereafter, the aim and scope of this thesis will be highlighted and finally, based on the released publications within this thesis, a novel technique for ORR catalyst layer evaluation will be presented and compared to the state-of-the-art techniques.

2. Theoretical Background

2.1. Fuel cells: Types, application and functional principle

Fuel cells are devices converting the chemical energy stored in a fuel such as methanol or hydrogen into electricity by electrochemical oxidation. Although the principle of a fuel cell was already discovered in 1839, the development of the technique is still in progress [25]. In general, there are different types of fuel cells, utilizing different kinds of fuel, operating at different conditions and each having their own advantages and disadvantages (see Table 1).

Table 1: Overview over the different types of fuel cells. Adapted from [26–28].

Type	Fuel	Electrolyte	Operating temperature	Catalyst
Polymer electrolyte membrane fuel cell (PEMFC)	H_2	Proton exchange membrane (perfluoro sulfonic acid)	<120 °C (Typically 80 °C)	PGM
Direct methanol fuel cell (DMFC)	CH_3OH	Proton exchange membrane (perfluoro sulfonic acid)	50-120 °C	PGM
Alkaline fuel cell (AFC)	H_2	Aqueous KOH / Anion exchange membrane	<100 °C	Non PGM (Ni, Fe Co, Ag)
Phosphoric acid fuel cell (PAFC)	H_2	Phosphoric acid soaked in a porous matrix	150 - 200 °C	PGM
Solid oxide fuel cell (SOFC)	H_2, CH_4, syngas	Yttria stabilized zirconia	500 - 1000 °C	Ceramics (yttria-stabilized zirconia and other types of zirconia)
Molten carbonate fuel cell(MCFC)	H_2, CH_4, syngas	Molten lithium, sodium or potassium carbonates soaked in a porous matrix	600 - 700 °C	Li titanates and Ni alloys

The high temperature types such as PAFC, SOFC and MCFC generally show the advantage of a high efficiency, a good tolerance to fuel impurities such as carbon monoxide and sulfur and because of the high operating temperature they are suited for combined heat and power production. On the other hand, these techniques show the disadvantage of long start-up and shut-down times and the high operating temperatures can be problematic regarding corrosion of cell components. AFCs show the advantage of alkaline environment, which is giving a wider range of stable and active materials and thus allows to utilize PGM free catalyst. However, conductivity and durability of the anion exchange membrane in new generation AFCs are still a remaining challenge [26–28].

PEMFCs combine a low operating temperature with high flexibility (quick start-up and shut-down) and a high efficiency and power density. For that reason, they are the most widespread type of fuel cell and attract major interest in the course of energy transition [29]. This can also be seen from the ongoing

commercialization of PEMFCs, especially in the transportation sector, where PEMFCs are already utilized in cars [17], busses [30], trains [31] and trucks [32]. Further applications being currently discussed include the utilization in airplanes [33] and ships [34]. Utilization of PEMFCs in the transportation sector is thereby in particular of interest in heavy duty transport, where a high range and fast refueling are of interest. Compared to battery electric vehicles (BEV), the advantage of fuel cell electric vehicles (FCEV) herein lies in the much greater energy storage density of hydrogen compared to lithium ion batteries. In personal transport and thus for smaller and lighter vehicles it is in contrast expected that BEV, showing a much higher energy conversion efficiency, will play the major role [35]. Besides the utilization in the transport sector, there are also combined heat and power plants for providing domestic heat and electricity available using PEMFCs [36].

In general, a PEMFC is built up as a stack of identical repeating units, the so-called membrane electrode assembly (MEA, see Figure 3). The MEA thereby consists of anode and cathode catalyst layer (typically Pt-based nanoparticles immobilized on high surface area carbon), separated by an ionomer membrane (typically perfluoro sulfonic acid), which is conducting protons, but not electrons and hinders crossover of hydrogen from anode to cathode side. Both catalyst layers are compressed between gas diffusions layers (GDL, typically carbon paper) with a microporous layer coating on top (MPL) for distribution of the reactant gases. Ionomer membrane, anode and cathode catalyst layer and two GDLs form a so-called five-layer MEA, which is then sandwiched between bi-polar plates, that harvest the electric current and introduce reactants and coolants [37]. Several hundred MEAs are combined to a fuel cell stack, for example the FCEV Hyundai Nexo utilizes a stack out of 440 MEAs giving a stack power of 95 kW [38]. Subsequently details on each component being part of a MEA will be introduced.

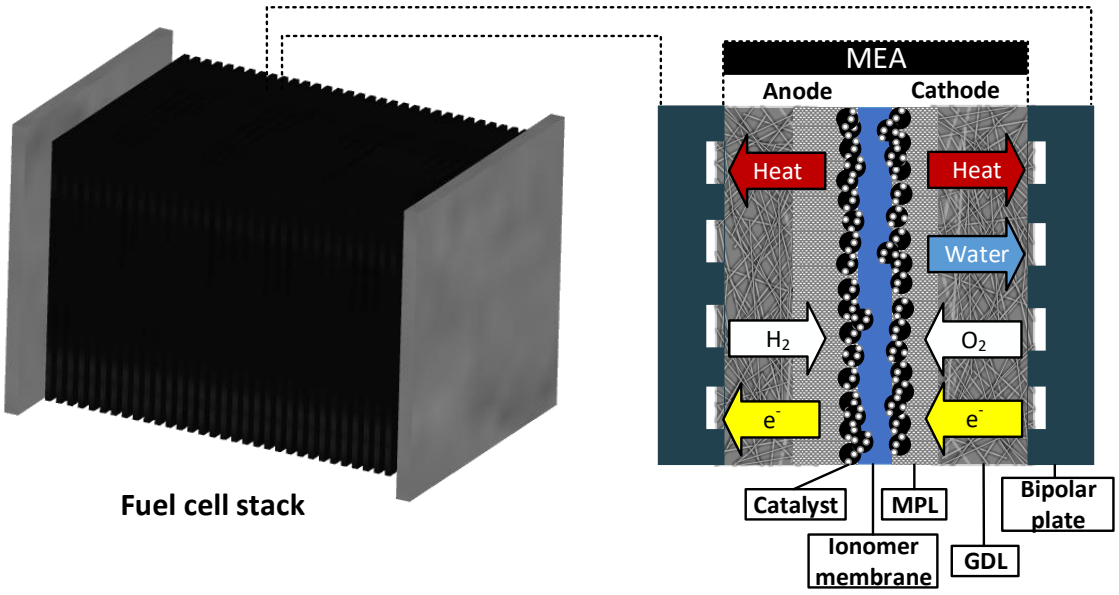

Figure 3: Functional principle of a PEMFC. Inspired by [39].

The most important function of the bipolar plate (BP) is to provide conducting path for electrons between the cells of a PEM stack and to distribute and barrier the reactant gases. To afford this, BPs have an optimized flow field design for uniform reactant distribution and to achieve effective water management. Besides that, they also enable to remove heat by introduction of coolants and to provide structural integrity of the PEM stack. Therefore, they are a key component to ensure all functions of a PEM stack while maintaining low cost of the device. Materials utilized for bipolar plates include metals (oftentimes with a corrosion resistant noble metal coating), which show high thermal and electrical conductivity, excellent mechanical stability and easy fabrication at low overall cost. Additionally, non-porous graphite materials are utilized as BP, showing superior corrosion resistance and thermal and electrical conductivity on one side, but higher cost on the other side [40]. GDLs being located between BP and catalyst layer (CL) have similar functionality compared to BPs regarding reactant transport to the CL, removal of liquid water and excess heat and to provide electron conductance between CL and BP. GDLs are typically carbon-based materials with an open pore network allowing gaseous reactant transport and water removal and a solid matrix for electron and heat removal. The two most prominent types of GDL are woven carbon-cloth and non-woven carbon paper. Due to the low cost in fabrication, carbon paper is hereby regarded as GDL material for commercialization of PEM fuel cells. Carbon paper is typically fabricated by carbonization of polyacrylonitril (PAN) fibers. After fabrication, carbon papers are treated with PTFE to provide hydrophobicity for effective water removal. On top of the GDL substrate, a MPL containing carbon powder (typically carbon black) and hydrophobic agents (mainly PTFE) is applied. MPLs are mediators for optimum water management, minimum resistance to the CL and also to facilitate catalyst deposition. The combination of GDL and MPL is typically 180 – 350 μm in thickness [39,41,42]. The role of the ionomer membrane is to exhibit high proton conductivity from anode to cathode CL and to avoid mixing of fuel and reactant gases while being chemically and mechanically stable in the fuel cell environment. The most popular type of ionomer membranes are perfluorocarbon-sulfonic acid ionomer membranes (e.g. Nafion®), showing high proton conductivity at low hydration level, thermal, mechanical and chemical stability, as well as low costs. The proton diffusion from anode to cathode side through the ionomer membrane generally involves two different mechanisms: vehicular diffusion (migration of hydronium ions) and structure or Grotthuss diffusion (jumps of protons from hydronium ions to adjacent water molecules). In order to improve the overall efficiency of a PEMFC stack by minimizing ohmic losses, ionomer membranes are fabricated as thin as possible while maintaining their functionality. Nowadays thicknesses down to 25 μm are therefore standard [25,43,44]. A CL is typically composed of a Pt/C catalyst and ionomer, forming a porous structure of platinum nanoparticles supported on high surface area carbon, surrounded by a thin ionomer film. Connection of the carbon support particles with each other ensures electronic transfer channels. The ionomer plays a key role in proton transport between polymer membrane and catalyst and also helps to remove product water. The

electrochemical reaction in a fuel cell takes part at three phase boundary of the catalyst, where electrons, protons and reactant gas get into contact. Therefore, optimization of the interface structure of GDL, CL and ionomer membrane is of great significance [45]. The reactions taking place in a PEMFC are the following: the anodic oxidation of hydrogen to protons and electrons (hydrogen oxidation reaction, HOR) and the cathodic reduction of oxygen with protons and electrons to water as the only reaction product (oxygen reduction reaction, ORR). The reactions are summarized below:

Anode (HOR): $H_2 \rightarrow 2\,H^+ + 2e^-$ (Eq. 1)

Cathode (ORR): $0.5\,O_2 + 2\,H^+ + 2\,e^- \rightarrow H_2O$ (Eq. 2)

As they are electrochemical cells, fuel cells directly convert chemical energy into electrical energy without intermediate degradation into heat. Therefore, fuel cells are not limited by the Carnot efficiency and have broad advantages over conventional heat engines [46]. The efficiency of a fuel cell can generally be calculated by dividing the electrical power output (product of cell potential and current) with the fuel input. The energy content of fuel input (F_{in}) can therefore be calculated with Equation 3 from the consumption rate of hydrogen (given by Faradays law) and its energy content, given as enthalpy (ΔH):

$$F_{in} = q_{H_2} \cdot \Delta H = \frac{M_{H_2} \cdot \Delta H}{n \cdot F} \cdot i \quad \text{(Eq. 3)}$$

Herein, M is the molecular weight of hydrogen, n ist the number of electrons transferred and F is Faraday's constant. The term $M_{H_2} \cdot \Delta H / n \cdot F = 1.428\,\text{V}$ is also called thermoneutral or reversible cell potential and is equal to the maximum electrical and thermal energy resulting from the electrochemical reaction. Since in a practical fuel cell only the free energy part (ΔG) can be converted into electricity because of irreversible entropy changes, the theoretical maximum potential of the fuel cell reaction (Eq. 2) at 25 °C and ambient pressure is 1.229 V. Thus, the maximum theoretical hydrogen fuel cell efficiency is $1.229\,\text{V} / 1.482\,\text{V} = 0.83$ [47]. However, in practical fuel cells the theoretical cell voltage of 1.229 V cannot be reached because of several effects causing voltage losses. These include activation and concentration losses at both cathode and anode, as well as resistive losses linked to limited conductivity of the electrolyte [37]. These losses result in the typical shape of the fuel cell polarization curve, which is the most important characteristic of a fuel cell and its performance and is introduced in Figure 4 and the text below. The fuel cell polarization curve is a plot of cell voltage versus current density and thus determines the maximum power that can be drawn from a fuel cell. The below polarization curve shows that the actual cell voltage deviates from the ideal voltage (given here for an operating temperature of 100 °C) depending on the current applied. The difference of the real open circuit voltage from the ideal voltage is mainly caused by factors such as fuel crossover from anode to cathode side. As current is drawn from the fuel cell, various kinds of voltage losses arise which will be introduced below.

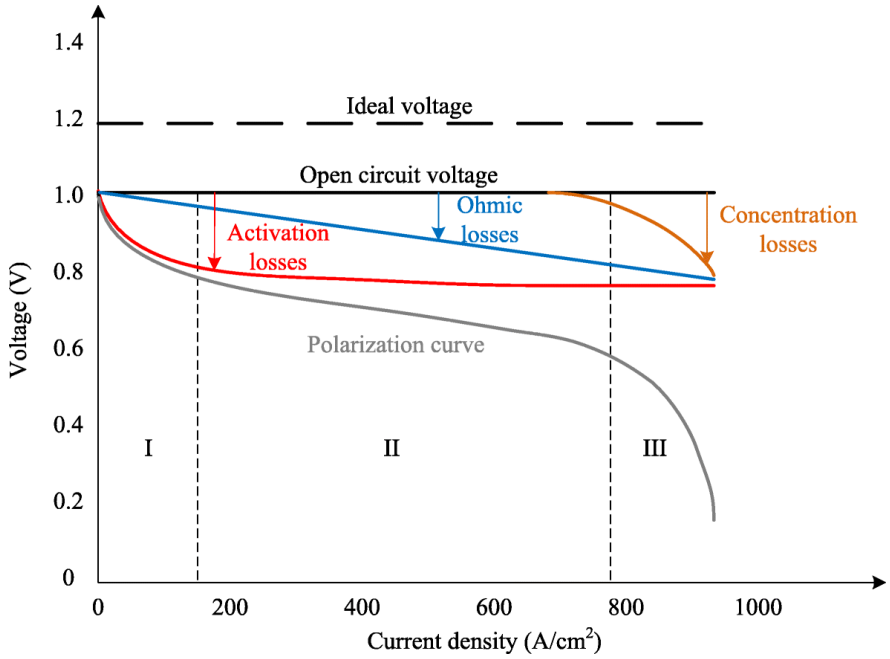

Figure 4: Example of a fuel cell polarization curve introducing the different sources of voltage losses. Reprinted from [48] (CC-BY).

In the low current density regime mainly *activation losses* are dominating, which are linked to high overpotentials being required to drive the electrochemical reactions. These losses depend on the catalyst material, reactant activities as well as the microstructure of the MEA. *Ohmic losses* are caused by the resistance of mainly the electrolyte, but also the electrodes and other connecting parts. This kind of voltage loss follows ohms' law and is thus proportional to the current density. In the high current density regime, the fuel cell power is mainly limited by *concentration losses*, that result from a drop in reactant concentration at the surface of the electrodes. The effects of these three factors causing voltage losses are easy to distinguish from a polarization curve. Thus, detailed investigation of a polarization curve, supported by using further electrochemical and physicochemical analytics, allows to analyze the cause of failure of a MEA [48].

A main focus of current research is to minimize activation losses in fuel cells by increasing activity of the utilized catalysts. While the anodic HOR generally requires only low overpotential and thus allows to use small amount of catalyst, the cathodic ORR is six or even more orders of magnitude slower and therefore holds enormous potential for improvement of the overall process [37]. Main reasons for the sluggish ORR kinetics can be summarized as follows: Generally, oxygen has higher bonding energies compared to hydrogen, therefore resulting in higher activation barriers. Furthermore, the ORR follows a complicated mechanism with multi-electron transfer processes, various elementary steps and different reaction intermediates. A process, that is still not fully understood up to now [49,50]. Deeper insights on the ORR mechanistics and a general overview on catalyst materials utilized for cathodic ORR in fuel cells and attempts to improve catalytic activity will be given in the following chapter.

2.2. Catalysts for the oxygen reduction reaction

A general reaction pathway proposed for the ORR is given in Scheme 1. Accordingly, oxygen can be either reduced directly to water via the 4-electron pathway or undergo two 2-electron pathways in series with adsorbed hydrogen peroxide as intermediate [51].

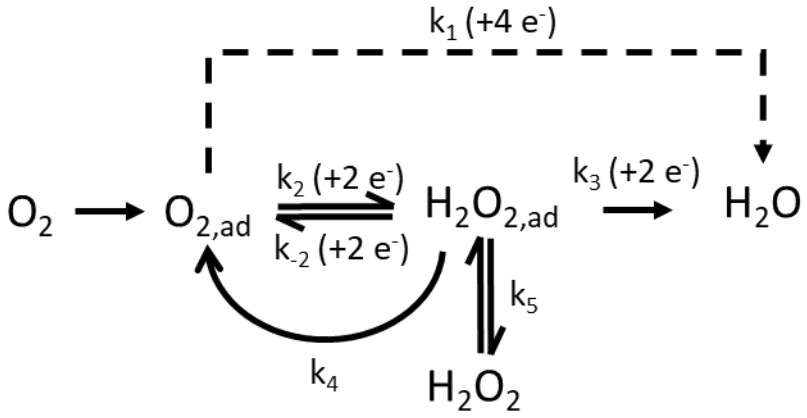

Scheme 1: Proposed reaction pathways for the ORR given by Wroblowa et al. [51].

The favored 4-electron reduction to water, can principally proceed dissociative (Initial step: O_2 → 2 *O) or associative (Initial step: O_2 → $*O_2$), depending on the oxygen dissociation barrier on the catalytic surface. The mechanism includes at least three oxygen-containing intermediates: *OOH, *OH and *O [52]. To design optimized catalysts, it is essential to understand, how to control the adsorption-free energies of these intermediates. In order to do so, for a variety of metal surfaces, Nørskov et al. have calculated the free energies of the intermediates as a function of the oxygen binding energy by the use of a density functional theory (DFT) approach. As a result, a volcano plot (see Figure 5) was obtained, pointing out that Platinum is near the top and the best pure metal ORR catalyst. Accordingly, for metals binding oxygen stronger than Pt, the lower activity is linked to a limitation introduced by the proton-electron transfer to *O and *OH. For metals binding oxygen weaker than Pt, the proton-electron transfer to $*O_2$ in the associative step or splitting of the O-O bond in the dissociative step is limiting, respectively.

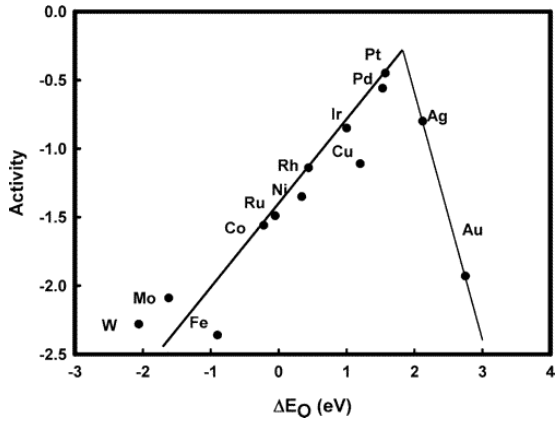

Figure 5: Theoretical ORR activity on different metal surfaces depending on the oxygen binding energy calculated by Nørskov et al. Reprinted with permission from [49]. Copyright 2004, American Chemical Society.

A main issue is that binding energies of the reaction intermediates cannot be decoupled easily. Therefore, in particular the universal scaling relation between *OOH and *OH, that is $\Delta G(*OOH) = \Delta G(*OH) + 3.2 \pm 0.2$ eV, is unfavorable. The optimum adsorption free energy difference between *OOH and *OH would be 2.46 eV [53]. Based on this scaling relation observed on most catalytic surfaces, even the best catalysts at the top of the volcano plot show onset potentials deviating 0.3 - 0.4 V from the ideal cell voltage [54]. Attempts to maximize the activity of Pt-based catalysts generally follow the idea to slightly decrease the oxygen binding energy compared to pure Pt by engineering of the d-band center, resulting in a shift more to the top of the volcano plot. The theory behind this approach is that the d-band center, which is the average energy of the surface atom d states to which the adsorbate binds, correlates with the surface bond energies. In case of the adsorption of oxygen on a metal surface, the oxygen 2p states couple with the metal d states, resulting in formation of bonding and antibonding states. The latter are filled depending on the shift of the d-band center relative to the Fermi level. While an upward shift of the d-band center relative to the Fermi level results in less filling of the antibonding states and a stronger bond, a downward shift of the d-band center results in weaker adsorbate binding due to increased occupation of the antibonding orbital [55,56].

One strategy to improve the Pt d-band center therefore is to tailor the structure of the Pt catalyst via shape-controlled synthesis of nanostructures. Accordingly, the ORR activity of single crystalline Pt facets follows the order (110) > (111) > (100) [57]. Based on these findings, numerous Pt-based catalysts with different exposed facets and morphologies, such as nanowires, nanocubes, nanotubes and nanocages have been presented [58]. Another promising attempt to optimize the d-band center and increase ORR activity is to modify the electronic structure of Pt by alloying with metals such as Ni, Co, Fe, V, Cr and Ti [57,59]. Theoretical and experimental studies have shown that the ORR activity of alloys of Pt with Ni and Co is thereby better than any other Pt alloy or pure Pt catalyst [60–63]. PtNi alloys still suffer from limited stability linked to dissolution of Ni and subsequent restructuring of the surface morphology and changes in composition, resulting in break-in of activity [64]. Pt_3Co alloy catalyst on the other hand is already commercialized and utilized for example in the FCEV Toyota Mirai [17]. Attempts to further improve these catalysts mainly focus on increasing stability. One promising approach therefore is the incorporation of a third metal, resulting in the formation of ternary alloys. This can allow not only to increase electrochemical stability, but also further fine tune the d-band center and maximize ORR activity. Promising materials include alloys such as PtNiMo, PtNiCu, PtNiCo and PtCoAu [65–68]. While the so far discussed approaches focus on increasing intrinsic activity by optimizing the d-band center of Pt, there still exist other possibilities to improve Pt-based PEMFC catalysts, that are summarized in Figure 6 and discussed below.

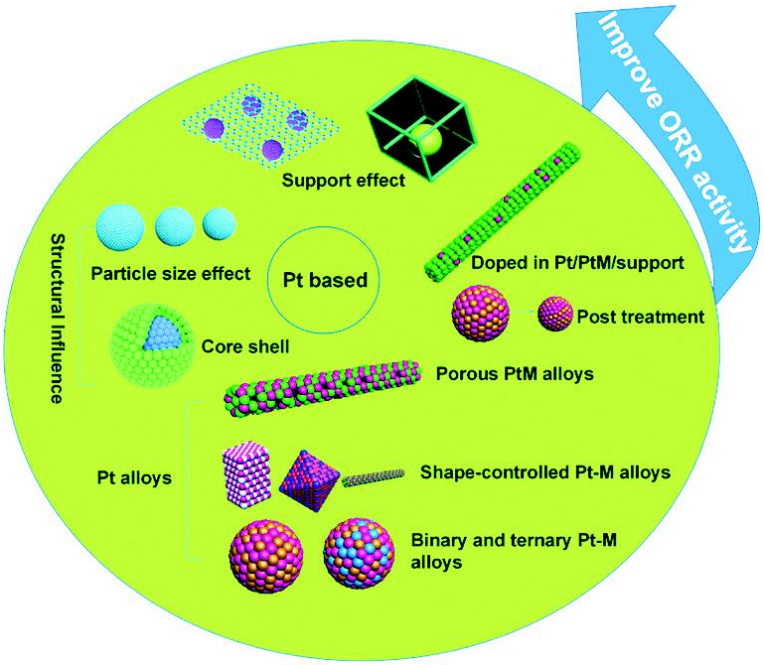

Figure 6: Strategies to improve Pt-based PEMFC catalysts. Reprinted from Zhang et al. [69] (CC BY-NC 3.0).

A general strategy for effective catalysis and to minimize the amount of active metal (in particular Pt) is to maximize the catalyst surface and thus the electrochemical active surface area (ECSA). Therefore, state-of-the-art fuel cell catalysts utilize nanosized particles of Pt dispersed on high surface area carbon powders. The optimum size of the nanoparticles is thereby a trade-off between high surface area and lower intrinsic activity: smaller nanoparticles show enhanced surface binding energies, resulting in lower ORR activity. Also smaller nanoparticles tend to agglomerate and are prone to Ostwald ripening resulting in loss of ECSA and decreasing ORR activity [70]. Regarding the optimum nanoparticle size for Pt/C catalysts, varying values are given in different studies, but the range is around 2-5 nm [71–73]. Another approach to maximize the number of exposed active sites is the formation of porous structures in several geometries such as nanotubes, nanocages and nanowires. However, these fragile structures suffer from poor stability [74–77]. Besides optimization of the active site, also the catalyst support can be optimized for better catalyst stability and also to improve activity via metal-support interaction, as well as accessibility of the active sites via optimization of the pore structure. Generally, requirements the catalyst support has to fulfill are a good electrical conductivity, high specific surface are and porosity, strong interaction with the Pt nanoparticles, as well as low cost and easy recycling of Pt after utilization [78–80]. The most common support for Pt-based catalysts is carbon black. Carbon black is manufactured by pyrolysis of hydrocarbons such as natural gas or oil fractions stemming from petroleum production. The structure of carbon black exhibits a morphological hierarchy (see Figure 7): spheroidal primary particles in the nanoscale range form aggregates with uniform particle size and these aggregates form larger agglomerates. Thereby, strong electrical forces ensure integrity of the aggregates and promote formation of the larger agglomerates [81]. A commonly used carbon black utilized in PEMFCs represents Vulcan XC-72, having a surface area around 250 $m^2\ g^{-1}$ [82].

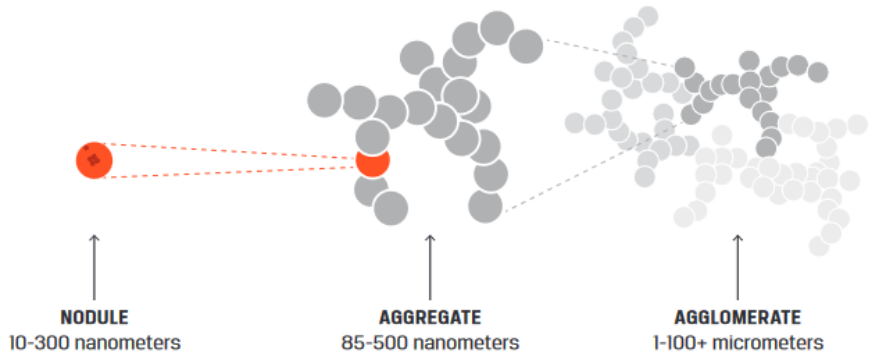

Figure 7: Sequence of the carbon black structure. Reprinted from [81]. Copyright International Carbon Black Association (ICBA).

However, carbon black tends to be instable at high potentials and can induce catalyst degradation due to weak Pt-C interaction. Therefore, attempts to improve carbon stability through graphitization or chemical modification such as boron and nitrogen doping attract attention [83–86]. Also the pore structure of many high surface area carbon blacks utilized in fuel cells cannot be seen as optimal, since they show deep micropores that can trap the catalyst nanoparticles, making them inaccessible to the reactants. Therefore, alternative carbon materials such as carbon nanotubes, mesoporous carbons and carbon nanoframes are of interest in current PEMFC research [82,87]. Besides that, also alternative materials such as TiMo oxides or tin-doped indium oxide, which can anchor Pt and show superior stability over carbon based materials, are investigated [88,89].

Besides the utilization of Pt based catalysts, recently, also non-precious metal catalysts have attracted major attention. Materials of special interest include metal-free functionalized carbons and pyrolyzed Fe-N-C and heteroatom doped carbons. These materials have been shown to reach the activity of pure Pt catalyst, but still suffer from unsatisfactory stability [90–94].

A general overview over the stage of development of the discussed materials and catalyst concepts is given in Figure 8. A key challenge thereby is the transfer of promising catalyst materials from lab-scale testing to real fuel cell application, which will be the focus of the following chapter.

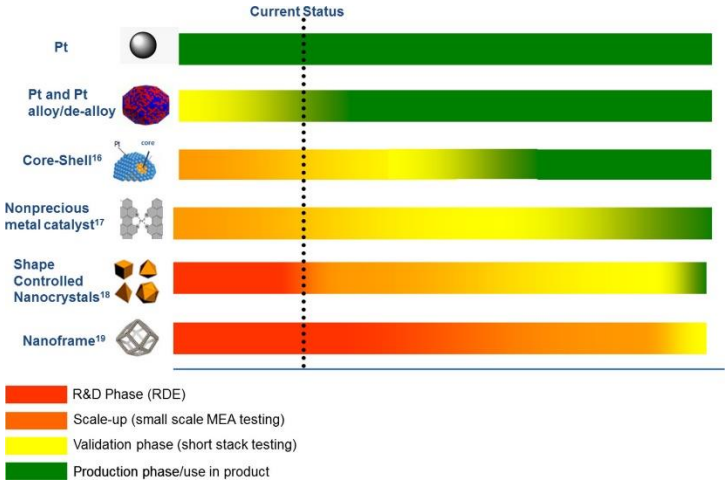

Figure 8: Current status and development timeline of catalyst materials utilized in PEMFCs. Reprinted with permission from [95]. Copyright 2017, American Chemical Society.

2.3. State-of-the-art techniques for testing of electrochemical ORR performance

Basically, there exist two wide-spread techniques for evaluation of the ORR activity of new catalyst materials: the thin-film RDE technique and single-cell MEA testing. While RDE testing is very popular in an early stage of catalyst testing due to its technical simplicity and fastness, MEA testing is much more complex, but can closely resemble the real fuel cell application, since it is carried out under identical operation conditions (temperature, pressure, humidification of gases) [96]. Since both techniques allow evaluation of the catalyst activity towards the identical reaction, for data interpretation it is crucial to be aware of the strengths and limitations of both techniques. Therefore, subsequently, both techniques will be compared to each other and important differences will be highlighted. Figure 9 gives a general overview of the measurement principle of both techniques and compares the most important measurement specifications during ORR evaluation.

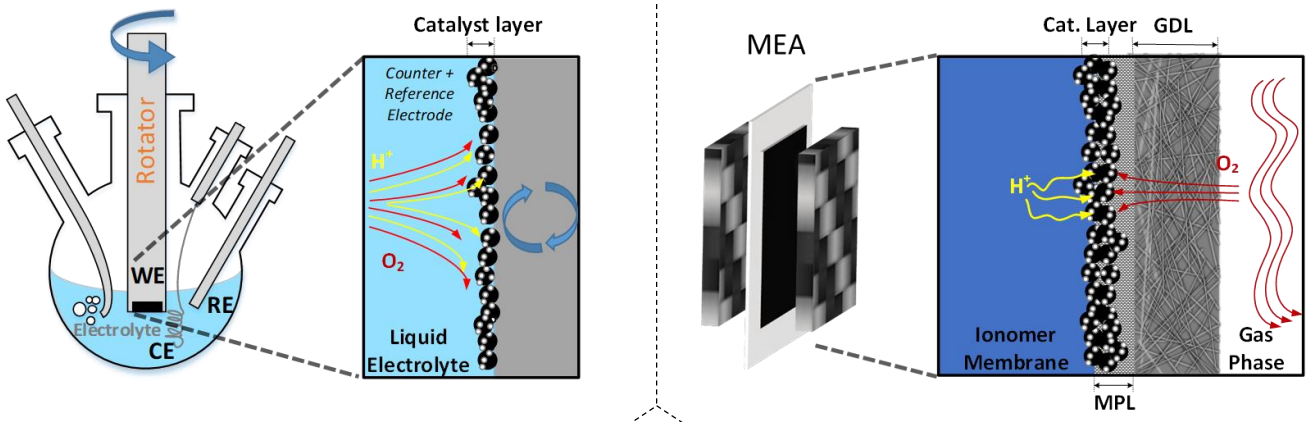

RDE	Technique	MEA
Typically 0.1 M $HClO_4$ (aq.)	**Electrolyte**	Proton exchange membrane (PEM, typically perfluoro sulfonic acid)
Glassy carbon electrode typically 0.196 cm^2 electrode area	**Substrate / electrode size**	PEM or GDL, compressed to five-layer MEA 5 – 25 cm^2 electrode area
Typically room temperature	**Temperature**	40-95 °C, typically 80 °C
Typically 6 mA cm^{-2}_{geo} at 1600 rpm	**Maximum current density**	> 4000 mA cm^{-2}_{geo}
Minutes to hours	**Experiment duration**	Days to weeks
< 10 mg for electrode preparation < 0.02 mg_{Pt} cm^{-2}_{geo}	**Catalyst amount / loading**	20-2000 mg for electrode preparation 0.1 – 0.5 mg_{Pt} cm^{-2}_{geo}

Figure 9: Visualization of the measurement environment and specification of typical measurement conditions in RDE and MEA. Inspired by [97]. Data extracted from [26,97,98].

In RDE evaluation a small amount of catalyst is deposited on a smooth glassy carbon electrode by drop casting of catalyst ink. After drying, the RDE is then rotated in oxygen saturated aqueous acidic electrolyte (typically 0.1 M $HClO_4$). Rotation of the RDE thereby ensures transport of reactant to the electrode surface and establishes a well-defined diffusion layer of 5-50 μm thickness, allowing to extract kinetic parameters. One important difference to MEA evaluation is that RDE testing is typically carried

out in a 3-electrode setup and all potentials are referred to a reference electrode, allowing to measure the isolated overpotentials towards the ORR and extraction of intrinsic reaction kinetics. In contrast, in MEA testing, the full cell potential is measured, containing overpotentials of both cathodic ORR and anodic HOR [99–101]. The catalyst loading in RDE evaluation is usually below 0.02 $mg_{Pt}\,cm^{-2}_{geo}$, while in MEA evaluation catalyst loadings in the range of 0.1 – 0.5 $mg_{Pt}\,cm^{-2}_{geo}$ on a bigger electrode area are typical. Thus, MEA testing also requires a much higher amount of catalyst, which can be problematic in early stages of catalyst development, where oftentimes only milligram amount of material is available. For MEA testing, the first step in evaluation is to prepare the five-layer MEA, consisting of anode and cathode catalyst layer, separated by the ionomer membrane and sandwiched between two GDLs (see Figure 9). Generally, two approaches for MEA fabrication can be distinguished: applying the catalyst to the GDL, called catalyst coated substrate (CCS) or applying the catalyst to both sides of the membrane, called catalyst coated membrane (CCM). Two CCSs can then be combined with a membrane or one CCM with two GDLs to form the five-layer MEA. Different techniques are utilized for preparation of CCS, CCM and MEA, respectively, including spray coating, doctor blading, vacuum filtration, decal transfer and hot-pressing [102,103]. Requirements needed to be optimized in this regard include to maximize the 3-phase boundary of the catalyst, i.e. by maximizing the catalysts ECSA and simultaneously minimizing barriers to reactant transport (protons and oxygen). Therefore, the catalyst particles should be electronically connected via the catalyst support, but not be trapped in the electrode structure and have ionic pathway for proton accessibility. The barrier to water diffusion should be low for effective removal of product water, but oxygen diffusion should be optimized at the same time by optimal distribution of the reactant gases through the GDL. This is a highly complex interplay of all components within a MEA and gives a huge variety of parameters needed to be optimized [102,104]. In RDE testing the situation is simpler and electrode manufacturing less time consuming: the main goal is to have an ultrathin catalyst coating with high uniformity, wherefore best practices under application of techniques such as rotational drying have been released [105–107]. In MEA evaluation not only electrode preparation is time-consuming, but also testing takes several days. Firstly, pre-test diagnostics have to be carried out to avoid problems such as gas leaks and electrical shorting. Then the MEA has to be conditioned over hours/days, before it attains peak performance and finally ORR activity can be determined. Thus, the overall evaluation takes days to weeks. Additional to heating and cooling, MEA testing requires also further technical periphery such as gas humidification [108]. RDE evaluation is technically much easier in this regard. It requires no sophisticated technology and oftentimes also no heating, since the measurements are mostly carried out at room temperature. The duration time of the whole evaluation therefore is only few hours. An important difference between RDE and MEA testing is the catalyst environment in both techniques. In RDE testing the catalyst is deposited on a smooth glassy carbon surface and surrounded by the liquid electrolyte, flooding the catalyst layer and providing both protons

and oxygen (solubilized in the electrolyte) for the ongoing reaction through the liquid diffusion boundary layer. As in any other electrochemical half-cell utilizing bulky electrode material, the dissolved reactant gas has to diffuse over a long distance in the bulk electrolyte to reach the catalytically active sites [109]. The combination of the resulting thick diffusion layer and the low diffusion coefficient in the liquid electrolyte, together with the low solubility of oxygen in the aqueous electrolyte (around 1 mmol L^{-1}) results in strong mass transport limitations in RDE testing, limiting the maximum achievable current density to around 6 mA cm^{-2}_{geo} at a typical rotation rate of 1600 rpm. This corresponds to minimum potentials, where activity can be determined of 0.9 V or even 0.95 V for highly active next generation catalysts. In contrast, in MEA testing the catalyst is in contact with the solid ionomer membrane for proton supply, thus no complete flooding of the catalyst layer, as obtained in RDE testing, occurs and oxygen is supplied by gas phase diffusion through the GDL. Thereby the thickness of electrolyte that oxygen must diffuse through to reach the catalyst surface, is significantly reduced. Together with the higher gas phase diffusion coefficient of oxygen compared to the liquid phase diffusion coefficient, this allows to reach technical current densities of more than 4000 mA cm^{-2}_{geo}. This corresponds to potentials down to 0.4 V, where ORR activity is determined [108,110,111]. The different catalyst environment between both techniques therefore can result in important uncertainties regarding interfacial phenomena, reactant solubility, differences in local and bulk pH and generally transport phenomena of reactants and product water [112]. For RDE testing many best practice advices have been released, allowing good inter-lab comparability of catalysts [104,106,107,110,111,113,114]. Nevertheless, due to the observed differences of the technique to MEA testing, in the recent years, challenges of transferring RDE activity to MEA experiments have moved into the limelight. The main issue therefore is that promising novel catalyst concepts such as multi-metallic and shaped nanomaterials cannot maintain their record activities observed in RDE testing, when embedded in real catalyst layers and tested in a MEA (see Figure 10) [23,24,115,116].

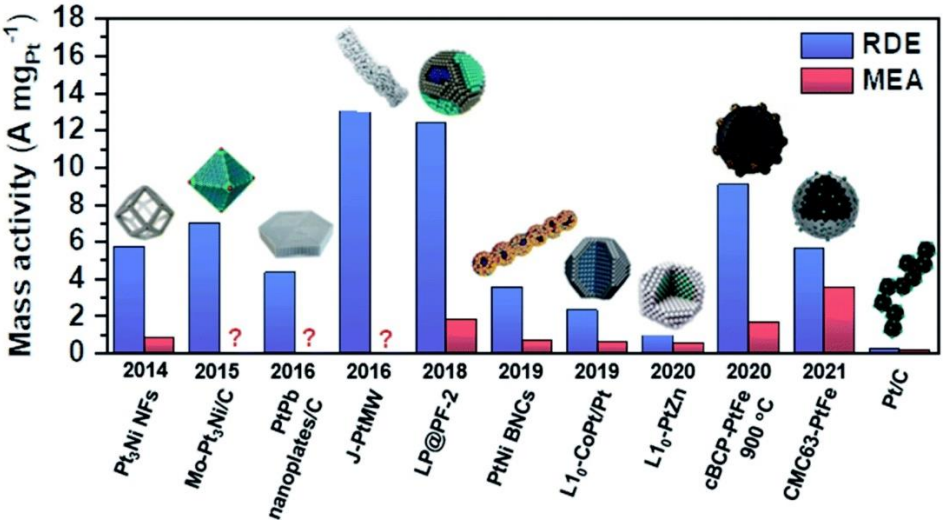

Figure 10: Comparison of the catalytic activity of different materials measured in RDE and MEA. Reprinted from Kim et al. [116] (CC BY-NC 3.0).

The main drawback of RDE testing therefore is that it cannot capture the complex interaction of the single MEA components in the high current density regime, which directly affects the maximum power density of the fuel cell device, as discussed above. One important metric needed to be optimized in MEA evaluation for high current density performance is the balance of a good pore structure for improved oxygen diffusion and a covering thin ionomer layer for sufficient proton accessibility. Therefore, the catalyst itself can be optimized regarding the carbon support pore structure and the location and dispersion of the Pt active nanoparticles on the carbon support [117–120]. Besides that, the interaction of ionomer and the catalyst support and also the distribution of the ionomer within the CL is a key to a high performing MEA. Accordingly, adding a sufficient amount of ionomer is crucial to ensure good proton conductivity, but adding excess ionomer can induce oxygen mass transport limitations resulting from a diffusion barrier through thicker ionomer films [121,122]. Besides optimizing the amount of ionomer by tuning the ionomer to carbon (I/C) ratio, the chemical structure of the ionomer can be optimized. Furthermore, distribution of the ionomer within the CL can be improved by tuning the interaction with the carbon support and by optimizing the ink formulation [123–128]. Catalyst layer optimization by fine-tuning the interplay of the discussed components holds huge potential to increase the energy efficiency of the fuel cell device. For example the power density of the FCEV Toyota Mirai could be improved by 15 % by mainly optimizing carbon support and ionomer [129]. RDE evaluation does not allow to describe the discussed interaction of the single CL components due to its limitation to low current densities and the differing catalyst environment. Regarding interaction with the ionomer, in RDE testing with the CL surrounded by liquid electrolyte providing protons, it has been shown that even measurements without ionomer are feasible and actually any ionomer added will negatively influence the activity. Ionomer is therefore mainly added to get a stable catalyst ink and a uniform coating. Also the negative effect of excess ionomer observed in the MEA mass transport regime cannot be captured [130]. Thus, these measurements are suited to describe intrinsic activity, but not to get a clear view of the interaction of catalyst and ionomer and its influence on proton accessibility in realistic catalyst layers. Overall, the presented findings highlight that activity trends observed in the low current density regime and in particular in aqueous model systems such as RDE, cannot automatically be translated to the high current density regime. As a result, it can be concluded that it is essential to test novel catalyst materials in the high current density regime already at an early stage of catalyst development. Therefore, MEA testing is an indispensable component in implementation of novel materials. However, it is expensive, material and time-consuming, technically complex and requires extensive catalyst layer optimization. Therefore, MEA testing might not be the best choice as standard tool in early stage catalyst evaluation and novel techniques giving access to the high current density regime but having advantages of the RDE technique such as simplicity, robustness and short evaluation time are required [97,131]. Approaches to achieve this goal will be the focus of the following chapter.

2.4. Approaches to bridge the gap between fundamental and applied ORR evaluation

To overcome the limitations of the RDE technique and allow for assessment of ORR activity in realistic current regimes at an early stage of catalyst development, several different approaches have been proposed. The most promising of which are microelectrodes, floating electrode (FE) and gas diffusion electrode (GDE). Microelectrodes are solid-state electrode setups, allowing to study the catalyst-membrane interface. Therefore, the catalyst is in direct contact with the ionomer membrane and mass-transport parameters at the interphase of the two of them can be examined [132–135]. A schematic of such a microelectrode setup is shown in Figure 11A. The setup allows to apply variable pressure to the electrode-membrane contact and also the surrounding pressure and temperature are controllable [132]. A major limitation of microelectrode setups is that the reactant gas has to diffuse through the ionomer membrane, resulting in similar mass transport limitations and low maximum current densities as observed in RDE testing [136]. Additionally, as microelectrodes represent a bulky electrode material, they cannot imitate the structure of realistic catalyst layers in a MEA. To overcome the mass transport limitations in half-cell ORR testing, Kucernak et al. invented a setup using similar measurement principle as in a real MEA. Thereby, the catalyst is loaded on a gold grid as electrode substrate and is in contact with an ionomer membrane. Oxygen is then provided from the backside of the thin electrode substrate as humidified gas, thereby by-passing the mass transport limitations observed in RDE testing and allowing to study the ORR performance across fuel cell relevant potentials [136]. The idea of this setup was later used to establish the FE approach for catalyst testing. Therefore, a porous polycarbonate substrate with well-defined pore size is sputtered with gold and coated with a thin layer of catalyst from one side, while the other side is treated hydrophobic by the application of a Teflon compound, to prevent flooding with electrolyte during the measurement. The resulting electrode is then placed to float on top of the electrolyte, providing protons, while gaseous reactant can be delivered from the backside directly to the catalyst, thus avoiding mass-transport limitations (see Figure 11B) [137–139].

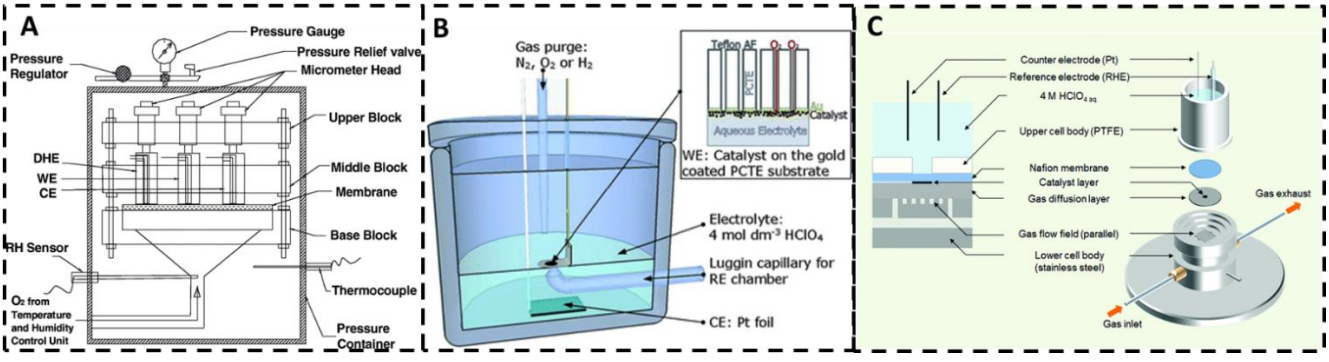

Figure 11: A: Schematic of a solid-state microelectrode setup. The catalyst is introduced between working electrode (WE) and membrane. Reprinted from Zhang et al. [132] with permission from Elsevier B.V. B: Experimental floating electrode setup with the catalyst layer being in contact with the liquid electrolyte and gas being delivered from the backside through a gas diffusion media. Reprinted from Zalitis et al. [137] with permission from Royal Society of Chemistry. C: Sketch of a gas diffusion electrode half-cell, utilizing the identical electrode as used in a MEA. Reprinted from Inaba et al. [140] with permission from Royal Society of Chemistry.

In the work of Zalitis et al. this approach allowed to achieve very high specific current densities up to 185 mA cm^{-2}_{spec} (around 800 mA cm^{-2}_{geo}) and no mass transport limitations could be observed in the fuel cell application relevant potential range of 0.6-0.8 V [137]. In newer studies even current densities up to 2800 mA cm^{-2}_{geo} could be realized [141]. Also, the FE approach was recently adapted for *in operando* studies using Fourier-transform and online mass spectrometry (MS) [142]. Furthermore, degradation studies using identical location transmission electron microscopy (IL-TEM) were presented [143]. However, the FE technique, similarly to the RDE, uses very thin and idealized catalyst layers (catalyst loading typically <0.02 mg_{Pt} cm^{-2}_{geo}) on a well-defined electrode surface. Therefore, it cannot precisely mimic the 3-phase boundary in real MEAs and cannot be used to examine the complex interaction of all electrode components, as discussed in the previous chapter. In order to further approach real fuel cell conditions in aqueous half-cell setups, therefore, gas diffusion electrode half-cells have been invented (see Figure 11C). This approach uses the same electrode substrate material as in a MEA, namely gas diffusion electrodes with a microporous layer on top. The measurement principle thereby is identical to the FE approach: the catalyst layer is in direct contact with the acidic electrolyte (perchloric acid in higher concentrations compared to RDE) for proton supply and gaseous reactant is directly transported to the catalyst via the porous gas diffusion media [140]. Thereby, catalyst loadings matching those of the industrial fuel cell application can be investigated [144]. GDE half-cells have already been used since the 1990's to study the effect on ORR performance of various parameters such as ionomer amount, PTFE content, particle size and temperature [145–150]. However, these studies have all presented mass transport limitation, hindering the study of fuel cell relevant potentials and current densities in GDE half-cells. Important works that could finally overcome these limitations by optimizing the experimental setups were presented by Pinaud et al. and Wiberg et al. [151–153]. In the work of Pinaud et al., therefore, a measurement cell with controlled convective gas flow to the GDE was established, thus hindering flooding issues during evaluation. This principle was further optimized by Ehelebe et al., allowing to reach geometric current densities up to 2000 mA cm^{-2}_{geo} without observable mass-transport limitations and good comparability to single-cell MEA testing [154]. The setup presented by Wiberg et al. was first established for measurements in phosphoric acid for high temperature PEMFCs and later adapted for evaluation of low temperature PEMFC catalysts with perchloric acid as electrolyte [140,153]. Thereby, lower catalyst loadings compared to the works of Pinaud et al. and Ehelebe et al. could be investigated at various temperatures and also with an ionomer membrane placed between catalyst layer and electrolyte [140,153].

In the past years, GDE half-cell setups were further developed for measurements at elevated temperature and pressure, and also coupling to various analytical equipment such as quadrupole MS, Inductively Coupled Plasma (ICP) MS, X-ray and neutron imaging, IL-TEM and small-angle X-ray scattering was presented to study both activity and stability [144,155–161]. This allows to study highly interesting

phenomena in realistic catalyst layers under application-oriented conditions and can give insights, which were not accessible so far with MEA testing alone. Also, it was recently presented that half-cell GDE setups can be used to investigate novel catalyst concepts for the PEMFC, such as Fe-N-C catalysts [162–164]. As a result, GDE half-cells are supposed to be a promising bridging tool between RDE and GDE (see Figure 12).

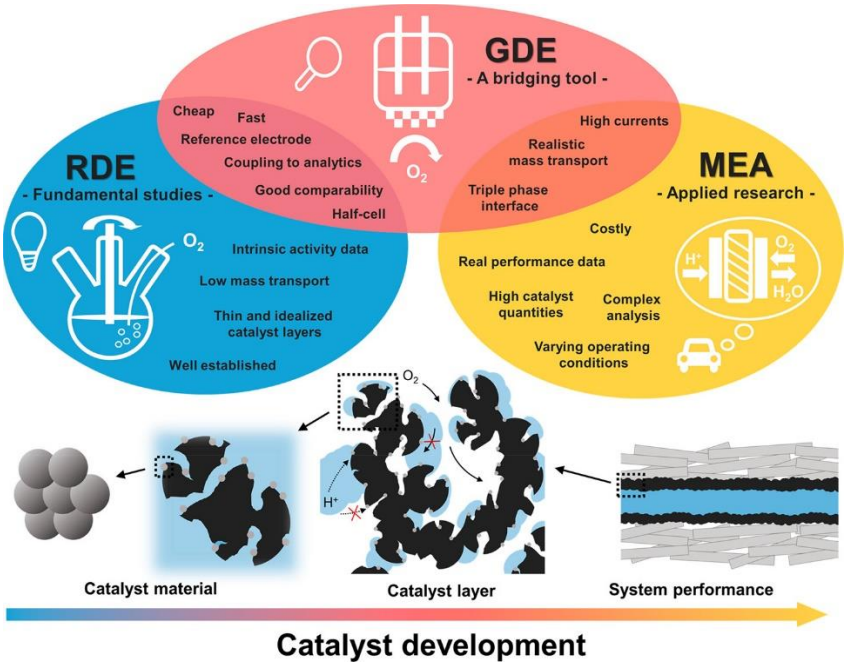

Figure 12: Introduction of gas-diffusion electrode half-cells as bridging tool between RDE and MEA. Reprinted from own publication [96]. Copyright 2022, American Chemical Society.

3. Aim and scope of the thesis

As presented in the previous chapter, promising ORR activity of next generation PEMFC catalysts derived from thin film RDE testing could so far not be transferred to real MEA devices. Therefore, the aim of this thesis is to establish a novel technique which can overcome the limited significance of fundamental lab-scale testing in aqueous half-cell setups. This technique should therefore allow to study realistic catalyst layers utilized in a MEA at fuel cell relevant current densities and potentials, while keeping the advantages of RDE testing, such as fast evaluation, utilization of a reference electrode, minimized material consumption and good comparability and reproducibility. This would allow on the one hand to identify catalysts where a tedious catalyst layer optimization for MEAs is worth to be carried out and could potentially also give insights to good catalyst layer compositions.

In order to face this concern, this thesis focusses on the half-cell gas diffusion electrode approach, introduced in the preceding chapter. Therefore, a commercially available half-cell configuration (Flexcell®, Gaskatel GmbH) is utilized. The thesis is built up upon the results published in three self-contained research articles, which are appended in the following chapter. The open scientific question addressed by these publications is how reproducible high current density testing in GDE half-cells can be carried out and which insights can be gained through the GDE approach in detail.

The first publication *"Oxygen reduction reaction measurements on platinum electrocatalysts in gas diffusion electrode half-cells: Influence of electrode preparation, measurement protocols and common pitfalls"* focusses on the development of dedicated protocols for GDE half-cell testing. A process which was necessary before for both RDE and MEA testing, and is the required base for trustworthy and comparable data. Therefore, the publication gives best practice advices for electrode preparation and ORR activity measurement and also generally highlights pitfalls during GDE characterization, such as electrolyte heating and falsified iR correction at elevated current densities. Considerations within this publication were also integrated in a collaborative and co-authored work, not included in this cumulative thesis. Thereby, activity of identical catalysts was assessed in different half-cell GDE setups in different laboratories by following identical measurement protocols, underlining the strength and reliability of the presented protocols and best practice advices [96].

The second paper *"How to maximize geometric current density in testing of fuel cell catalysts by using gas diffusion electrode half-cell setups"* focusses on further development of the GDE technique to allow analyzing the full current density regime of MEA testing. Thereby, measures are presented to minimize ohmic losses within the half-cell setup, which limited the accessible current range in earlier publications on GDE testing linked to the compliance voltage limitation of the utilized potentiostat. With this, ORR current densities up to 4000 mA cm^{-2}_{geo} could be tested and even absolute current densities as high as 10500 mA cm^{-2}_{geo} were feasible, making the technique applicable for future generation catalysts or high catalyst loadings.

In the third paper *"Which insights can gas diffusion electrode half-cell experiments give into activity trends and transport phenomena of membrane electrode assemblies?"*, finally, the comparability of GDE half-cell and MEA testing is assessed. Therefore, two model catalyst systems are comparatively analyzed by using both techniques. Thereby, it can be shown that the correct prediction of catalyst performance in a GDE half-cell strongly depends on the limiting transport mechanism (proton accessibility and oxygen transport limitation) and the critical component within the catalyst layer, limiting the catalyst performance. In particular, it is presented that for differences in catalytic activity being linked to oxygen mass transport, GDE evaluation can very well give trends for catalytic activity in a MEA and is superior compared to RDE testing in this regard. However, due to the differing interphase catalyst layer/solid ionomer membrane in MEA and catalyst layer/liquid electrolyte in GDE testing, trends in catalytic activity being linked to proton transport and accessibility can less be described using the GDE half-cell in the presented configuration.

Thus, overall, the publications within this thesis allow to answer both scientific questions mentioned beforehand: it is shown that fast and simple half-cell GDE testing, allowing to analyze ORR activity in fundamental research along the full current and potential range of a real fuel cell device, can be carried out with high reproducibility by following the measurement protocols and general measures presented within this thesis. Additionally, important differences in GDE testing and MEA testing are identified, resulting from the differing catalyst interphase in both techniques. Based on this, it is presented that GDE half-cell testing can reliably describe oxygen mass transport behaviour for real MEAs at industrial relevant current densities. Figure 13 presents the general chronology of this thesis.

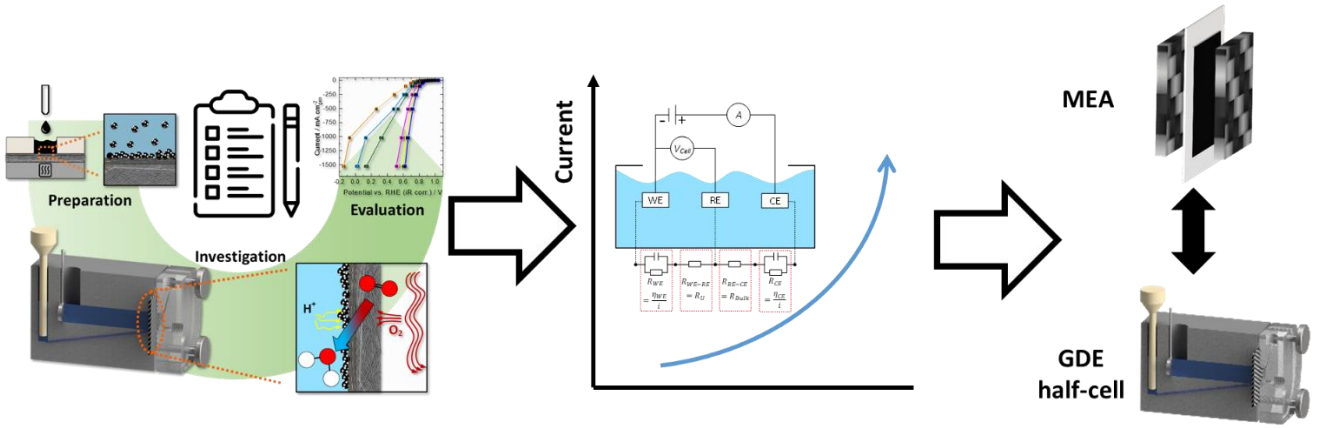

Figure 13: Chronology of the present cumulative thesis: In the first step measurement protocols for half-cell GDE evaluation were proposed. Thereafter, the technique was developed to reach higher geometric current density. Finally, different model catalysts were comparatively analyzed in GDE half-cell and single-cell MEA testing.

4. Publications within this cumulative thesis

4.1. Oxygen reduction reaction measurements on platinum electrocatalysts in gas diffusion electrode half-cells: Influence of electrode preparation, measurement protocols and common pitfalls

Authors: Nicolai Schmitt, Mareike Schmidt, Gerold Hübner, Bastian J.M. Etzold

Journal: Journal of Power Sources

Publisher: Elsevier

Bibliography: Volume 539, 231530
© 2022 The Authors. Published by Elsevier B.V.

Date: 15 August 2022

DOI: https://doi.org/10.1016/j.jpowsour.2022.231530

Reprinted under the terms of the Creative Commons CC-BY license.
https://creativecommons.org/licenses/by/4.0/

Journal of Power Sources 539 (2022) 231530

Contents lists available at ScienceDirect

Journal of Power Sources

journal homepage: www.elsevier.com/locate/jpowsour

Oxygen reduction reaction measurements on platinum electrocatalysts in gas diffusion electrode half-cells: Influence of electrode preparation, measurement protocols and common pitfalls

Nicolai Schmitt [a], Mareike Schmidt [a], Gerold Hübner [b], Bastian J.M. Etzold [a,*]

[a] Technische Universität Darmstadt, Ernst-Berl-Institute for Technical Chemistry and Macromolecular Science, Alarich-Weiss-Straße 8, 64287, Darmstadt, Germany
[b] Volkswagen AG, Konzernforschung, 38436, Wolfsburg, Germany

HIGHLIGHTS

- GDE measurements for evaluation of oxygen reduction reaction catalysts.
- Best practice guidelines on electrode preparation and activity determination.
- Facile and reproducible catalyst layer application.
- Pitfalls in GDE half-cell measurements.

GRAPHICAL ABSTRACT

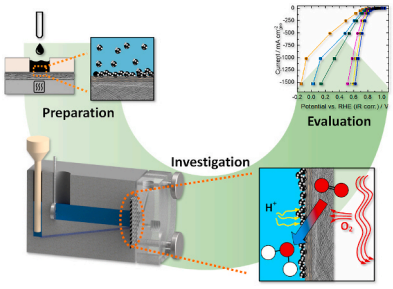

ABSTRACT

Recently, half-cell gas diffusion electrode (GDE) setups have been presented as a powerful tool and promising alternative to rotating-disk electrode (RDE) as also membrane electrode assembly (MEA) testing of oxygen reduction reaction (ORR) catalysts. While RDE testing aims to extract isolated kinetic data, GDE testing allows characterization of realistic fuel cell catalyst layers at application relevant current densities and potentials, where also phenomena besides catalyst kinetics play a role. Nevertheless, while for RDE as also MEA testing dedicated protocols for reliable electrode preparation and assessment of activity were developed, and are backdrop for trustworthy and comparable data, these are missing for the novel half-cell GDE testing. This work identified key challenges in running and evaluation of half-cell GDE measurements, which are *e.g.* ink composition and electrode preparation, falsification of electrochemical active surface area using hydrogen uptake measurements, influence of joule heating at high current densities and importance of solution resistance correction. A commercial half-cell GDE, as well as a commercial catalyst, were employed, allowing fast application of the developed protocols, while the general findings can also be translated to other GDE setups.

1. Introduction

In the past years proton-exchange membrane fuel cells (PEMFCs) have reached an initial state of commercialization for automotive, portable and stationary applications, as can be seen from several major automotive companies that are selling fuel cell electric vehicles and the increasing utilization of the technology in micro-combined-heat-and-power systems [1–3]. However, similar to other technology with ongoing strong research and development after initial commercialization, for fuel cells there are remaining challenges including durability, performance at high current densities and cost, which need to be addressed [2,4]. Especially the still sluggish kinetics of the cathode

* Corresponding author.
E-mail address: bastian.etzold@tu-darmstadt.de (B.J.M. Etzold).

https://doi.org/10.1016/j.jpowsour.2022.231530
Received 6 August 2021; Received in revised form 21 March 2022; Accepted 23 April 2022
Available online 18 May 2022
0378-7753/© 2022 The Authors. Published by Elsevier B.V. This is an open access article under the CC BY license (http://creativecommons.org/licenses/by/4.0/).

oxygen reduction reaction (ORR), on commercially used, cost intensive and critical platinum electrocatalysts results in high overpotentials and represents a major obstacle to a more widespread use of the PEMFC [5–7]. The cathodic ORR is also of great importance in other electrochemical conversion devices, such as metal-air-batteries, and dominates the overall efficiency and performance of the respective processes [8]. For that reason, finding more efficient, durable and cheap electrocatalysts for the ORR is still a main goal in fuel cell research and also in other fields of electrocatalysis [3,9].

Currently, cathode catalyst layers in commercial PEMFCs use PtCo alloy nanoparticles on a carbon support, showing higher ORR mass activity versus pure Pt nanoparticles and enhanced stability compared to alloys of Pt with other transition metals (*e.g.* Ni, Fe, Cr) [2,10,11]. However, studies in liquid half-cells under well-defined conditions have presented several next-generation Pt-electrocatalysts, that can outperform the current state-of-the art catalysts by tuning their particle sizes, shapes and surface compositions [12]. For instance, Stamenkovic et al. have presented PtNi nanoframes showing a mass activity of 5.7 A mg_{Pt}^{-1} at 0.9 V, which is more than an order of magnitude higher than the U.S. Department of Energy's target of 0.44 A mg_{Pt}^{-1} set in 2017 [13]. Li et al. showed a procedure to synthesize jagged nanowires out of pure Pt by leaching Ni out of PtNi nanowires. The resulting surface area is exceptionally high and enables a record-breaking mass activity of 13.6 A mg_{Pt}^{-1} at 0.9 V in a liquid half-cell [14]. Other highly promising Pt-based catalyst concepts include transition-metal doped PtNi octahedral nanoparticles and PtPb nanoplates [15,16]. Besides that, recently, non-precious metal catalyst, including transition-metal oxides and carbon-based materials (*e.g.* metal-free functionalized carbons, pyrolyzed Fe–N–C and heteroatom-doped carbons) have attracted numerous interest and can surpass the activity of the state of the art Pt catalysts, while the stability is still unsatisfactory [17–21]. A big problem of all these promising results derived from low current density half-cell studies is that they could not or only partially be transferred to the real membrane electrode assembly and single cell or stack studies [22,23].

Thus, in ORR catalyst research the problem arises that a technique allowing to extract kinetic parameters at well-defined reaction conditions, while being fast and using only very small amounts of catalyst is needed. The widely accepted thin-film rotating disk electrode (RDE) technique, where the catalyst is immobilized on smooth glassy carbon electrodes, is fulfilling these criteria [24–28]. Additionally, the data should be transferable to the technical application and must be meaningful also within the technical relevant conditions applied in fuel cells. In this sense RDE studies on novel PEMFC electrocatalysts have shown extraordinary performance, which, however, could not be transferred to the real fuel cell device [23]. Major reason for this differing results are first of all the catalyst environment in an RDE (thin layer on a small area glassy carbon disk) which differs substantially from the much thicker catalyst layers on larger electrodes in practical fuel cells. Furthermore, the solubility of oxygen as reactant gas in the commonly used aqueous-acidic electrolytes in combination with the laminar film at the rotating electrode is limiting the maximum achievable current density to approx. 6 mA cm^{-2} at a typically used rotation rate of 1600 rpm. This corresponds depending on the catalyst to a minimum potential, where activity can be determined, of 0.9 V and for highly active next generation catalysts even 0.95 V. Contrary to that real fuel cell devices achieve three magnitude higher current densities up to 3000 mA cm^{-2} and are operated approx. down to 0.6 V [25,29]. For that reason, RDE measurements oftentimes cannot capture catalytic behavior at elevated current densities and high overpotentials and thus only give limited information about trends in catalytic activity in the real fuel cell operation range [23,30]. In order to overcome the limitations of the RDE technique while preserving its advantages such as good comparability of results, fast testing, no need for sophisticated membrane electrode fabrication tools for high reproducibility, known working electrode potential and isolated analysis of ORR kinetics, half-cell setups using gas diffusion electrodes have been presented as a powerful tool to examine fuel cell electrocatalysts [31–35]. Utilizing a self-developed setup, Pinaud et al. [32,35] were able to measure ORR activity by using realistic catalyst loadings (0.3 mg_{Pt} cm^{-2}) up to a current density of 1750 mA cm^{-2} with good comparability to single cell MEA measurements. Arenz et al. [31,33] meanwhile presented a setup with similar functional principle that enables to examine Pt-based ORR catalysts at low loadings (down to 5 μg_{Pt} cm^{-2}) and also allows experiments at elevated temperature and under introduction of a Nafion membrane to better mimic fuel cell conditions. Ehelebe at al. [34] took the cell setup presented by Pinaud et al. as a role model and carried out some further optimization. By doing so, they could measure ORR activity up to a current density of 2000 mA cm^{-2}. Furthermore, a Pt-loading variation in the range of 0.02 mg_{Pt} cm^{-2} to 0.4 mg_{Pt} cm^{-2} demonstrated that specific and mass-specific activities do not change with layer thickness in a wide potential range, implying that no major mass transport resistances do occur in the used setup.

As can be seen from several principle and best practice studies concerning the RDE methodology and MEA testing, detailed instructions on experimental execution, including sample preparation and measurement protocols, is essential for meaningful research and comparability of results [24]. In RDE testing reliable and reproducible catalytic activity could be observed, once protocols on production of uniform electrodes and detailed electrochemical measurement protocols were established [24–26,36–38]. The reliable evaluation of new materials in single cell MEA measurements is even more challenging, since the setup contains multiple complex interacting components (*e.g.* pore network and ionomer network within the catalyst layer, ionomer membrane, GDLs including microporous layer (MPL), gaskets as compression stops, flow-field plates and current connectors) that are all evaluated at once. Therefore, in single cell testing, detailed instructions on the fabrication of the MEA are at least as important as standardized measurement protocols as provided by the U.S. Department of Energy [39–42].

Due to the novelty of the GDE-half-cell testing approach, major pitfalls of this measurement technique were not determined up to now and no best practice measurement protocols were developed. E.g. up to now cyclic voltammetry with potential control [31,33] as also galvanostatic steps [32,34] are employed for determination of ORR activity. In order to increase comparability of cross-lab results of this novel methodology, in this work, major pitfalls were identified and a measurement protocol development based on well-founded scientific observations is presented. This covers the fabrication of catalyst coated GDEs, the determination of the ECSA, the influence of joule heating at high current densities during the measurement of polarization curves and the influence of electrolyte concentration and the type of GDL. A commercial GDE-half-cell equipment was employed (see the assembled half-cell and a sketch highlighting the measurement principle in Fig. 1), as well as commercial catalyst, which is easily available as reference material, allowing fast transfer of the protocol, while the general findings can of course be transferred to other GDE-half cells.

2. Experimental

2.1. Formulation of catalyst ink and electrode preparation

For catalyst ink preparation 4 mg of Pt/C 50% catalyst (Elyst Pt50 0550, Umicore) were mixed together with deionized water (<1.1 μS cm^{-1}, VWR chemicals), ultrapure ethanol and ionomer (Aquivion® D98-25BS, Sigma-Aldrich) in an eppendorf tube and finely dispersed with the use of an ultrasonic processor (Hielscher, UP200St). The total volume of ethanol and water was set to a value of 4.85 mL. The ionomer/carbon ratio was held at 0.5 g g^{-1} and in standard measurements the volume percentage of ethanol in the catalyst ink was set to a value of 45%. In order to check the influence of the ethanol content in the catalyst ink, the ethanol percentage was varied in a range of 0–100% in a separate measurement series. As further preparation step, the

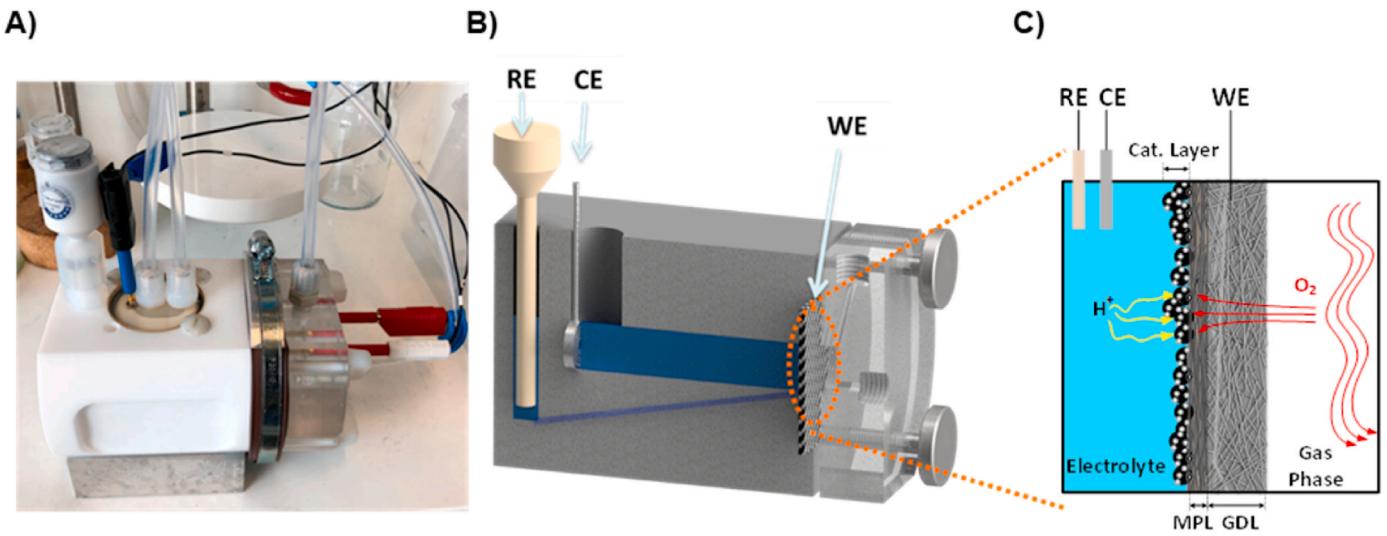

Fig. 1. A) Photograph of the assembled half-cell gas diffusion electrode setup. B) Cross-section of the cell showing the position of working (WE), counter (CE) and reference electrode (RE) and the connection of the reference electrode via a luggin-capillary. C) Function principle of the characterization technique. Gas flow is provided from the backside of the GDL, while the catalyst coated microporous layer (MPL) side is in contact with the electrolyte, providing protons for the ongoing reaction.

accordingly prepared ink was diluted with a water/ethanol mixture considering the respective volume percentage of ethanol. The dilution was adapted to reach a target loading of platinum on the GDL in the range of 10–200 $\mu g_{Pt}\ cm^{-2}$. For application of the catalyst on the gas diffusion media, a GDL piece of 30 × 45 mm is fixed in a self-designed mask, consisting of an alumina body and a PTFE cover that is positioned with the help of three stainless steel pins (details see Fig. S1), with the MPL side facing towards the PTFE cover. The PTFE cover has a round hole of 0.785 cm^{-2} surface area, which is restricting the catalyst coated area. The assembled mask is preheated to 125 °C on a heating plate and finally, 400 μL of the respective catalyst ink dilution is pipetted into the hole of the PTFE mask and let dried. Important to note is that too high concentrated catalyst inks results in elevated deposition of catalyst on the PTFE cover. Therefore, catalyst loadings above 100 $\mu g_{Pt}\ cm^{-2}$ had to be prepared by multiple application of lower concentrated catalyst inks. Due to the restriction of the area with the PTFE mask, only a part of the electrode being in contact with the electrolyte later (full area = 3 cm^2) is coated with catalyst. In order to account for minimal losses of catalyst to the PTFE mask during the coating procedure, the exact loading amount after drying of the catalyst ink is determined by using equation (1).

$$Catalyst\ loading_{real} = Catalyst\ loading_{theoretical} \cdot \frac{ECSA_{CO,\ with\ mask}}{ECSA_{CO,\ without\ mask}} \quad (1)$$

Therefore, the ECSA of the respective catalyst determined from CO-stripping is calibrated by carrying out the drop casting procedure without PTFE mask and thus guaranteeing full deposition of the catalyst on the GDL. Afterwards the ECSA obtained with PTFE mask is set in relation with the obtained value without mask in order to calculate the exact catalyst loading amount on the GDL. Further details on the coating procedure can be found in the Supporting Information.

2.2. Contact angle measurements

For measurement of the static contact angle of catalyst inks with various ink solvent composition (ethanol percentage) on gas diffusion media, a contact angle device OCA35 from Dataphysics at standard climate conditions was used. Therefore, 10 μL droplets of the respective catalyst ink diluted for a target loading of 20 $\mu g_{Pt}\ cm^{-2}$ (see supporting information) were pipetted on the MPL side of a Sigracet 29 BC gas diffusion layer and the drop shape analysis was done by Young−Laplace fitting. For each catalyst ink composition at least five droplets were measured and an average value was determined, whereby the error represents the standard deviation. Catalyst inks with an ethanol percentage ranging from 0 to 100 Vol-% were investigated in this study.

2.3. GDE half-cell setup and cell assembly for the electrochemical characterization

As measurement cell, a commercially available half-cell (FlexCell® PTFE, Gaskatel GmbH) was utilized at room temperature using perchloric acid (ROTIPURAN®Ultra 70%, Carl-Roth), that was diluted with ultrapure water, as electrolyte. In standard measurements an acid concentration of 2 mol L^{-1} was used. In order to check for the influence of the electrolyte concentration, the $HClO_4$ concentration was varied in a range of 0.1–4 M in a separate series of measurements. The utilized cell consists of a gas chamber and an electrolyte chamber, that includes a separate reservoir for the reference electrode (RE, Hydroflex, Gaskatel GmbH), which is connected to the working electrode (WE) via a Luggin-capillary. The commercial cell was slightly modified for the given task. On one hand the cover of the electrolyte chamber was replaced by a self-built cover with pipe connectors from em-technik for being able to purge the electrolyte with nitrogen in order to guarantee inert gas atmosphere. Furthermore, a Viton O-ring (⌀ 80 mm, Cafiro) was mounted around the opening between gas and electrolyte with the help of two alumina bodies and a pipe clamp for additional sealing. The utilized cell also includes a PtIr-wire as counter electrode (CE). For the electrochemical measurement, the GDE is sandwiched between two silicon gaskets for sealing and placed between gas chamber and electrolyte chamber with the catalyst coated side facing the electrolyte chamber. The GDE is electrically contacted via two banana plugs that are screwed into the gas chamber. After installation of the GDE, the additional O-ring sealing can be mounted and the cell is filled with approx. 25 mL of electrolyte. For ensuring electrical contact between reference and working electrode, it is important to remove any air bubbles in the luggin capillary by sucking the electrolyte several times through the opening of the RE compartment using an eppendorf pipette. Finally, the reference electrode can be screwed into the RE compartment while avoiding the introduction of air and the gas pipes (PFA, 6 × 1 mm) can be connected to the electrolyte and gas chamber. During the electrochemical measurements, the gas flow to the gas compartment and the electrolyte chamber is controlled via mass flow controllers (EL-Flow Select, Bronkhorst). The electrolyte can be purged with N_2, while the gas compartment can individually be

purged with either N_2, O_2 (99.999%, Air Liquide), CO (99.999%, Air Liquide), H_2 (99.999%, Air Liquide) or synthetic air (20.5% O_2 in N_2, Air Liquide). For monitoring of the electrolyte temperature during the ongoing measurements, a type K thermocouple was introduced through the cover of the electrolyte chamber close to the working electrode and the temperature profile was recorded by using a data logger (TC08, picolog Technology).

2.4. Electrochemical characterization using the GDE half-cell

Electrochemical measurements were carried out on a Ivium Multichannel Potentiostat (Octostat 5000) which is controlled by IviumSoft software. The electrochemical active surface area (ECSA) was determined by integrating the hydrogen desorption area (H_{UPD}) of the CVs in N_2-atmosphere at a scan rate 100 mV s^{-1}, carried out after 200 activation cycles between 0.05 and 1.2 V vs. RHE at 500 mV s^{-1}. Additionally, CO-Stripping was carried out at a scan rate of 20 mV s^{-1} for determination of the ECSA. For ORR activity measurements two different protocols, which both start with a reduction of the Pt-surface by application of a potential of 0.1 V, were utilized. The first one consists of potentiostatic steps that are conducted both backward (1.05–0.1 V) and forward (0.1–1.05 V). The second protocol is based on the protocol presented by Pinaud et al. [32] and Ehelebe et al. [34] and consists of galvanostatic steps. For both protocols the last 3 s of each step were used to construct the resulting polarization curves, considering only the anodic sweep (also see Fig. S3). The uncompensated resistance (*iR* drop) in the utilized GDE setup was determined using electrochemical impedance spectroscopy (EIS) and was used for post-correction of all measured potentials. For each experiment at least two samples have been tested. A detailed overview about the utilized measurement protocols is given in Table 1. During the course of the measurement, the electrolyte chamber is constantly purged with 50 mL min^{-1} N_2, while the gas flow to the gas chamber is adapted for the respective method.

2.5. RDE measurements

RDE characterization was used to benchmark the ECSA of the utilized Pt/C catalyst by using both H^+- and CO-Stripping. The RDE measurements were carried out on a Ivium Multichannel Potentiostat (Octostat 5000) which is controlled by IviumSoft software. A leak-free double-junction Ag/AgCl electrode (Aldrich) was used as RE and a Pt wire (PINE) as CE. All potentials reported in this work were calibrated against a reversible hydrogen electrode (RHE) using hydrogen evolution-oxidation reaction on a Pt electrode. A glassy carbon rotating disk electrode (GC-RDE, 5 mm diameter, PINE) was used as WE. Further details on the RDE measurements are summarized in the Supporting Information.

2.6. Data repository

All data presented in this study is available from an open access repository.

URL: https://tudatalib.ulb.tu-darmstadt.de/handle/tudatalib/2774.

3. Results

Since several critical processes that do influence each other were discovered during the development process of the subsequently presented measurement protocol, critical issues for avoiding pitfalls in GDE measurement cannot strictly be discussed in a chronological order and

Table 1
Protocol for the electrochemical characterization.

	Step	Method	Parameter	
1	Determination of iR drop	EIS galvanostatic	Gas flow	N_2 (~300 mL min^{-1})
			EIS frequency range	10000-1 Hz
			EIS amplitude	0.05 A
			Current	0 mA
2	Electrochemical cleaning	Cyclic voltammetry (CV)	Gas flow	N_2 (~300 mL min^{-1})
			Potential limits	0.05–1.2 V
			Scan rate	500 mV s^{-1}
			Number of cycles	~200 (until CV constant)
3	ECSA (N_2)	CV	Gas flow	N_2 (~300 mL min^{-1})
			Potential limits	0.05–1.2 V
			Scan rate	100 mV s^{-1}
			Number of cycles	3
4	Formation of CO-monolayer	Chronoamperometry (CA)	Gas flow	First 2 min: CO (~200 mL min^{-1})
			Potential	Remaining time: N_2 (~500 mL min^{-1})
			Time	0.1 V
				60 min
5	ECSA (CO)	CV	Gas flow	N_2 (~300 mL min^{-1})
			Potential limits	0.1–1.0 V
			Scan rate	20 mV s^{-1}
			Number of cycles	3
6a[a]	ORR (O_2)	Potentiostatic staircase	Gas flow	O_2 (~200 mL min^{-1})
			Pt-reduction step	0.1 V for 300 s
			ORR potential range	1.05–0.1–1.05 V
			Step size	10 mV
			Holding time at each point	10s
6b[a]	ORR (O_2)	Galvanostatic staircase	Gas flow	O_2 (~200 mL min^{-1})
			Pt-reduction step	0.1 V for 300 s in N_2 (~300 mL min^{-1})
			Current steps (holding time)	OCV (600s);
				−0.04 mA; −0.08 mA (90 s);
				−0.20 mA; −0.40 mA (60 s);
				−0.80 mA; −2.00 mA; −4.00 mA; −8.00 mA (30 s)
				−20 mA; −40 mA; −80 mA; −200 mA; −400 mA; −800 mA; −1200 mA (5 s)
				→in negative and positive direction
7	ORR (Synthetic air)	See 6b[a]		

[a] Protocol 6a was only used during the protocol development process. All later measurements were carried out using protocol 6b.

isolated from each other. E.g. the results on establishing a functioning and reproducible preparation procedure of the GDEs goes somehow hand in hand with identifying how to reliably measure the ECSA in a GDE half-cell can be realized, what is presented in section 3.1 and 3.2. Insights from the variation of the catalyst loading and the effect of temperature changes at higher current densities have led to an optimized protocol for measurement of polarization curves, and is discussed in section 3.3 and 3.4. Finally, in section 3.5 and 3.6 the influence of the electrolyte concentration and GDL type could trustworthy be analyzed.

3.1. Determination of the electrochemical active surface area in the GDE setup

In RDE measurements the most common technique to determine the ECSA is to use the charge associated with hydrogen adsorption (Hydrogen underpotential deposition, H_{UPD}) or desorption (H^+-stripping) out of CVs in N_2-atmosphere. Another approach is to use CO-stripping, which is relying on the charge associated with the oxidation of a monolayer of carbon monoxide, resulting in very similar ECSA compared to proton-stripping when working on pure Pt electrocatalysts [43]. In order to check the suitability of both techniques for determination of the ECSA in GDE measurements, a comparison of the respective measurements between RDE and GDE was carried out. Fig. 2 shows the comparison of CVs recorded in N_2-atmosphere and CO-stripping voltammetry for an identical amount of catalyst on the working electrode in both RDE and GDE measurements. For this series of measurements, the catalyst was applied on the GDE without utilization of the PTFE cover described in section 2.1, in order to ensure full deposition of the catalyst on the GDL by avoiding any loss due to deposition on the PTFE cover (see also discussion of electrode preparation in section 3.2 and supporting information).

As can be seen in the CVs in nitrogen in Fig. 2 A, RDE and GDE measurements do nearly perfectly overlay in the double layer regime and in the Pt–O-regime. However, bigger differences do appear in the hydrogen regime, where an onset of faradaic current is observed in the GDE measurement. Based on the possible reactants, this is most likely the hydrogen evolution reaction (HER), nevertheless, potentials would be above the Nernst potential of 0 V vs. RHE. Reasonable explanation for this observation is most likely the enhanced removal of evolved hydrogen through the GDL and to the gaseous N_2-stream. The resulting lowering of the hydrogen partial pressure induces a positive shift of the Nernst-potential of the HER [44]. As a direct consequence in GDE-half-cell measurements the range typically associated with proton adsorption and desorption is compromised with additional faradaic HER current. For that reason, in the cathodic sweep the area associated with proton adsorption cannot be determined isolated from HER and the correct lower integration limit is difficult to identify due to the high slope of the curve. In the anodic sweep loss of adsorbed protons to the nitrogen stream on the backside of the GDL in form of gaseous hydrogen results in a comparable lower integral current. As a result, determining the ECSA with H_{UPD} or H^+-stripping in GDE measurements underestimates the ECSA. For the reference catalyst employed, the ECSA of 48 $m^2\ g_{Pt}^{-1}$ determined within the RDE is not reached and an ECSA falsified by 16.7% results from the determination with GDE. Interestingly the measurement error within the RDE is 4.97% and for the GDE with 1.58% comparable lower, demonstrating the high precision of the GDE measurements.

Employing CO-stripping voltammetry results for both RDE and GDE in very similar shape of the CO-oxidation signal, as also integral current. Interestingly, the CO-oxidation peak from GDE measurement is shifted to lower potentials compared to the RDE measurement. Most likely this is caused by the enhanced gas transport through the GDL and a lowering of the partial pressure of formed carbon dioxide due to the stream of N_2 in the gas chamber, thus shifting the Nernst potential of CO-Oxidation (identical to the effect on HER discussed above). Besides that, additionally, the higher concentrated electrolyte could trigger competing adsorption of electrolyte anions for Pt active surface sites, influencing desorption of CO. The ECSA calculated from CO-Stripping of the RDE and the GDE measurement matches within the low fitting error excellently and highly accurate and precise results can be obtained.

As a conclusion, in GDE measurements data close to 0 V vs RHE needs to be interpreted with caution as faradaic current from HER might be included and for a more accurate determination of the ECSA CO-stripping voltammetry is recommended. For the following results, always CO-stripping voltammetry was applied.

3.2. Catalyst ink formulation and catalyst layer preparation

When depositing the catalyst on the hydrophobic MPL side of the GDL, it gets directly obvious that the wetting behavior of the catalyst ink has a strong influence on the resulting catalyst layer. To optimize the wetting behavior, the ethanol percentage in the total solvent amount (volume of ethanol + water) was varied in a range of 0–100 vol.-%. Fig. 3 A shows the wetting behavior of the catalyst ink on the GDL depending on ethanol amount and Fig. 3 B highlights the resulting contact angle of catalyst ink droplets on the MPL side of Sigracet 29 BC gas diffusion media. Strong repulsion can be observed when pure water is used. Water/ethanol-mixtures with an ethanol content up to 30 vol.-

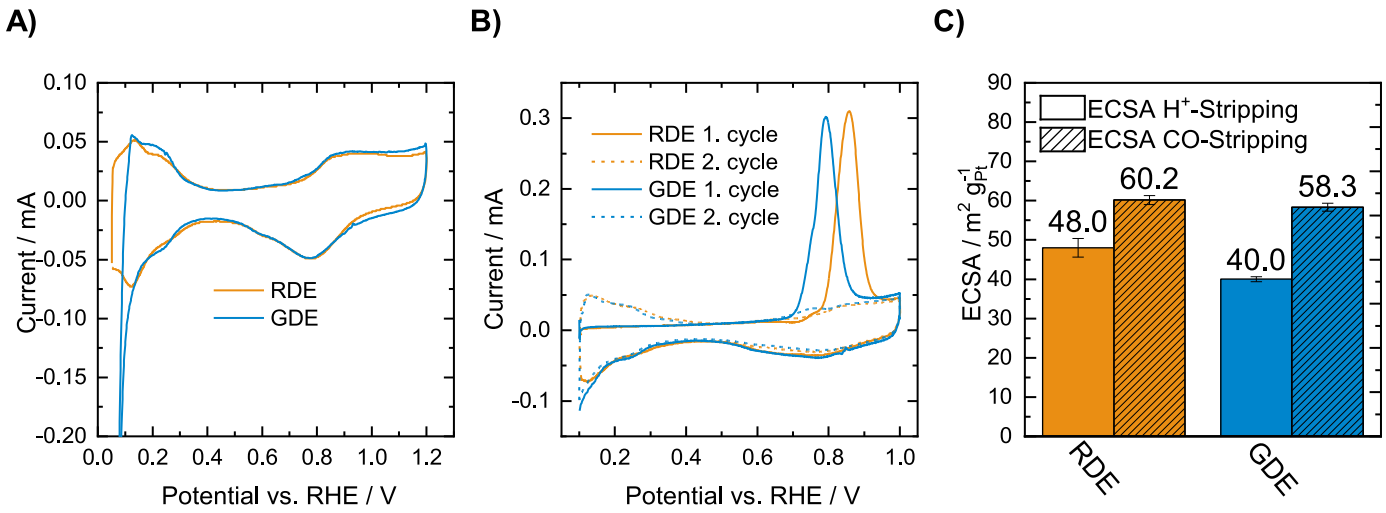

Fig. 2. Determination of the ECSA in RDE and GDE measurements at room temperature for an identical amount of catalyst applied in both techniques. RDE: 0.1 M $HClO_4$; GDE: 2 M $HClO_4$ A) Comparison of CVs in N_2-atmosphere. B) Comparison of CO-Stripping voltammetry. C) Calculated values for the ECSA.

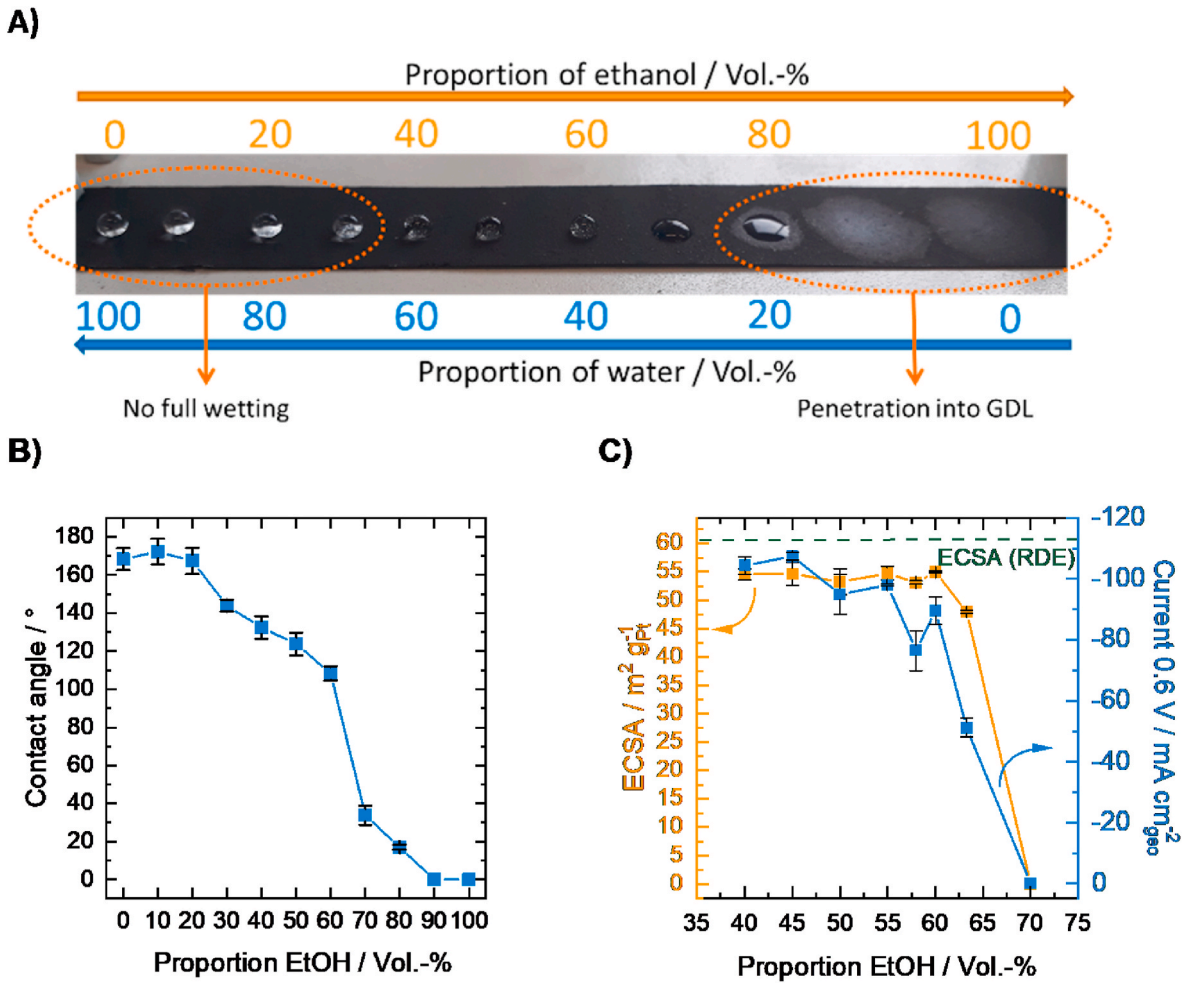

Fig. 3. Influence of the solvent composition in the catalyst ink on the wetting behavior and the resulting GDE performance. A) Wetting behavior of different water/ethanol mixtures on a Sigracet 29 BC GDL. B) Resulting contact angle of catalyst ink droplets on the MPL side of the GDL. C) ECSA and ORR current density of GDEs prepared with catalyst ink containing a varying percentage of ethanol in the water/ethanol solvent mixture; values refer to a full deposition of the target catalyst loading of 20 μg_{Pt} cm^{-2}. Catalyst: Elyst Pt50 0550, Umicore.

% do not fully wet the hydrophobic MPL side of the GDL, as can be seen from a plateau of the contact angle in this range. Starting with 80 vol.- % of ethanol the solution is clearly sucked into the pore structure of the MPL/GDL through capillary forces, as also reflected by the contact angle approaching 0°. When depositing catalyst for the very repelling solutions with 0–30 vol.-% of ethanol it can be observed by eye that very inhomogeneous layers result. Thus only, mixtures between 30 and 70 vol.-% ethanol, showing wetting of the GDL while avoiding intrusion, were studied subsequently.

To probe the influence on the accessibility of the catalyst, the ECSA was determined in the GDE setup for catalyst layers deposited with varying ethanol content and are compared in Fig. 3 C to the ECSA determined within the RDE for this catalyst. The obtained values for the ECSA are independent on the ethanol percentage in the catalyst ink solvent for values between 40 and 60 vol.-% and form a stable plateau, indicating full electrolyte contact of the deposited catalyst on these GDEs. For an ethanol percentage higher than 60%, the ECSA is dropping dramatically. Most likely the catalyst particles penetrate into the MPL/GDL pore structure, resulting in an insufficient electrolyte contact due to the hydrophobic MPL. Comparing the ECSA determined within the plateau from 40 to 60 vol.-% to the benchmark RDE measurement reveals that the maximum achieved ECSA in GDE testing is slightly lower (54.98 ± 0.09 m^2 g_{Pt}^{-1} vs. 60.16 ± 1.13 m^2 g_{Pt}^{-1}). By eye it was observed that some catalyst particles can stick to the PTFE cover, thus the lower ECSA can be attributed to some minor catalyst losses during the coating procedure due to deposition on the utilized PTFE cover. This cover is employed to fix the surface area which is coated and to be able to give geometric surface area dependent values. Due to the observed sticking of catalyst to the cover for the study in 3.1 no PTFE cover was employed and while no specific geometric surface area could be given a complete deposition was assured. Here an ECSA of 58.33 ± 1.00 m^2 g_{Pt}^{-1} results, which is within the measurement error very close to the RDE derived value.

After studying the accessibility of the catalyst, the as prepared GDEs were also analyzed regarding ORR current density at 0.6 V vs. RHE (see Fig. 3 C). The activities show a similar trend with a plateau for low ethanol contents and a strong decline at high ones. Carefully looking at the plateau reveals that for the activity it is less pronounced when compared to the ECSA. Starting with 50 vol.-% of ethanol a decreasing trend as also increasing error bars can be observed, while the highest and most stable activities result for 40 and 45 vol.-%. Therefore, an ethanol content of 45 vol.-% was employed for the subsequent experiments. The reason for the trend of ECSA and ORR activity between 50 and 60 vol.-% of ethanol remains unclear during this study. It might be that starting with 50 vol.-% the ink starts to penetrate into the structure of the MPL slightly. During CO-stripping voltammetry for ECSA determination and the resulting low currents these catalyst particles might be still accessible, while during ORR and high current densities, these particles don't contribute to activity. Fig. S4 shows the trend also at a higher potential of 0.85 V vs. RHE and thus in the kinetic regime. Here

the trend is very similar to the one obtained for the ECSA in Fig. 3 C. Therefore, we hypothesize that higher Ethanol content results in deeper penetration of the MPL structure and can change the wetting behavior. This can most likely effect the gas transport within the GDL and result in decreasing performance at higher overpotentials.

In summary, the study shows that the optimum ink solvent composition for the utilized catalyst needs to be determined through activity measurements and not only ECSA determination. Since the catalyst itself and especially the carbon support might also influence the wetting behavior of the catalyst ink, the optimum found herein might be different for another catalyst system. Furthermore, slight losses during deposition of the catalyst might occur, when employing a cover for limiting the area of deposition. Despite additional analysis of the Pt content on the resulting GDL *e.g.* through ICP or XRF measurements, the CO-stripping voltammetry could be applied with and without cover. The measurement without cover calibrates the ECSA measurement for a specific catalyst and can be validated by RDE measurements. Afterwards, in every GDL testing the ECSA determined with cover can be employed to accurately and fast determine the correct amount of Pt deposited. Subsequently, all Pt masses were corrected using this approach (also see section 2.1).

3.3. Influence of the ORR protocol on the electrolyte temperature

Prior discussing how higher Pt loadings affect the accessibility and activity (section 3.4), a major pitfall occurring at high total currents needs to be addressed, which is the heat release and a possible increase of the cell electrolyte temperature. In order to analyze the ORR protocols 6a and 6b (see Table 1) regarding a possible temperature evolution, the electrolyte temperature was monitored during the ongoing measurements by introduction of a thermocouple close to the GDE. Fig. 4 A shows for a catalyst loading of 200 μg_{Pt} cm^{-2} the temperature evolution and resulting currents during the ORR protocol 6a (see section 2.2 and Table 1), where potentials were applied and the resulting current was measured, which is typical in RDE testing. Constant potential steps and holding times of at least 10 s should guarantee stationary operation of the half-cell. The results show that a significant rise in temperature of around 14 °C is observed during application of protocol 6a. Especially the Pt reduction step carried out in oxygen atmosphere at a potential of 0.1 V prior to the activity measurement leads to a dramatic increase in cell temperature. In order to get a better understanding of how different current loads do influence the electrolyte temperature, chronopotentiometry was carried out at different current densities over a time period of 5 min in Fig. 4 B. The results show that for a preset current density of −200 mA cm_{Pt}^{-2} no significant rise in temperature and no obvious change in the measured potential can be observed. For higher current densities of −500 mA cm_{Pt}^{-2} and −1000 mA cm_{Pt}^{-2} (total current = −785 mA), the electrolyte temperature increases significantly by 4.2 and 14.0 °C. Besides that, at −1000 mA cm_{Pt}^{-2} also a significant decrease in the overpotential that is needed to reach the preset current density of 134 mV is observed, which could be a hint for an influence of temperature changes on the catalytic activity and/or the uncompensated resistance.

As a consequence, in order to minimize the electrolyte heating and its possible influence on the measured activity, especially the total time under high current should be minimized.

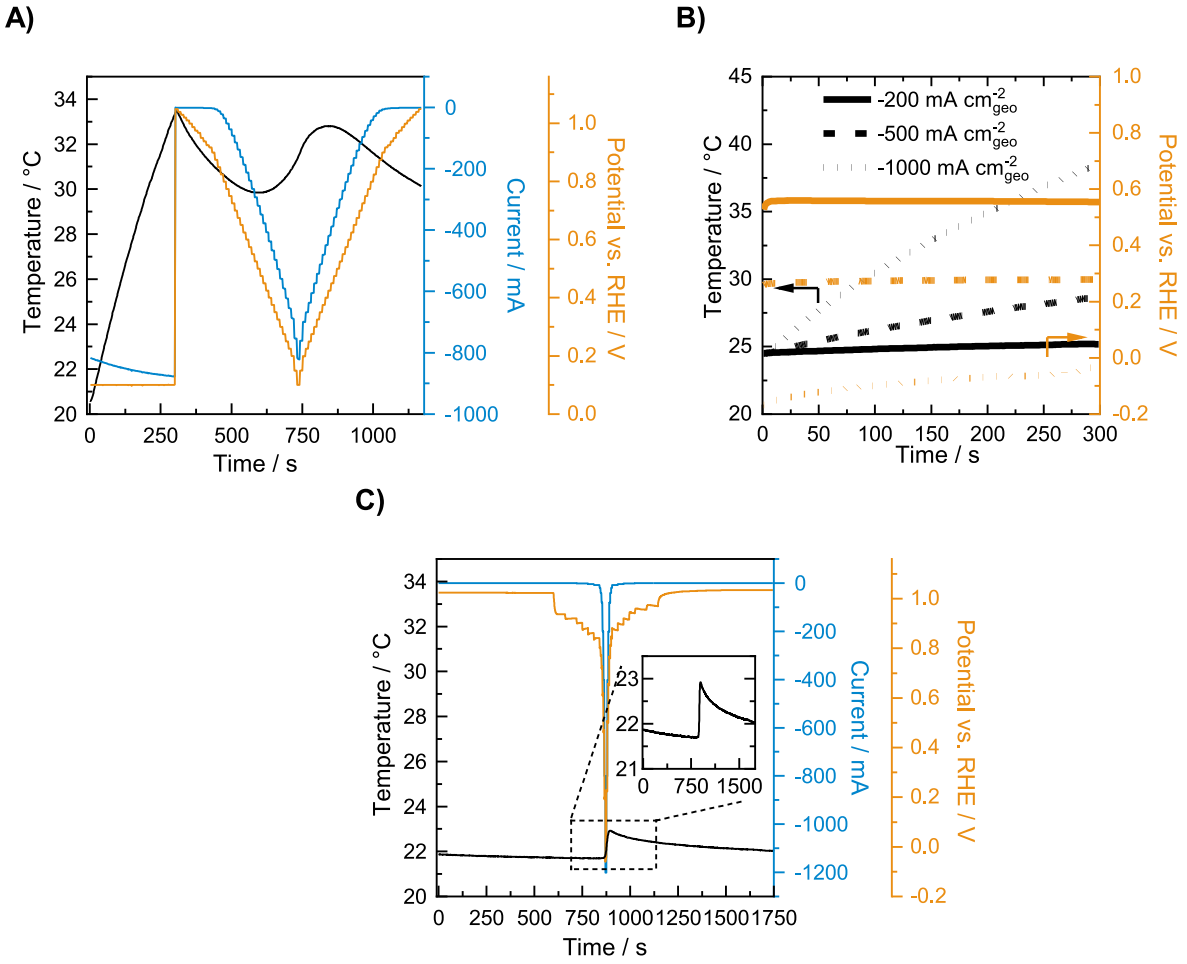

Fig. 4. Temperature evolution of the cell electrolyte during application of ORR protocol 6a (A)) and ORR protocol 6b (C)) The measurements were carried out on a GDE with a catalyst loading of 200 μg_{Pt} cm^{-2}. Graph B) shows the evolution of the electrolyte temperature and the measured potential at different current loads.

To prevent the falsification of the kinetic data due to varying electrolyte temperatures, similar to Ehelebe et al. [34], within this work a lower number of measurement points at high current densities and lower overall holding time is proposed. Furthermore, the initial Pt reduction step shall be carried out under nitrogen atmosphere to avoid heating due to the ongoing ORR reaction and, in order to ensure better comparability when comparing catalysts with different activity or different catalyst loading amounts, polarization curves should be obtained with a preset of current densities and measurement of the resulting potentials. All these best practices are realized within this study through protocol 6b described in Table 1. As given in Fig. 4 C measures with this protocol allow to limit the increase in electrolyte temperature to around 1 °C. All later shown ORR results were collected using protocol 6b.

Essential for reliable extraction of activity data out of the measurement results is to accurately correct for the *iR* drop, which shows huge impact due to the high currents reached during GDE measurements. The significance of correct iR-compensation was already stressed by Ehelebe et al. [34]. In this study, additionally, details on how the correct value for the uncompensated resistance R_U can be extracted out of impedance data is given. The Nyquist plots in Fig. S5 A indicate that the impedance curves show a semi-circuit, which is size dependent of the preset current density due to the changing charge transfer resistance and some measurement artifacts in the high frequency range. These measurement artifacts can most likely be referred to inductance of the reference electrode and should not be considered in determination of the *iR* drop. Therefore, the data was fitted by using a suited equivalent circuit model, as shown in Fig. S5 B, under exclusion of measurement points being referred to measurement artifacts. The value of "R1" in the equivalent circuit model represents the uncompensated resistance and was measured at varying current densities. Fig. S5 C shows that the value for R_U is approx. independent of the current density, even for higher currents. Thus, we can correct all of the measured potentials using the same value of R_U, without overcorrecting our data. For that reason, in difference to the measurement protocol presented by Ehelebe et al., we renounce to carry out impedance analysis at every current step, which would increase the overall measurement time, also at high current densities, and thus provoke heating of the electrolyte. Ehelebe et al. are using a higher electrode area, resulting in a much higher absolute current compared to our setup (4 A vs. 1.2 A). This could be a hint for a higher rise in temperature during the measurements presented by Ehelebe et al. and could well explain their observed decrease in *iR* drop at higher current densities.

As a conclusion, the obtained results do highlight the following demands to a robust and reliable ORR protocol for GDE measurements: 1. The Pt-reduction prior to the activity measurement should be carried out in N_2-atmosphere in order to avoid an increase in cell temperature. 2. The increase in cell temperature should be minimized by decreasing the number of measurement points and the holding time at high current densities. 3. A galvanostatic stepwise based ORR protocol should be used, since the preset of a certain potential will result in different currents for different catalytic systems and different catalyst loading, leading to bad comparability due to the influence of measured current on the cell temperature. 4. Exact iR-compensation is essential to obtain reliable kinetic data. Therefore, a critical interpretation of EIS data and using an appropriate model to extract the uncompensated resistance is required. Also a possible change of the *iR* drop at higher current densities must be considered.

3.4. Influence of thicker catalyst layers and higher mass loadings

In order to test the influence of higher platinum loadings and thus also thicker catalyst layers deposited on the GDE, the amount of platinum was varied in the range of 10–200 $\mu g_{Pt}\ cm^{-2}$ (details see supporting information). The as-prepared GDEs were thereafter analyzed regarding their ECSA and ORR performance. Fig. 5 A shows for the loading variation the recorded CV curves in N_2-atmosphere and Fig. 5 B the resulting ECSA from both H^+ - and CO-stripping. It can be seen that the measured ECSA is independent of the platinum loading in the complete range of 10–200 $\mu g_{Pt}\ cm^{-2}$. For the different catalyst loadings, values for the ECSA via CO-Stripping between 54.10 ± 1.27 $m^2\ g_{Pt}^{-1}$ and 59.13 ± 1.94 $m^2\ g_{Pt}^{-1}$ were obtained. Using equation (1) for the calculation of the real catalyst loading and assuming a value of 58.33 ± 1.00 $m^2\ g_{Pt}^{-1}$ for deposition of catalyst without PTFE mask, this results in maximum losses to the PTFE mask during coating of 7.25%. Thus, the presented coating procedure is suitable also for higher catalyst loadings and does guarantee full accessibility of the catalyst to the electrolyte even for increased catalyst layer thickness.

The polarization curves for determining the ORR performance are given in Fig. 6 A and the resulting mass specific activities are presented in Fig. 6 B. The later one indicates that the MSA is independent of the catalyst loading and that there are no mass transport limitations at the first look. In order to have closer look on the dependency of the MSA on the catalyst loading and possible transport limitations, mass specific currents at fixed potentials of 0.85 V and 0.65 V were determined by interpolation (see SI Fig. S7). At a potential of 0.85 V (corresponding to currents of max. 100 mA cm_{Pt}^{-2}), the MSA is independent of the catalyst loading, while at a potential of 0.65 V, it is decreasing with increasing loading amount. Thus, at low/intermediate overpotentials the intrinsic catalyst activity can be assessed without influence of the catalyst loading and at much higher currents and catalyst loadings compared to RDE

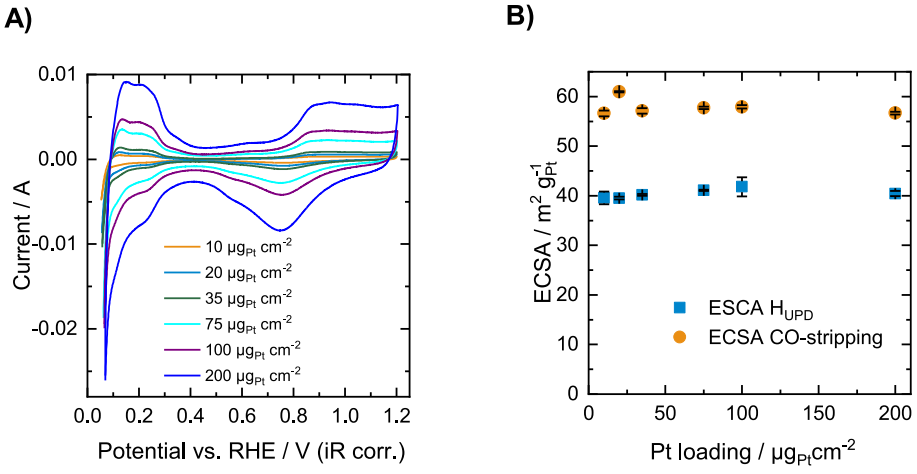

Fig. 5. Electrochemical properties of GDEs with varying catalyst loadings. A) CVs in N_2-atmosphere at 100 mV s^{-1} and B) the resulting ECSA derived from H^+- + CO-Stripping.

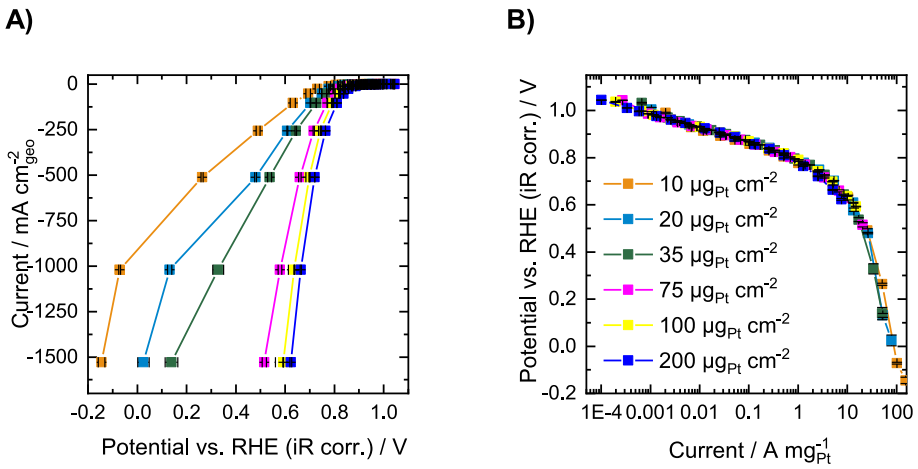

Fig. 6. A) ORR polarization curves and B) mass specific activity (MSA) in oxygen atmosphere for varying catalyst loading on the GDE measured in 2 M $HClO_4$ in O_2-atmosphere by application of protocol 6b.

measurements. However, at higher overpotentials and, thus, high reaction rates, there seem to be some transport limitations arising for higher catalyst loadings. The origin of the limitation needs to be studied in more detail in the future. The results also highlight that the applied drop casting procedure allows accurate control of the catalyst amount, while being fast and easy to apply.

As a side note in the supplementary information in Fig. S6 also the resulting activities for the catalyst loading variation are given when using protocol 6a, which induces a catalyst loading dependent temperature increase during the measurement (also see section 3.3). It becomes obvious, that the determined effective activities are falsified and the counterintuitive trend of increasing mass related activity with higher catalyst loading would result. Reason for that is the more pronounced temperature increase for higher loadings, which could be suppressed for the data presented in Fig. 6 through applying protocol 6b.

3.5. *Influence of the electrolyte concentration*

The influence of the $HClO_4$ concentration in the herein utilized setup was studied in detail in a range of 0.1–4 M for GDEs with a loading of 100 µg$_{Pt}$ cm^{-2}. Fig. 7 shows the influence of the electrolyte concentration on the CV curves in N_2-atmosphere and on the resulting ECSA derived from both H^+- and CO-Stripping voltammetry. As can be seen from the results, in the CV curves the onset of the Pt oxidation potential is slightly shifted to higher potentials, while hydrogen adsorption slightly shifts to lower potentials with increasing electrolyte concentration. Nevertheless, the overall influence on the resulting ECSA is negligible and the obtained values are on a constant level and independent of the electrolyte concentration. This highlights that no irreversible blocking of catalytic active sites by impurities and/or perchlorate anions does occur in the presented measurements. This observation, however, might change when investigating on lower loaded GDEs that might be more harmful to impurity/adsorption effects for high electrolyte concentrations.

Fig. 8 A displays the results of the ORR activity measurements. It highlights that the maximum current density can only be reached for electrolyte concentrations $\geq$ 2 M. Limiting currents were assessed through CV cycling in O_2 and synthetic air (despite nitrogen). CV curves recorded in synthetic air are given in Fig. 8 B. The observed limiting current does scale approximately linearly with increasing electrolyte concentration for 0.1–0.5 M $HClO_4$, while a further increase in concentration does enable only a smaller increase of the obtained limiting current (also see SI Fig. S8). Since similar behavior and identical limiting currents were observed in pure oxygen atmosphere (see SI Fig. S8), which should have a lowering effect on a possible diffusion limitation of oxygen reactant, as obtained in synthetic air, it can be excluded that the observed limiting current is related to limitations in oxygen transport. Briefly checking the measurement data reveals that in the plateau region the Potentiostat is displaying a Potential overload which can be related to a limitation introduced by the compliance voltage. Therefore, a too

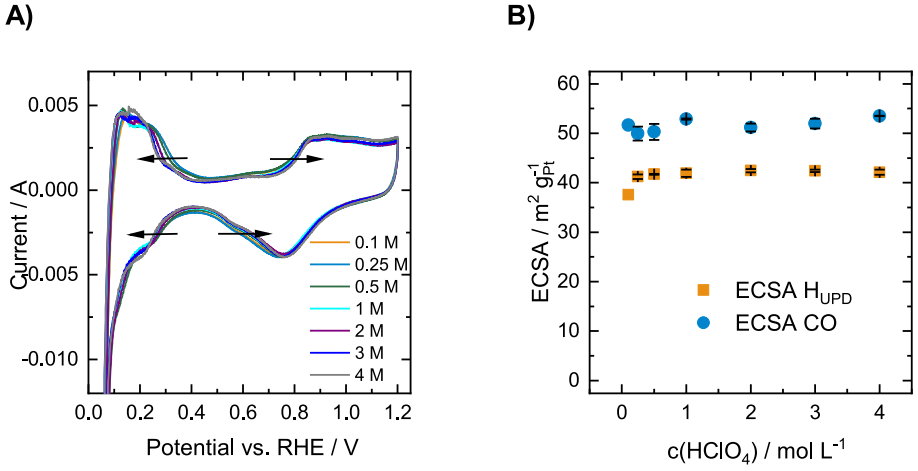

Fig. 7. Influence of the electrolyte concentration on A) CVs in N_2-atmosphere at 100 mV s^{-1} and B) the resulting ECSA (derived from H^+- + CO-Stripping) for GDEs with a loading of 100 µg$_{Pt}$ cm^{-2}.

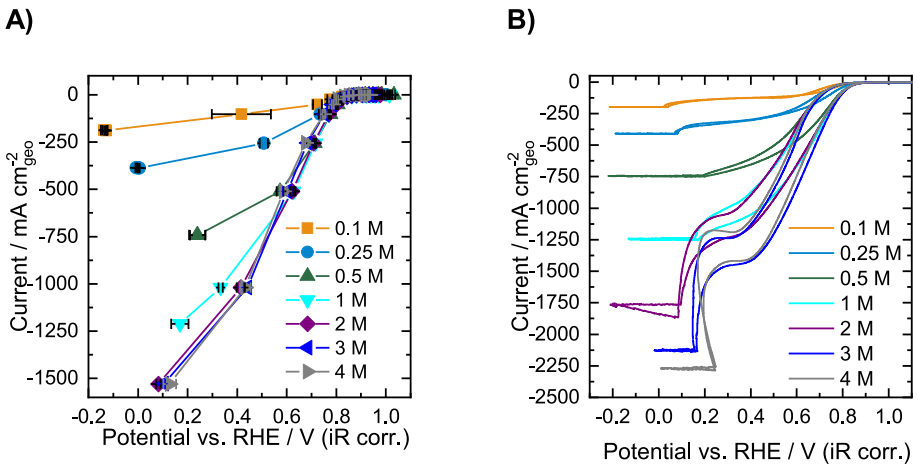

Fig. 8. Influence of the electrolyte concentration on the ORR activity measured for GDEs with a loading of 100 μg_{Pt} cm^{-2} in synthetic air. A) influence on the overall polarization curves B) Influence on CV curves in synthetic air, relating to a $HClO_4$-concentration dependent limiting current.

low electrolyte concentration can cause a limitation introduced by the specifications of the utilized Potentiostat. Details on this limitation and how to avoid it need to be clarified in future works.

For electrolyte concentrations $\geq$ 2 M the measured CV curves do point to an additional pitfall, when determining ORR activities in GDE-half-cells. As the limiting current at high electrolyte concentrations allows to reach potentials below 0.4 V vs. RHE, a plateau is observed between 0.4 and 0.2 V vs. RHE. This can be related to both ORR and HER taking place at the same time in this potential regime. The influence of the HER can also be seen when comparing anodic and cathodic sweep in the CV curves at potentials around 0.3–0.4 V vs. RHE. In the cathodic sweep adsorption of protons from the electrolyte solution does block active sites for the ORR, resulting in lower current compared to the anodic sweep. This is in accordance with the results shown by Zalitis et al. [45] and using the floating electrode technique. It highlights that for accounting only for the ORR activity of utilized catalysts in the GDE setup only potentials $\geq$ 0.4 V should be considered.

Additionally, to have a closer look on the effect of the electrolyte concentration on the ORR activity, the measured potentials at certain low and high current densities were plotted depending on the electrolyte concentration in Fig. S9. At a current density of 500 mA cm^{-2}, in both oxygen and synthetic air, the measured activity is independent of the electrolyte concentration in the shown range of 0.5–4 M. For even higher current densities of 1000 and 1500 mA cm^{-2}, when proton diffusion seems to become crucial, an increase in c($HClO_4$) allows little improvement in ORR activity. For the lowest current densities, however, one actually can recognize a reverse trend. While the measured potentials (and thus ORR activities) up to current densities of 0.5 mA cm^{-2} are independent of the electrolyte concentration in the range of 0.1–0.5 M, in both oxygen and synthetic air a further increase in electrolyte concentration results in a lowering in the measured activity. In order to exclude that this phenomenon is related to a Nernst-effect of the acid concentration on the utilized reversible hydrogen reference electrode, the open circuit potential in different electrolyte concentrations was measured while purging the gas chamber of the cell with hydrogen. Fig. S10 shows that the potential of the reference electrodes does not change with increasing c($HClO_4$) and that no Nernst-effect is taking responsible for the observation. Thus, the obtained results do highlight an additional pitfall. Although, the ECSA showed no blocking effect at high electrolyte concentration, it seems like reversible blocking of active sites by impurities and/or perchlorate ions for high perchloric acid concentrations can influence ORR activity. As a conclusion, a $HClO_4$ concentration of 2 M is proposed as optimum electrolyte concentration in the used setup with non-limiting H^+ transport at the highest current densities and less pronounced impurity/adsorption effects compared to even higher concentrations.

3.6. Influence of the GDL type

In order to check for the influence of the gas diffusion media on the resulting ORR performance, the same catalyst layers with a loading of 100 μg_{Pt} cm^{-2} were deposited on various commercial GDLs as a substrate (Freudenberg: H14C9, H14C10 and H23C8; SGL carbon: Sigracet 29 BC and Sigracet 39 BC). All of the used GDL types are having a PTFE treated microporous layer and slightly differ in their thickness and their mechanical and physical properties (see Table 2).

Fig. S11 shows the recorded polarization curves and Pt surface specific activity Tafel plots using the different types of GDLs as substrate. The data shows that no significant differences are present for potentials >0.7 V vs. RHE, indicating that the measured ORR activity is independent of the type of GDL for lower overpotentials. However, when entering the high current density regime, differences in the performance of the different GDEs become evident. The best performance is observed by utilizing the GDL Sigracet 39 BC and Freudenberg H14C9, while the GDL Freudenberg H23C8 is showing the worst performance with a potential difference of approx. 100 mV at the highest current density. Thus, in the high current density regime, where mass transport can become critical, there seem to be some performance differences regarding gas transport of the reactant to the catalytically active sites between the different GDL types and limitations caused by the GDL and not the catalyst itself can arise. For the non-limiting GDLs it seems like a maximum activity is approached. From Table 2 it is difficult to link differences in the specifications to the observed performance differences. As a summary, the choice of the GDL type does show an influence on the GDE half-cell results. With Freudenberg H14C9 and SGL 39 BC two GDEs showing similar maximum performance were identified. If within the GDE half-cell measurement the activity of the catalyst itself

Table 2
Specifications of the utilized GDL types. Values taken from Refs. [46,47].

GDL type	FB H14C9	FB H14C10	FB H23C8	SGL 29 BC	SGL 39 BC
Thickness/µm	180	170	230	235	325
Area weight/g m^{-2}	100	97	135	90	105
TP electrical resistance/ mΩ cm^{-2}	7	5	8	8.5–9.5	11–12
TP gas permeability (Gurley)/cm^3 $cm^{-2}s^{-1}$	–	–	–	0.9–1.3	1.0–1.5
TP gas permeability (Gurley)/s	30	70	90	–	–

shall be studied, a non-limiting GDE needs to be identified prior. Furthermore, the results show that the GDE half-cell measurements can be employed to study the interplay of mass transfer in the GDE and catalytic activity.

3.7. Summary: key parameters for accurate determination of ORR catalyst activity in gas diffusion electrode half-cells

Critical factors for obtaining reliable data in half-cell GDE characterization are the catalyst coating procedure, the methodology for the determination of the ECSA, the protocol and the electrochemical technique for the measurement of ORR polarization curves, the choice of the electrolyte concentration and finally, with some smaller impact, the choice of the GDL type as gas diffusion media. The catalyst coating methodology should allow control over the catalyst loading amount and the coated area. The results show that this can be guaranteed by using a simple and fast drop casting procedure. For the presented procedure, the catalyst ink solvent composition represents the decisive factor for the wetting behavior of the ink solution on the GDL and is the key to optimize the 3-phase-boundary. In order to optimize the catalyst ink composition, it is recommended to check its influence on both ECSA and ORR activity. Using the optimum found for the catalyst ink herein, it could be shown in a loading variation on the GDE between 10 and 200 μgPt cm^{-2} that the utilized drop casting procedure is a fast and easy to apply tool to produce high performing GDEs regarding the ORR activity with full accessibility to the electrolyte up to high catalyst loadings under precise control of the applied amount of catalyst. For accurate determination of the ECSA in the GDE setup we find that, in difference to H^+-stripping, CO-Stripping can avoid underestimation of the active surface area and shows great accordance with RDE measurements. Regarding the measurement of ORR polarization curves, it is of great importance to adopt the measurement protocol in order to avoid heating of the cell electrolyte during the course of the experiment. Therefore, it is crucial to limit the measurement points and the holding time at higher current densities. In general, galvanostatic steps do result in better comparability between different catalyst loadings (and thus also different catalysts) than an ORR protocol using potentiostatic control. Also, the validity of *iR* correction should be checked by measuring the value of the *iR* drop depending on current density. Important to note is that proton adsorption/HER and ORR are taking place in parallel in GDE half-cells for potentials below 0.4 V. Therefore, only potentials above this value should be considered for ORR activity determination. Another important issue is to minimize limitations of the setup on the measured ORR activity. A key factor for the measured ORR activity represents the concentration of the electrolyte. A $HClO_4$ concentration of 2 M is proposed as optimum electrolyte concentration in the presented setup which can avoid a limitation introduced by the compliance voltage and shows less pronounced impurity/adsorption effects, that affect adversely the ORR activity at small current densities, compared to higher concentrations. Finally, it is shown in the comparison of five different GDLs as gas diffusion media that at high current densities, when diffusion of the reactants to the catalyst becomes crucial, the wrong GDL type can result in transport limitations. A brief overview of the herein discussed key parameters for accurate and meaningful evaluation of ECSA and ORR activity in gas diffusion electrode half-cells is given as a workflow in Fig. S12 SI.

4. Conclusion

GDE half-cells allow the characterization of ORR catalysts in catalyst layer structures, current and potential regimes comparable to MEA tests while keeping the high speed and good comparability of half-cell experiments and represent a powerful tool to bridge between fundamental electrocatalysis using the TF-RDE technique and applied fuel cell research via MEA testing. While for RDE and MEA testing at first dedicated protocols for reliable electrode preparation and measurement of activity had to be developed for assessing trustworthy and comparable data, these were so far missing for the novel half-cell GDE testing. This work provides a detailed protocol for the half-cell GDE characterization of ORR catalysts by using a commercially available setup as well as commercial catalyst covering these issues. Explicit experimental procedures and measurement protocols are given and the impact of various experimental parameters in GDE half-cell measurements is demonstrated. Key challenges in running GDE half-cells that were identified in this work include the catalyst coating procedure (influence of the catalyst ink composition), avoiding pitfalls in measurement and comparison of activity data (falsification of ECSA using the charge associated with hydrogen adsorption or desorption and falsification of kinetic data due to heating of the electrolyte) and avoiding limitations of the setup that are influencing the measured activity (electrolyte concentration and GDL type). Our presented approach can easily be transferred to other laboratories and can be seen as the foundation stone for a broad-based application of the technique for fast and reliable characterization of ORR catalysts under application-oriented conditions. Furthermore, the work identified how different parameters can limit the maximum achievable current density and thus sets a starting point for developing the technique to higher current densities in future work.

CRediT authorship contribution statement

Nicolai Schmitt: Conceptualization, Methodology, Investigation, Visualization, Formal analysis, Writing – original draft. **Mareike Schmidt:** Investigation, Writing – review & editing. **Gerold Hübner:** Project administration, Writing – review & editing. **Bastian J.M. Etzold:** Supervision, Project administration, Funding acquisition, Writing – review & editing.

Declaration of competing interest

The authors declare that they have no known competing financial interests or personal relationships that could have appeared to influence the work reported in this paper.

Acknowledgements

This work was supported financially by the Volkswagen AG. The authors thank Sebastian Kirsch, Jonathan E. Mueller and Philipp Stehle from Volkswagen AG for the scientific discussion. The results, opinions and conclusions expressed in this publication are not necessarily those of Volkswagen Aktiengesellschaft. The authors also acknowledge the funding from the European Research Council (ERC) under the European Union's Horizon 2020 research and innovation program (grant agreement No. 681719).

Appendix A. Supplementary data

Supplementary data to this article can be found online at https://doi.org/10.1016/j.jpowsour.2022.231530.

References

[1] A. Arsalis, Renew. Sustain. Energy Rev. 105 (2019) 391–414.
[2] T. Yoshida, K. Kojima, Interface Mag. 24 (2015) 45–49, https://doi.org/10.1149/2.F03152if.
[3] D. Banham, S. Ye, ACS Energy Lett. 2 (2017) 629–638, https://doi.org/10.1021/acsenergylett.6b00644.
[4] B.G. Pollet, S.S. Kocha, I. Staffell, Curr. Opin. Electrochem. 16 (2019) 90–95, https://doi.org/10.1016/j.coelec.2019.04.021.
[5] C. Cui, L. Gan, H.-H. Li, S.-H. Yu, M. Heggen, P. Strasser, Nano Lett. 12 (2012) 5885–5889.
[6] X. Tan, S. Prabhudev, A. Kohandehghan, D. Karpuzov, G.A. Botton, D. Mitlin, ACS Catal. 5 (2015) 1513–1524.
[7] G.-R. Zhang, S. Wöllner, Appl. Catal. B Environ. 222 (2018) 26–34.
[8] X. Tian, X.F. Lu, B.Y. Xia, X.W.D. Lou, Joule 4 (2020) 45–68.

[9] Y. Li, Q. Li, H. Wang, L. Zhang, D.P. Wilkinson, J. Zhang, Electrochem. Energy Rev. 2 (2019) 518–538.
[10] R.L. Borup, A.Z. Weber, FC-PAD: Fuel Cell Performance and Durability Consortium, 2018.
[11] R.L. Borup, A. Kusoglu, K.C. Neyerlin, R. Mukundan, R.K. Ahluwalia, D.A. Cullen, K.L. More, A.Z. Weber, D.J. Myers, Curr. Opin. Electrochem. 21 (2020) 192–200.
[12] Y.-J. Wang, N. Zhao, B. Fang, H. Li, X.T. Bi, H. Wang, Chem. Rev. 115 (2015) 3433–3467.
[13] C. Chen, Y. Kang, Z. Huo, Z. Zhu, W. Huang, H.L. Xin, J.D. Snyder, D. Li, J. A. Herron, M. Mavrikakis, Science 343 (2014) 1339–1343.
[14] M. Li, Z. Zhao, T. Cheng, A. Fortunelli, C.-Y. Chen, R. Yu, Q. Zhang, L. Gu, B. V. Merinov, Z. Lin, Science 354 (2016) 1414–1419.
[15] X. Huang, Z. Zhao, L. Cao, Y. Chen, E. Zhu, Z. Lin, M. Li, A. Yan, A. Zettl, Y. M. Wang, Science 348 (2015) 1230–1234.
[16] L. Bu, N. Zhang, S. Guo, X. Zhang, J. Li, J. Yao, T. Wu, G. Lu, J.-Y. Ma, D. Su, Science 354 (2016) 1410–1414.
[17] K. Ehelebe, T. Ashraf, S. Hager, D. Seeberger, S. Thiele, S. Cherevko, Electrochem. Commun. 116 (2020), 106761.
[18] Y. Wang, J. Li, Z. Wei, J. Mater. Chem. 6 (2018) 8194–8209.
[19] L. Yang, J. Shui, L. Du, Y. Shao, J. Liu, L. Dai, Z. Hu, Adv. Mater. 31 (2019), 1804799.
[20] X. Ge, A. Sumboja, D. Wuu, T. An, B. Li, F.T. Goh, T.A. Hor, Y. Zong, Z. Liu, ACS Catal. 5 (2015) 4643–4667.
[21] C. Tang, Q. Zhang, Adv. Mater. 29 (2017), 1604103.
[22] B. Han, C.E. Carlton, A. Kongkanand, R.S. Kukreja, B.R. Theobald, L. Gan, R. O'Malley, P. Strasser, F.T. Wagner, Y. Shao-Horn, Energy Environ. Sci. 8 (2015) 258–266.
[23] I.E.L. Stephens, J. Rossmeisl, I. Chorkendorff, Science 354 (2016) 1378–1379.
[24] Y. Garsany, O.A. Baturina, K.E. Swider-Lyons, S.S. Kocha, Experimental Methods for Quantifying the Activity of Platinum Electrocatalysts for the Oxygen Reduction Reaction, ACS Publications, 2010.
[25] K. Shinozaki, J.W. Zack, S. Pylypenko, B.S. Pivovar, S.S. Kocha, J. Electrochem. Soc. 162 (2015) F1384.
[26] K. Shinozaki, J.W. Zack, R.M. Richards, B.S. Pivovar, S.S. Kocha, J. Electrochem. Soc. 162 (2015) F1144.
[27] V.R. Stamenkovic, B. Fowler, B.S. Mun, G. Wang, P.N. Ross, C.A. Lucas, N. M. Marković, Science 315 (2007) 493–497.
[28] V. Beermann, M. Gocyla, S. Kühl, E. Padgett, H. Schmies, M. Goerlin, N. Erini, M. Shviro, M. Heggen, R.E. Dunin-Borkowski, J. Am. Chem. Soc. 139 (2017) 16536–16547.
[29] A.R. Kucernak, E. Toyoda, Electrochem. Commun. 10 (2008) 1728–1731.
[30] M.K. Debe, Nature 486 (2012) 43–51.
[31] M. Inaba, A.W. Jensen, G.W. Sievers, M. Escudero-Escribano, A. Zana, M. Arenz, Energy Environ. Sci. 11 (2018) 988–994.
[32] B.A. Pinaud, A. Bonakdarpour, L. Daniel, J. Sharman, D.P. Wilkinson, J. Electrochem. Soc. 164 (2017) F321.
[33] G.W. Sievers, A.W. Jensen, V. Brüser, M. Arenz, M. Escudero-Escribano, Surfaces 2 (2019) 336–348.
[34] K. Ehelebe, D. Seeberger, M.T.Y. Paul, S. Thiele, K.J.J. Mayrhofer, S. Cherevko, J. Electrochem. Soc. 166 (2019) F1259.
[35] A. Bonakdarpour, J. Kwan, B.A. Pinaud, L. Daniel, G. Afonso, D.P. Wilkinson, ECS Transactions 80 (2017) 367.
[36] K. Shinozaki, J.W. Zack, S. Pylypenko, R.M. Richards, B.S. Pivovar, S.S. Kocha, Int. J. Hydrogen Energy 40 (2015) 16820–16830.
[37] Y. Garsany, J. Ge, J. St-Pierre, R. Rocheleau, K.E. Swider-Lyons, J. Electrochem. Soc. 161 (2014) F628.
[38] Y. Garsany, I.L. Singer, K.E. Swider-Lyons, J. Electroanal. Chem. 662 (2011) 396–406.
[39] G. Tsotridis, A. Pilenga, G. de Marco, T. Malkow, JRC Science for Policy Report 27632, 2015.
[40] V. Yarlagadda, S.E. McKinney, C.L. Keary, L. Thompson, B. Zulevi, A. Kongkanand, J. Electrochem. Soc. 164 (2017) F845.
[41] F.S.E. Center, Test Protocol for Cell Performance Tests Performed under DOE Contract# DE-FC36-06G016028. Vol. DOE# DE-FC36-06G016028, US Department of Energy, Arlington, Virginia, 2009.
[42] M.B. Sassin, Y. Garsany, B.D. Gould, K.E. Swider-Lyons, Fabrication Method for Laboratory-Scale High-Performance Membrane Electrode Assemblies for Fuel Cells, ACS Publications, 2017.
[43] D.F. van der Vliet, C. Wang, D. Li, A.P. Paulikas, J. Greeley, R.B. Rankin, D. Strmcnik, D. Tripkovic, N.M. Markovic, V.R. Stamenkovic, Angew. Chem. 124 (2012) 3193–3196.
[44] R.N. Carter, S.S. Kocha, F. Wagner, M. Fay, H.A. Gasteiger, ECS Transactions 11 (2007) 403.
[45] C. Zalitis, A. Kucernak, X. Lin, J. Sharman, ACS Catal. 10 (2020) 4361–4376.
[46] R. Schweiss, C. Meiser, T. Damjanovic, I. Galbati, N. Haak, SIGRACET® gas diffusion layers for PEM fuel cells, SIGRACET® gas diffusion layers for PEM fuel cells, electrolyzers and batteries. https://www.sglcarbon.com/loesungen/material/sigracet-brennstoffzellenkomponenten/.
[47] Freudenberg Performance Materials SE & Co. KG, Freudenberg gas diffusion layers technical data. https://fuelcellcomponents.freudenberg-pm.com/-/media/Files/fuelcellcomponents,-d-,freudenbergpm,-d-,com/FPM_technical_data_sheet_gdl_ENG_2020-08-24.pdf.

Supporting information

Oxygen Reduction Reaction Measurements on Platinum Electrocatalysts in Gas Diffusion Electrode Half-cells: Influence of Electrode Preparation, Measurement Protocols and Common Pitfalls

Nicolai Schmitt[1], Mareike Schmidt[1], Gerold Hübner[2], Bastian J.M. Etzold[1]

[1]Technische Universität Darmstadt, Ernst-Berl-Institute for Technical Chemistry and Macromolecular Science, Alarich-Weiss-Straße 8, 64287 Darmstadt

[2]Volkswagen AG, Konzernforschung, 38436, Wolfsburg, Germany

Corresponding authors: Prof. Bastian J.M. Etzold

Tel.: +49 (6151) 1629983. Fax: +49(6151) 1629982.

Email: bastian.etzold@tu-darmstadt.de

All data presented in this supporting information is available from an open access repository.

URL: https://tudatalib.ulb.tu-darmstadt.de/handle/tudatalib/2774

RDE measurements

RDE measurements were carried out on a Octostat5000 Multichannel Potentiostat by Ivium Technologies and controlled by IviumSoft software. A leak-free double-junction Ag/AgCl electrode (Aldrich) was used as reference electrode and a Pt wire (PINE) as counter electrode. All potentials shown in this work were calibrated against reversible hydrogen electrode (RHE) using hydrogen evolution-oxidation reaction on a Pt electrode. A glassy carbon rotating disk electrode (GC-RDE, 5 mm diameter, PINE) was used as working electrode. Before every measurement the RDE was cleaned by ultrasonication in ethanol, acetone and ultrapure water. In order to coat the RDE with catalyst at first a catalyst ink was prepared. Therefore, the catalyst powder was placed in an eppendorf tube together with 5 wt-% Nafion® solution and an ethanol/water-mixture as solvent. The amount of Nafion® solution was adapted to achieve an ionomer-to-carbon ratio (I/C ratio) of 0.35. The amount of solvent was chosen to achieve a Pt concentration in the catalyst ink of 0.196 mg mL^{-1}. The catalyst was finely dispersed in the solvent by ultrasonic treatment using an ultrasonic processor (Hielscher, UP200St). Afterwards 10 µL of the homogeneous catalyst ink were pipetted on the RDE to achieve a Pt loading on the electrode of 10 µg cm^{-2}. In order to ensure a uniform catalyst layer on the RDE the catalyst ink was dried under rotation at 700 rpm. The electrochemical measurements were conducted at room temperature in N_2-saturated 0.1 M $HClO_4$ solution. For determination of the electrochemically active surface area (ECSA), the catalyst was first electrochemically cleaned via potential cycling between 0.05 and 1.2 V (vs. RHE) at 500 mV s^{-1} for at least 200 cycles until the hydrogen adsorption/desorption signal was stable. Thereafter, CV curves in N_2-saturated 0.1 M HClO4 in a potential range between 0.05 and 1.2 V (vs. RHE) at 20 mV s^{-1} were measured and the charges associated with the hydrogen desorption signals were used to calculate the final ECSA, assuming 210 µC cm^{-2} for calibrating the desorption charge of a monolayer of hydrogen on a Pt surface. For determination of the ECSA via CO-Stripping, CO-gas was bubbled through the electrolyte for 10 min, followed by 45 min of bubbling with N_2 in order to remove any excess CO from the electrolyte. During this procedure, the potential was held at 0.1 V to promote CO adsorption on the catalyst surface sites. Finally, three cycles were performed between 0.1 and 1.0 V vs. RHE with a scan rate of 20 mV s^{-1}: the first one being the CO-stripping voltammetry, and the last two as baseline and to verify the absence of residual CO in the electrolyte solution. For the determination of the ECSA the charge related to CO oxidation was determined out of

the CO-Stripping peak and was then normalized using the theoretical value of 420 µC cm^{-2} for a two-electron transfer assuming the oxidation of one CO to CO2 per Pt atom.

Formulation of catalyst ink and electrode preparation

For catalyst ink preparation 4 mg of Pt/C 50 % catalyst (Elyst Pt50 0550, Umicore) were mixed together with deionized water (<1.1 µS cm^{-1}, VWR chemicals), ultrapure ethanol and ionomer (Aquivion® D98-25BS, Sigma-Aldrich) in an eppendorf tube and finely dispersed with the use of an ultrasonic processor (Hielscher, UP200St). The total volume of ethanol and water was set to a value of 4.85 mL. The ionomer/carbon ratio was held at 0.5 g g^{-1} and in standard measurements the volume percentage of ethanol in the catalyst ink was set to a value of 45 %. Before application on the GDL, the accordingly prepared ink was diluted with a water/ethanol mixture considering the respective volume percentage of ethanol. The dilution was adapted to reach a target loading of platinum on the GDL in the range of 10 to 200 μg_{Pt} cm^{-2} (see Table 1). For application of the catalyst on the gas diffusion media, a GDL piece of 30x45 mm is fixed in a self-designed mask, consisting of an alumina body and a PTFE cover that is positioned with the help of three stainless steel pins (details see Figure S1), with the MPL side facing towards the PTFE cover. The PTFE cover has a round hole of 0.785 cm^{-2} surface area, which is restricting the catalyst coated area. The assembled mask is preheated to 125 °C on a heating plate and finally, 400 µL of the respective catalyst ink dilution is pipetted into the hole of the PTFE mask and let dried. A step by step summary of the coating procedure is given in Figure S2. Important to note is that too high concentrated catalyst inks results in elevated deposition of catalyst on the PTFE cover. Therefore, catalyst loadings above 100 μg_{Pt} cm^{-2} had to be prepared by multiple application of lower concentrated catalyst inks.

Table 1:Dilution of the prepared catalyst ink for achievement of specific target loadings.

Target loading / µg cm^{-2}	V(undiluted ink) / µL	V(EtOH)	V(H_2O)
10	150	1282	1567
20	300	1215	1485
40	600	1080	1320
75	1125	844	1031
100	1500	675	825

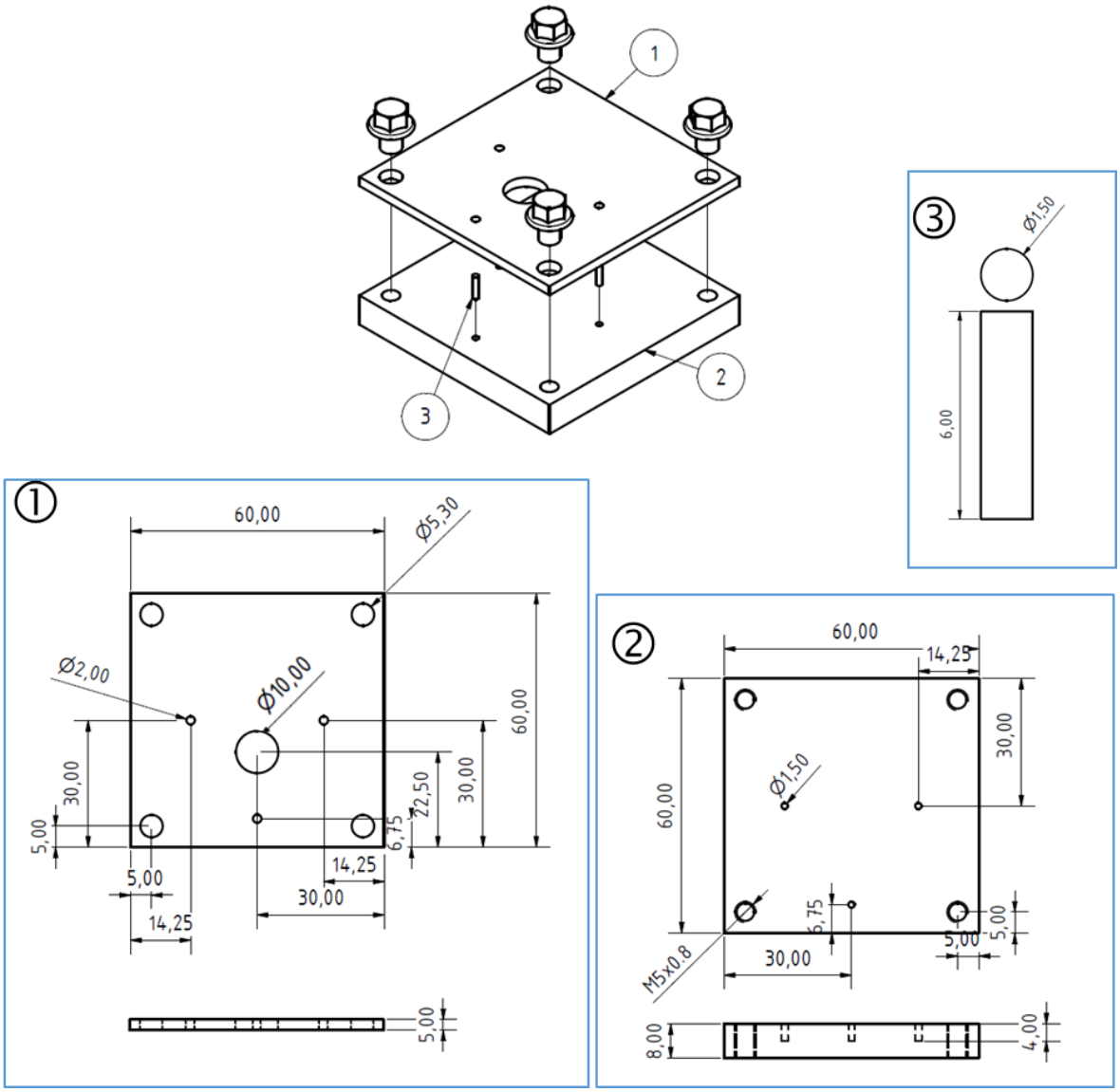

Figure S1: Technical drawing of the mask, utilized for coating of GDLs. The mask consists of a PTFE cover (1), an alumina body (2) and three stainless steel pins (3) for positioning of GDL and PTFE cover. The PTFE cover is fixed with 4 screws.

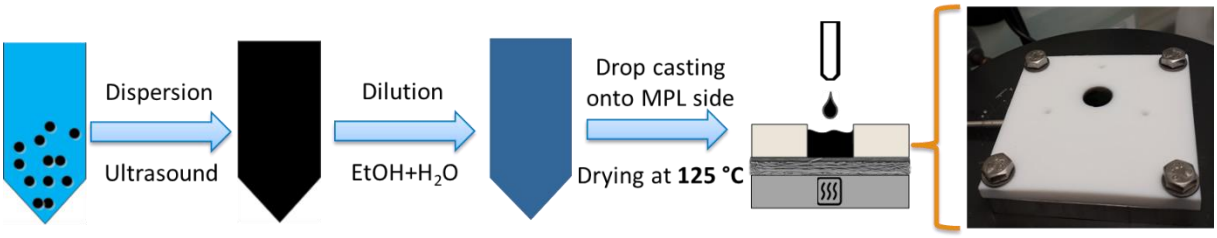

Figure S2: Step by step summary of the coating procedure. A catalyst ink is prepared and further diluted with respect to the target loading. Finally a volume of the diluted ink of 400 µL is pipetted into the opening of the mask described in Figure S1, which contains the GDL and is preheated to 125 °C on a heating plate.

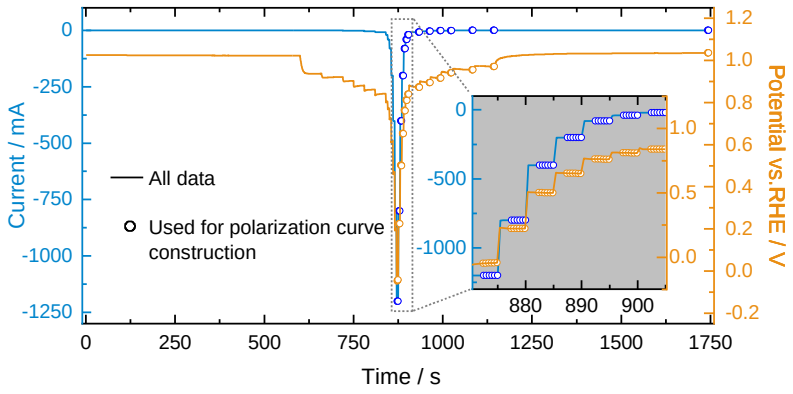

Figure S3: Highlighting of data points that are used for the construction of ORR polarization curves from the Current/Potential vs. Time plot obtained during the galvanostatic staircase protocol.

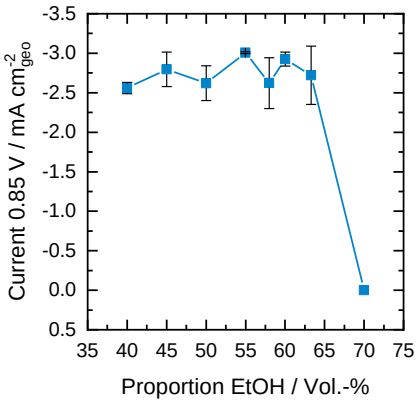

Figure S4: ORR current density at a potential of 0.85 V vs. RHE of GDEs prepared with catalyst ink containing a varying percentage of ethanol in the water/ethanol solvent mixture; values refer to a full deposition of the target catalyst loading of 20 μg_{Pt} cm^{-2}. Catalyst: Elyst Pt50 0550, Umicore.

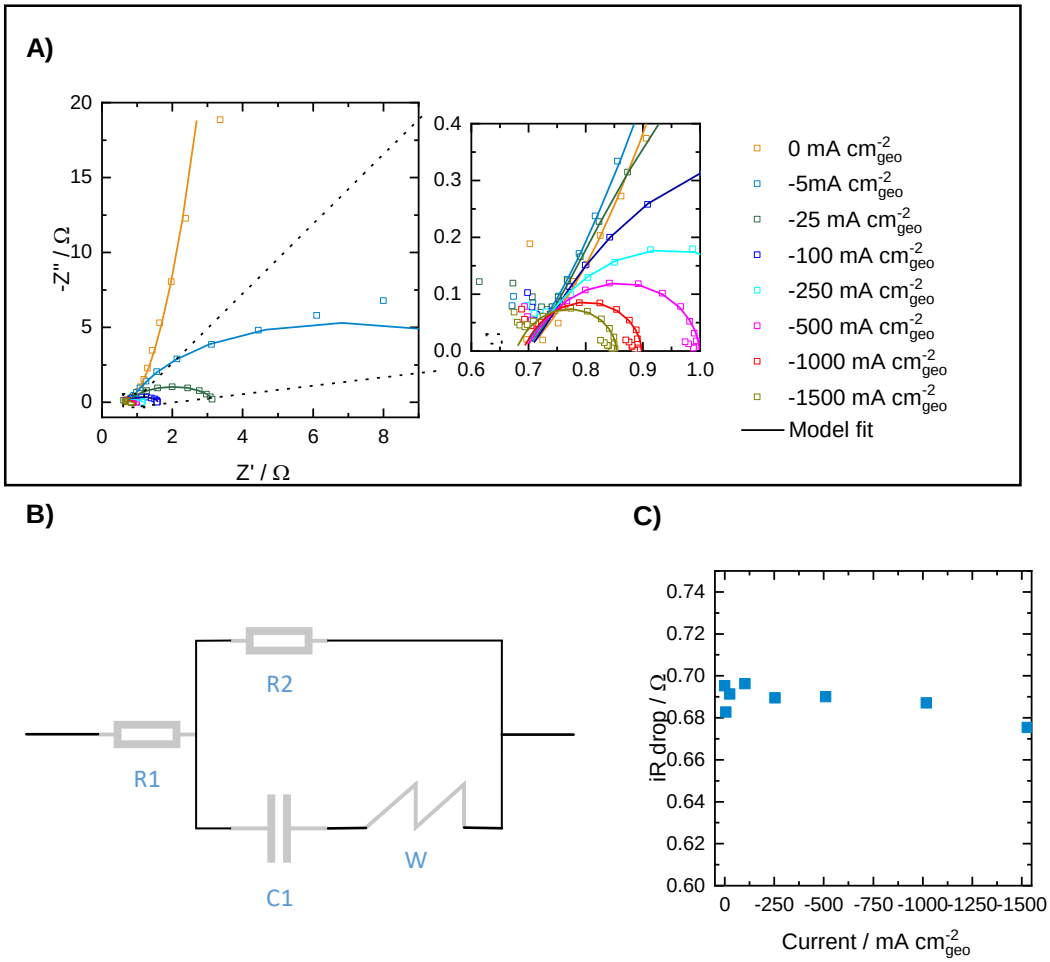

Figure S5: A) Nyquist Plots resulting from galvanostatic EIS measured at varying current density on a GDE with a catalyst loading of 100 μg_{Pt} cm^{-2} and the respective fit functions using the equivalent circuit shown in B). Data points of the inductive loop at high frequencies, stemming from the inductance of the reference electrode, are not being considered in the data fit. C) iR drop determined out of the measured impedance curve by application of the equivalent circuit shown in B).

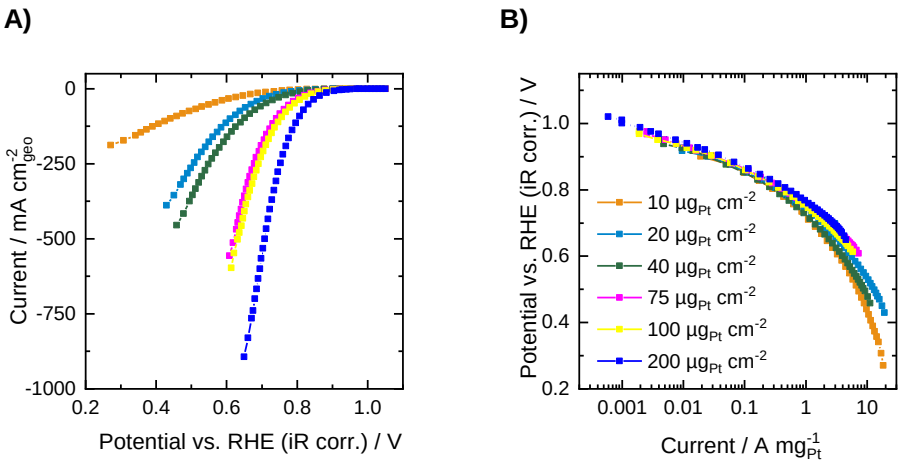

Figure S6: A) ORR polarization curves and B) mass specific activity (MSA) in oxygen atmosphere for varying catalyst loading on the GDE measured by application of protocol 6a. Higher loadings result in higher MSA for protocol 6a, highlighting falsification of kinetic data due to heating of the cell electrolyte.

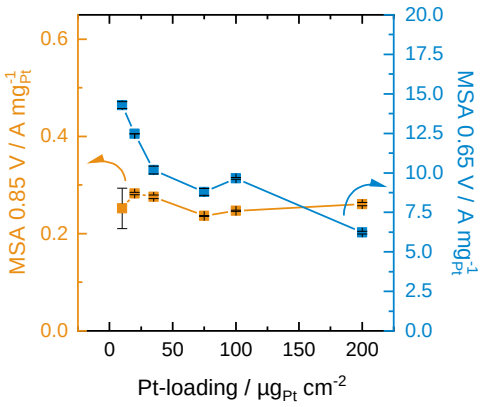

Figure S7: Mass specific ORR activity determined by interpolation out of the recorded polarization curves shown in Figure 6 in O_2-atmosphere depending on the catalyst loading.

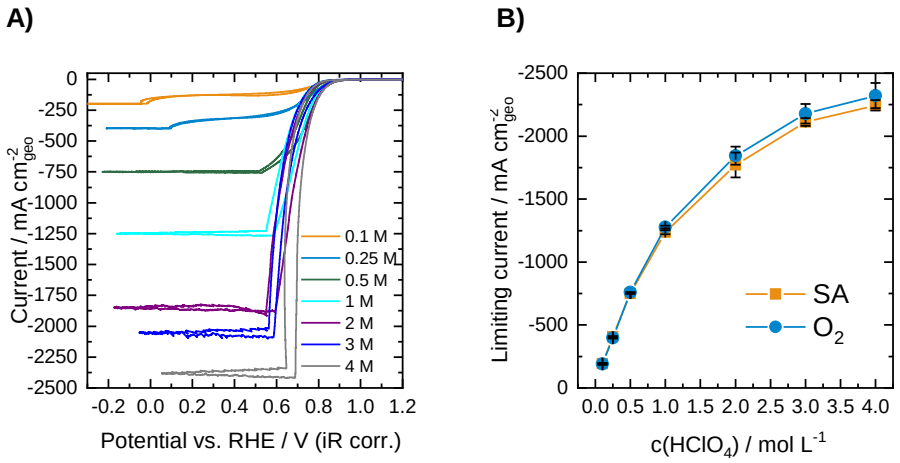

Figure S8: Influence of the electrolyte concentration on the ORR activity measured for GDEs with a loading of 100 µg$_{Pt}$ cm^{-2}. A) influence on CV curves in O_2-atmosphere. B) influence on the limiting current in O_2 and synthetic air derived from the plateau of the respective CV curves.

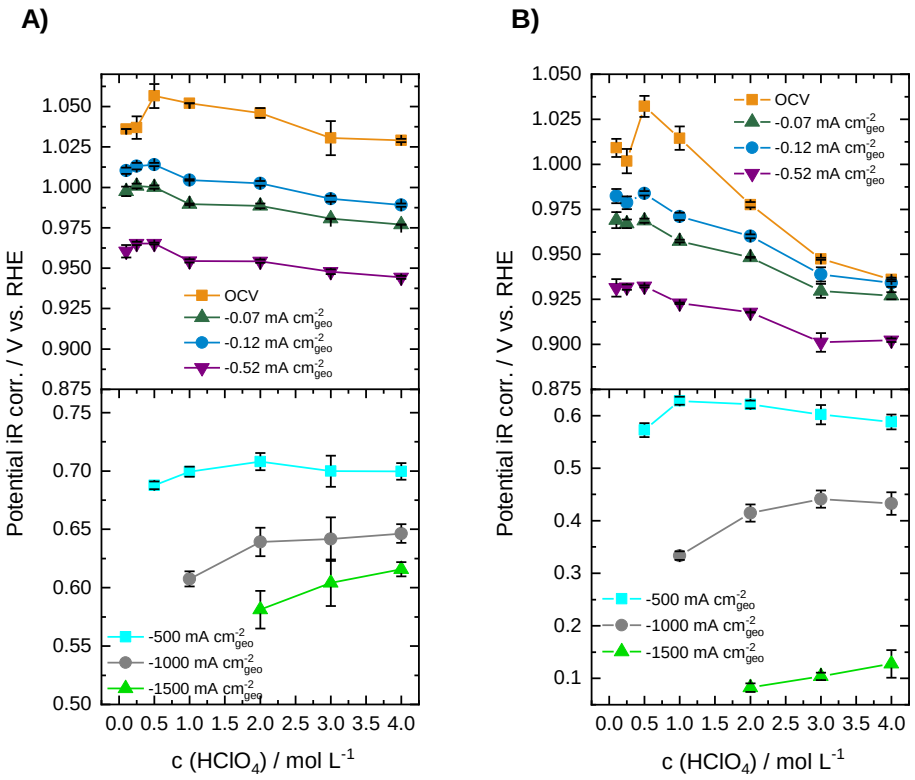

Figure S9: Influence of the electrolyte concentration on the measured potentials (relating to the ORR activity) for GDEs with a loading of 100 μg_{Pt} cm^{-2} for low and high current densities in O_2 (IA)) and synthetic air (B)). Some values are missing, because for concentrations ≤ 1 M not all of the higher current densities could be reached due to the observed limiting current.

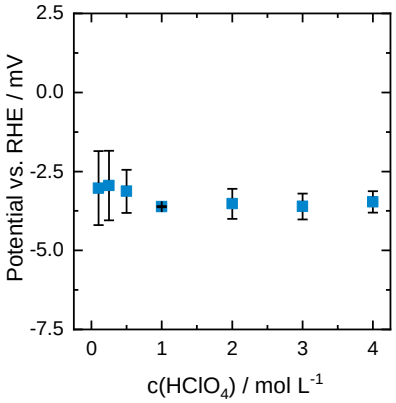

Figure S10: Influence of the electrolyte concentration on the potential of the utilized reversible hydrogen reference electrodes. For the experiment, the gas chamber with a built-in Pt/C coated GDE was purged with hydrogen and the resulting open circuit potential was monitored over a time period of 10 min. The shown potentials are mean values of three independent measurements with three different reference electrodes

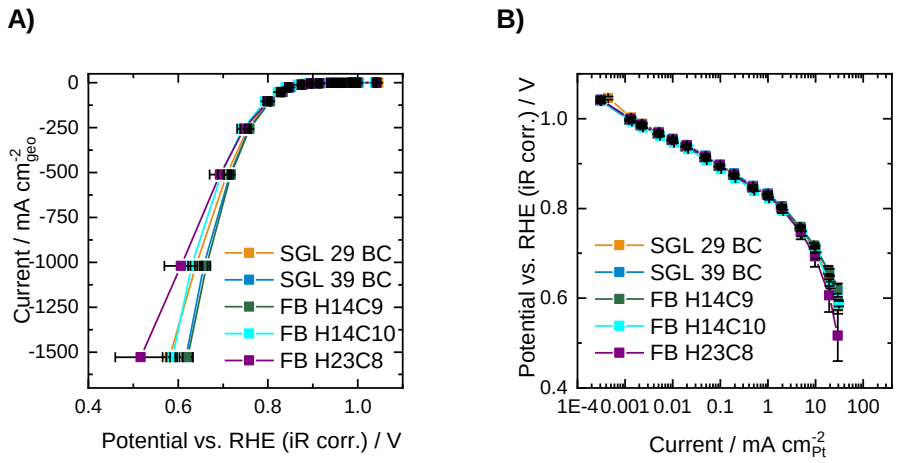

Figure S11: Influence of the GDL type on the ORR activity measured for GDEs with a loading of 100 μg_{Pt} cm^{-2} in O_2 in 2 M $HClO_4$. A) influence on the overall polarization curves B) Influence on the specific activity.

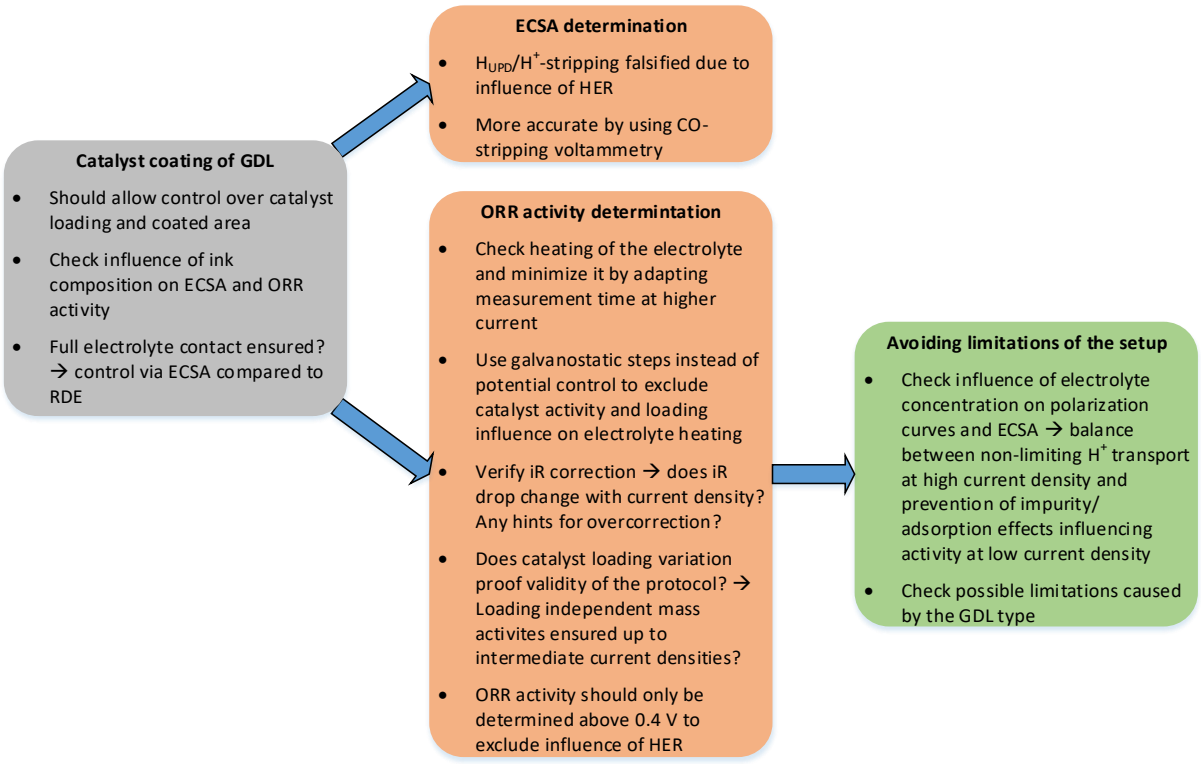

Figure S12: Workflow for accurate and meaningful evaluation of ECSA and ORR activity in gas diffusion electrode half-cells.

4.2. How to maximize geometric current density in testing of fuel cell catalysts by using gas diffusion electrode half-cell setups

Authors: Nicolai Schmitt, Mareike Schmidt, Jonathan E. Mueller, Lasse Schmidt, Bastian J.M. Etzold

Journal: Electrochemistry Communications

Publisher: Elsevier

Bibliography: Volume 141, 107362
© 2022 The Authors. Published by Elsevier B.V.

Date: August 2022

DOI: https://doi.org/10.1016/j.elecom.2022.107362

Reprinted under the terms of the Creative Commons CC-BY-NC-ND license.
https://creativecommons.org/licenses/by-nc-nd/4.0/

Electrochemistry Communications 141 (2022) 107362

Contents lists available at ScienceDirect

Electrochemistry Communications

journal homepage: www.elsevier.com/locate/elecom

How to maximize geometric current density in testing of fuel cell catalysts by using gas diffusion electrode half-cell setups

Nicolai Schmitt [a], Mareike Schmidt [a], Jonathan E. Mueller [b], Lasse Schmidt [b], Bastian J. M. Etzold [a,*]

[a] Technical University of Darmstadt, Department of Chemistry, Ernst-Berl-Institut für Technische und Makromolekulare Chemie, 64287 Darmstadt, Germany
[b] Volkswagen AG, 38436 Wolfsburg, Germany

ARTICLE INFO

Keywords:
Oxygen reduction reaction
Pt/C
Gas diffusion electrode
Compliance voltage
Setup limitations
Fuel cells

ABSTRACT

Half-cell gas diffusion electrode (GDE) setups have recently been shown to allow characterization of oxygen reduction reaction (ORR) catalysts at fuel cell relevant current densities and potentials while offering the advantage of fast screening and requiring only minimal sample usage. Most recently, publications suggesting best practices for GDE half-cell characterization have highlighted key challenges in running GDE experiments and have presented measurement protocols that allow excellent Inter-lab comparability. This step can be seen as the cornerstone for broad-based utilization of GDE half-cells. However, what is still missing, is an understanding of what limits the maximum achievable current density in GDE measurements. In this study we highlight the influence of various setup parameters (electrode area, electrolyte concentration, as well as size and position of the counter electrode) on the maximum achievable current density in an automated GDE setup. Furthermore, we present the metrics that need to be considered when adapting the electrochemical protocol for recording ORR polarization curves at higher current densities. The findings observed in this study are not limited to testing the ORR, but can be transferred to any other electrocatalytic reaction tested in a half-cell GDE at high current densities.

1. Introduction

Proton-exchange membrane fuel cells (PEMFCs), which allow the release of electrical energy from hydrogen and air, will play a key role in the transition to renewable energy [1]. Remaining challenges for widespread commercialization of PEMFCs include durability, performance at high current densities and cost. Especially, the sluggish kinetics of the oxygen reduction reaction (ORR) at the cathode, even on the commercially-used, cost-intensive and critical platinum-based electrocatalysts, result in high overpotentials, and hinder a more widespread use of PEMFCs [2,3]. Thus, optimizing the cathode catalyst layer offers great potential for improving PEMFC technology [4].

Herein, a major issue in development of new and superior ORR catalysts is that promising data obtained in fundamental rotating disk electrode (RDE) measurements has not yet been successfully transferred to technically more relevant membrane electrode assembly (MEA) measurements, corresponding to performance in a real fuel cell device [5–7].

These discrepancies in transferability are most likely due to the strongly differing reaction conditions for the ORR in these systems. On one hand, the catalyst environment in RDE testing, where a thin catalyst layer is deposited on a small area and smooth glassy carbon surface, differs substantially from the much thicker catalyst layers on larger gas permeable electrodes in MEA testing [4,8–10]. Additionally, the limited solubility of oxygen as reactant gas in the commonly used aqueous-acidic electrolytes introduces mass transport limitations at higher overpotentials and limits the maximum achievable current density to approx. 6 mA cm_{geo}^{-2} at the typical rotation rate of 1600 rpm [11,12]. Together with the need to apply the Koutecky-Levich (K-L) correction, this corresponds to a minimum potential of approximately 0.9 V or even 0.95 V where activity can be determined [13]. In contrast, current densities three orders of magnitude greater (i.e. up to 3000 mA cm_{geo}^{-2}) and potentials down to about 0.6 V are practicable in MEAs [4].

To bridge the gap in transferability of fundamental kinetic measurements in RDE testing to technologically more relevant MEA testing, different measurement setups with increased mass transport properties

* Corresponding author.
E-mail address: bastian.etzold@tu-darmstadt.de (B.J.M. Etzold).

https://doi.org/10.1016/j.elecom.2022.107362
Received 5 August 2022; Received in revised form 12 September 2022; Accepted 13 September 2022
Available online 14 September 2022
1388-2481/© 2022 The Author(s). Published by Elsevier B.V. This is an open access article under the CC BY-NC-ND license (http://creativecommons.org/licenses/by-nc-nd/4.0/).

have been introduced, including floating electrode (FE) and gas diffusion electrode (GDE) apparatuses [14–20]. Both of these techniques use different kinds of gas-permeable electrodes in half-cell setups to retain advantages of the RDE technique (e.g. fast testing, no need for complex membrane electrode fabrication tools, exact determination of the working electrode potential and isolated analysis of ORR kinetics), while avoiding the mass transport limitations of RDE measurements [21,22]. In FE measurements, a gold sputtered polycarbonate substrate with controlled pore size is coated with an ultra-thin catalyst layer and placed to float on top of the electrolyte, enabling gaseous reactants to be transported directly to the catalyst active sites and geometric current densities of up to 2800 mA cm_{geo}^{-2} to be reached [20]. GDE half-cell setups on the other hand use the same electrode substrate material as in MEA testing, namely carbon paper based gas diffusion layers with a microporous layer on top. GDE testing goes back to the end of the 1990′s [23–27], but has attracted increased interest following the introduction of setups that avoid mass transport limitations in the past several years [14–16]. Most recently, key parameters for GDE testing were identified and published along with best practices [28–30]. These publications presented key challenges for obtaining reproducible kinetic data from GDE experiments and highlighted the importance of a uniform catalyst coating and using appropriate measurement protocol. Thereby, in an Inter-lab comparison using different GDE setups ORR activity data up was reported for current densities up to 2000 mA cm_{geo}^{-2}.

Past research has successfully focused on making GDE studies reliable and reproducible, while maximizing the experimental current density. However, in order to test next generation ORR catalysts in GDE experiments the present maximum current density of 2000 mA cm_{geo}^{-2} could still be limiting and also does not cover the mass transport limited regime of MEAs. Therefore, we asked ourselves which effects limit the current densities in these studies. In order to address this question, we will elucidate the influence of several setup parameters (e.g. size and position of working and counter electrode, and properties of the utilized electrolyte) on current limitations in GDE testing. This approach will help to avoid current limitations in future GDE testing and thus help to further improve the technique.

2. Experimental

2.1. Formulation of catalyst ink and electrode preparation

For catalyst ink preparation we utilized a drop casting procedure presented in our recent publication [29] by utilization of Pt/C 50 % catalyst (Elyst Pt50 0550, Umicore), resulting in a catalyst loading of 100 μg_{Pt} cm_{geo}^{-2}. The coated area is hereby restricted by a PTFE mask, that is mounted onto an alumina body and having a round hole of varying diameter. In the present work PTFE masks resulting in catalyst coated areas of 0.196, 0.5, 0.785 cm^{-2} and 3 cm^2 were utilized. Details on ink preparation and coating are presented in the Supporting Information.

2.2. GDE testing

GDE measurements were carried out using a commercially available half-cell (FlexCell® PTFE, Gaskatel GmbH), that was utilized at room temperature using 2 M perchloric acid (ROTIPURAN®Ultra 70 %, Carl-Roth), diluted with ultrapure water, serving as the electrolyte. The GDE setup is automatically controlled by using a self-developed LabVIEW-based software application. Details on the specifications of the cell setup and on assembly of the cell are given in our recent publication [29]. Further information about the automated setup and the detailed measurement protocol is highlighted in the Supporting Information.

In order to investigate the influence of various setup parameters (e.g. size and position of working and counter electrode, and properties of the utilized electrolyte) on the maximum current we can draw from our GDE half-cell, CV cycling was carried out at a scan rate of 200 mV s^{-1} in oxygen atmosphere. These measurements aim for visualization of the current limit. Important to mention is that iR corrected data from CV curves recorded in GDE half-cells tends to be falsified (see [28] for details), wherefore in this work only polarization curves recorded using the galvanostatic protocol are corrected for the iR drop and used for ORR activity assessment.

3. Results

In our previous publication [29], we investigated the influence of the perchloric acid concentration on the resulting ORR polarization curves in our GDE half-cell setup and found a clear correlation between electrolyte concentration and maximum achievable current density (see Fig. S4). Hereby, in the maximum current regime (which is given as a plateau) the Potentiostat displayed a voltage overload, which is related to a limitation introduced by the compliance voltage. In order to provide deeper insights, in the Supporting Information we introduce the theoretical background on the compliance voltage.

As a brief summary, Eq. (1) shows the relationship between the maximum current we can draw from our cell, the compliance voltage ($V_{compliance}$) and various sources of voltage losses, that are present in our system. Herein, R_{WE} and R_{CE} indicate activation losses at WE and CE, respectively [31,32]. R_{WE-RE} and R_{RE-CE} on the other hand represent ohmic losses stemming from limited conductivity of our electrolyte and the distance separating our electrodes [33].

$$i_{driven,\ max} = \frac{V_{compliance}}{R_{WE} + R_{WE-RE} + R_{RE-CE} + R_{CE}} \quad (1)$$

3.1. How to maximize the current in GDE half-cell measurements

Based on Eq. (1), measures can be discussed to maximize the current in GDE half-cell measurements. An obvious solution is to utilize a Potentiostat with a higher compliance voltage, which is proved in Fig. S5. However, the improvement is only little and limited, wherefore we subsequently want to focus on how to minimize the various kinds of voltage losses, presented in Eq. (1) as resistances.

In order to investigate how a reduction of the activation losses at WE and CE influences the current limit, we tried to minimize R_{CE} and R_{WE} by using a CE with a higher surface area and by increasing the catalyst loading at the WE.

Fig. 1 A) shows that a decrease of R_{CE} by increasing of the area of the Pt spiral CE from 2.6 cm^2 to 8.2 cm^2 (A photograph of both electrodes is shown in Fig. S6) can shift the limitation of the maximum current density from −2750 to −3075 mA cm_{geo}^{-2}. Fig. 1 B) and C) show CV curves in oxygen atmosphere and EIS curves recorded at a potential of 0.8 V vs RHE for different catalyst loadings on the WE (the size of the CE was 8.2 cm^2 during these measurements). Although the impedance curves indicate a decrease of the size of the semicircuit with increasing catalyst loading, indicating a decreasing charge transfer resistance at the WE, no significant increase in the maximum current can be observed. Thus, the influence of the value of R_{WE} on the maximum current density is negligible.

The latter finding is of great interest, because it allows us to manipulate our system by minimizing the catalyst coated area of our GDE, resulting in similar absolute current, but much higher geometric current density. To prove this, we prepared gas diffusion electrodes while utilizing PTFE masks of different sizes during the drop casting procedure to achieve round catalyst spots on the GDE with areas of 0.196, 0.5, 0.785 and 3 cm^2. The measured CV curves for visualization of the current limit and also polarization curves using the galvanostatic protocol for ORR activity assessment are presented in Fig. S7. As awaited, the maximum achievable current is approximately independent of the coated area. As a result, minimizing the catalyst coated area to 0.196 cm^2 allows to measure current densities up to –7000 mA cm_{geo}^{-2}, before the compliance voltage is limiting. Fig. S7 also compares the polarization curves obtained using galvanostatic control. For the highest

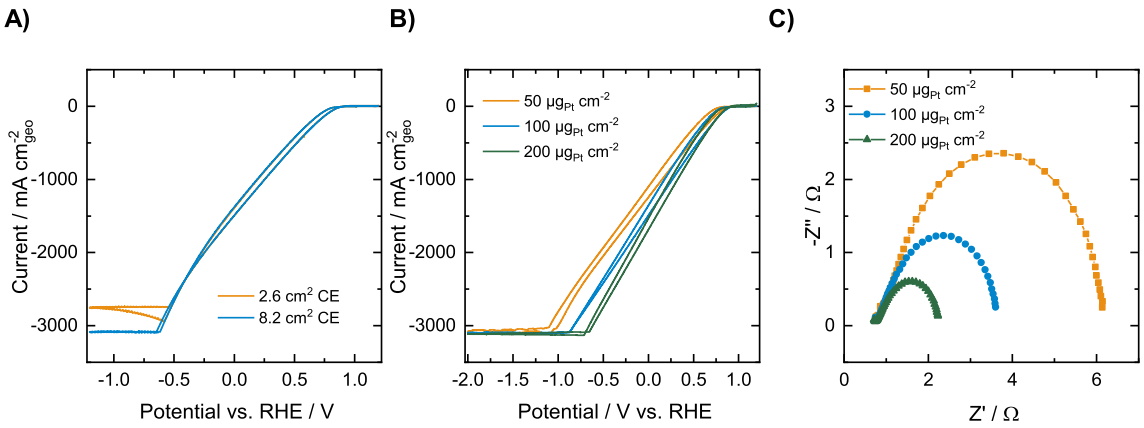

Fig. 1. A) Influence of the size of the CE on the maximum current in CV curves recorded in oxygen atmosphere. B) Influence of the catalyst loading on the WE on the maximum current in CV curves recorded in oxygen atmosphere. C) EIS curves recorded with varying catalyst loading at a potential of 0.8 V vs RHE. All measurements were carried out on GDEs with a catalyst-coated area of 0.5 cm^2 in 2 M $HClO_4$ and in a cell with the standard configuration (distance CE-RE = 6.7 cm).

electrode area of 3 cm^2 no current densities above –500 mA cm$^{-2}_{geo}$ can be reached due to the limitation caused by the compliance voltage, while for the smallest electrode area current densities up to –4000 mA cm$^{-2}_{geo}$ are measured at 0.4 V. Higher current densities are not shown for this sample using the galvanostatic protocol, because for potentials below 0.4 V vs RHE the ongoing hydrogen evolution reaction will affect the ORR measurement. These results highlight excellent overlap of the curves before the current limitation is reached for the respective catalyst coated area, indicating that the geometric current is independent of the catalyst spot size. This is underlining the suitability of decreasing the catalyst spot size for achieving higher geometric current densities.

Reduction of the ohmic losses R_{WE-RE} and R_{RE-CE} is possible by increasing the conductivity of the electrolyte and minimizing the distance separating the electrodes. The relation between electrolyte concentration and the current limit was already presented in our earlier publication [29]. In Fig. S9 we show that the increase in the current limit in higher concentrated $HClO_4$ solution is directly linked to a decreasing iR drop (identical to R_{WE-RE}). Thus, an increase of the electrolyte concentration increases the conductivity and will minimize both R_{WE-RE} and R_{RE-CE}. As further method to decrease the ohmic losses, we varied the positions of the electrodes in our GDE half-cell. Since the position of WE and RE is fixed, we therefore varied the position of the CE and brought it closer to the RE. Subsequently, the distance of CE to RE indicates the distance between CE and the tip of the Luggin capillary, which ends directly in front of the WE and connects electrolyte chamber and RE compartment.

Fig. 2 A) and B) show the influence of the position of the CE (CE size = 8.2 cm^2) on ORR polarization curves recorded using the galvanostatic protocol and on CV curves recorded in oxygen atmosphere. While for the standard galvanostatic protocol recorded up to –2500 mA cm$^{-2}_{geo}$, as expected, the distance of the CE to the RE does not influence the measured activity, but a dramatic increase of the achievable current is observed in the CV curves when bringing the CE closer to the RE. At a minimum distance of 0.2 cm between CE and RE, current densities up to –10500 mA cm$^{-2}_{geo}$ can be reached. To the best of our knowledge, this is the highest value reported for GDE experiments in the literature so far. Problematic at such close distance between RE and CE is that the CE is positioned directly in front of the WE and strong gas evolution at the CE can disturb the electric field. This also becomes obvious in the CV curve, that shows strong oscillation at the highest current densities. In order to check, which of the resistances in Eq. (1) become influenced by bringing the CE closer to the RE, we carried out impedance analysis. Therefore, we measured EIS curves one time with the Pt wire CE utilized as working electrode and the GDE as CE, and the other time vice versa. The EIS curves can be found in Fig. S8. The data clearly shows that the EIS curves with cathodic GDE as WE are not influenced by the position of the Pt wire CE and also the iR drop shows a stable value. This fulfills our expectations, since the distance between RE and WE does not change. In contrast, the EIS curves recorded with the anodic Pt wire as WE are clearly shifted to lower resistances in the high frequency regime with decreasing distance of Pt wire and RE. These curves allow us to calculate the uncompensated resistance between RE and the Pt wire CE by EIS

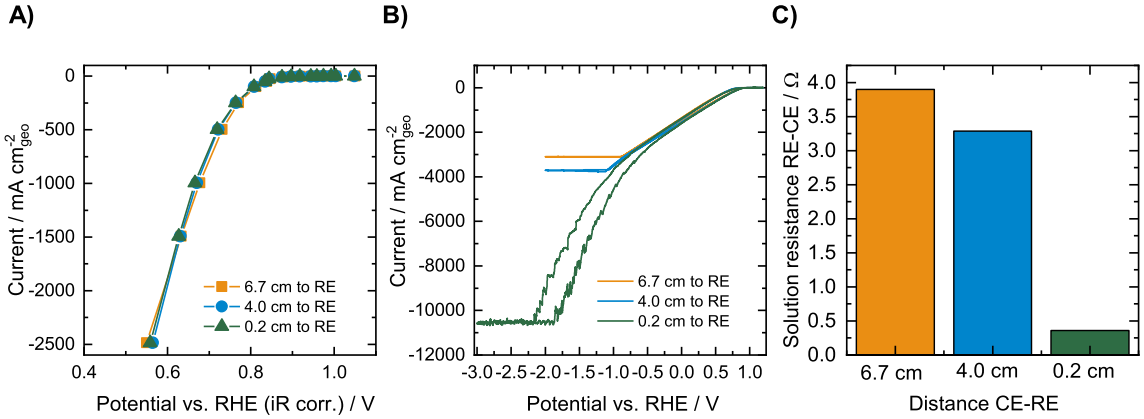

Fig. 2. A) Influence of the position of the CE on ORR polarization curves recorded in oxygen atmosphere for current densities of up to –2500 mA cm$^{-2}_{geo}$. B) Influence of the position of the CE on the maximum current in CV curves recorded in oxygen atmosphere. C) Influence of the position of the CE on the solution resistance between RE and CE. All measurements were carried out on GDEs with a Pt loading of 100 µg cm^{-2} and a catalyst coated area of 0.5 cm^2 in 2 M $HClO_4$.

fitting, what is shown in Fig. 2 C). The data clearly reveal, that bringing the Pt wire CE closer to the RE strongly minimizes the value of R_{RE-CE} and can thus increase $i_{driven,\ max}$ in Eq. (1).

3.2. Importance of iR correction technique at high current densities

Previous publications on GDE testing have already stressed the significance of iR correction at high current densities [14,28] and have proposed determining the iR drop separately at every current step via EIS. However, in our previous publication [29], we showed that carrying out EIS at every current step can lead to additional, unwanted heating of the electrolyte by prolonging the measurement time. Since an increase in the electrolyte temperature will result in a decreasing solution resistance [34], this will decrease the iR drop and therefore can falsify iR correction if not accurately controlled/measured. In order to show the correlation between the iR drop and the electrolyte temperature in our setup, we carried out impedance spectroscopy at electrolyte temperatures ranging from 25 to 60 °C. As can be seen in Fig. S10, there is a strong correlation between the temperature and the iR drop in our cell. Even a minimal increase in electrolyte temperature from 25 °C to 30 °C results in a decrease in iR drop of 0.105 Ω, corresponding to a deviation in the iR correction of 131 mV at an imaginary current density of –2500 mA cm^{-2}_{geo} for the 0.5 cm^2 catalyst spot size. Thus, to avoid erroneous iR corrections in the high current density regime, we subsequently compare different approaches for correcting the iR drop. First, we measured the temperature of the electrolyte during the course of the polarization curve measurement with and without EIS measurement at every current step for a catalyst spot size of 0.5 cm^2. Herein, the time to measure EIS data is about 5 s and thus doubles the holding time at the higher current densities. As an alternative technique for determining the iR drop, current interrupt (CI) was applied at every current step from –25 to –2500 mA cm^{-2}_{geo}. CI allows several orders of magnitude smaller measurement times with a single measurement taking only 2 ms. As a result, determination of the iR drop via CI at every current step does not lead to increased temperature evolution over the standard measurement. In contrast to that, adding EIS at every current step to the ORR protocol prolongs the measurement time and results in a significantly higher increase in electrolyte temperature of 4.3 °C in Fig. 3 A). Consequently, as highlighted in Fig. 3 B), the iR drop decreases more strongly with increasing current density utilizing EIS at every current step than it does utilizing CI. Important is, that the values obtained via CI are overall slightly higher than the values derived from EIS. This is probably the case, because CI will deliver an overall resistance including resistance of the GDL and the contact resistance [35], while EIS data fitting allows the extraction of the isolated resistance causing the iR drop. Interestingly, the difference in heating of the electrolyte is clearly reflected in the resistances determined using both techniques and follows the trend observed in the evolution of the electrolyte temperature with lower resistance in the anodic sweep (higher temperature) than in the cathodic sweep (lower temperature). Fig. 3 C) shows the resulting iR corrected polarization curves using the different techniques. As can be seen, the curve obtained with post correction using a uniform value for the iR drop measured prior to the measurement at OCV overcorrects data at high current densities. The data obtained by correcting current dependent and using CI reflects changes in the iR drop at higher currents and yields more accurate results for the iR correction in the high current density regime. Problematic here is that CI slightly overestimates the solution resistance, since it delivers an overall resistance, as discussed above. When using EIS at every current step for the iR correction, the polarization curves reveal significant differences in the corrected potentials for the two highest current densities of –1500 and –2500 mA cm^{-2}_{geo}, with a deviation of the potential of around 130 mV at –2500 mA cm^{-2}_{geo} compared with the CI corrected curve. Problematic here could be that the EIS spectra are always recorded after the current measurement and thus after the electrolyte temperature has been increased, so that the temperature where the iR drop is determined will always be slightly higher than during the chronopotentiometry (CP) step, resulting in slight underestimation of the iR drop. In order to check for the error this could introduce, we carried out the following sequence of measurements at the highest current density: EIS at –2500 mA cm^{-2}_{geo}, CP at –2500 mA cm^{-2}_{geo} (5 s) and again EIS at –2500 mA cm^{-2}_{geo}. The difference in the iR drops due to electrolyte heating between the first and the second EIS measurement was used to estimate the standard deviation of the measurement. The measured potential is shown as the red point in Fig. 3 C). It can be seen that the value is in good agreement with the previous measurement (green curve). Thus, the potential can be measured and the iR correction applied with excellent accuracy, without being biased by any preceding electrolyte heating. The difference in iR drop measured before and after the single point measurement at –2500 mA cm^{-2}_{geo} equals 0.018 Ω, resulting in a standard deviation of 13.5 mV. This confirms that the error introduced due to differences in electrolyte temperature between when the potential is measured and when the iR drop is determined, is negligible.

In summary, these results highlight that activity data obtained at very high current densities in GDE half-cells should be interpreted very careful regarding the iR correction. In particular, we have shown that

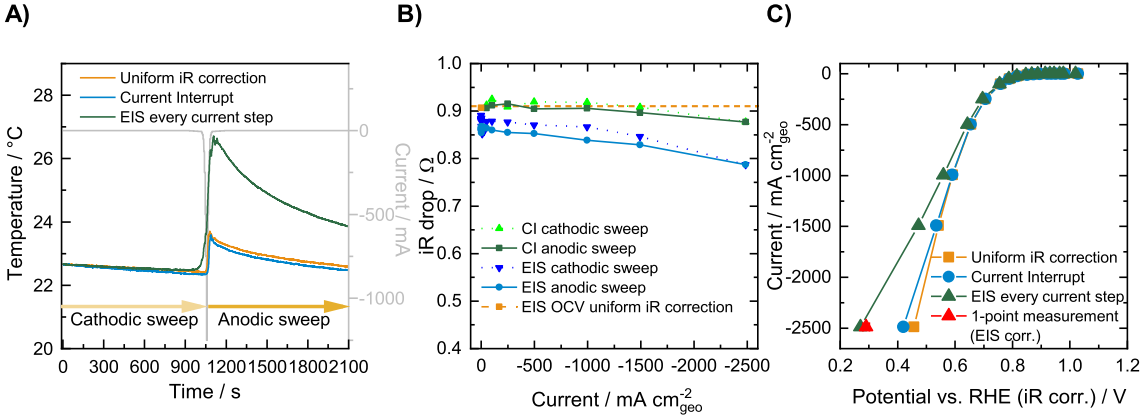

Fig. 3. Comparison of different iR-correction techniques for post-measurement processing of recorded ORR-activity data. A) Temperature evolution of the cell electrolyte during the polarization curve measurement when adding EIS and CI for post measurement determination of the iR drop. B) iR drop depending on the current density measured via EIS and CI. C) Overall polarization curves with different iR corrections. The red point shows a single point measurement, where EIS was carried out before and after the potential measurement and is used to give the standard deviation due to the temperature related change of iR drop during the measurement time of this single point. Measurements were carried out on GDEs with a Pt loading of 100 μg cm^{-2}. (For interpretation of the references to colour in this figure legend, the reader is referred to the web version of this article.)

the iR drop can be determined with the highest reliability when EIS measurements are performed at every single current step. Furthermore, the results demonstrate the high sensitivity of the solution resistance to slight temperature changes and the consequences for iR correction. Although we obtained the most accurate iR correction via EIS, excessive heating of the electrolyte should be avoided due to possible effects on catalyst layer activity, particularly when going to even higher currents than those presented here, where active control of the electrolyte temperature might be useful. Ultimately, overcorrecting the iR drop could be excluded by only carrying out EIS at every current step for high currents of interest.

4. Conclusion

This work reveals that the maximum achievable current density in the characterization of ORR catalysts in gas diffusion-electrode half-cells is primarily limited by the Potentiostats compliance voltage due to the charge transfer resistance at the counter electrode and ohmic losses related to the electrolyte solution resistance. Besides using a Potentiostat with a higher compliance voltage, measures identified in this work to achieve higher geometric current densities include minimizing the charge transfer resistance at the CE by increasing its size, and decreasing ohmic losses by decreasing the distance between CE and RE and using perchloric acid electrolyte in sufficiently high concentration. Herein, decreasing ohmic losses holds especially great potential for maximizing the current in the utilized half-cell and enabled a geometric current density of up to –10500 mA cm_{geo}^{-2} in our setup at a minimal distance of CE and RE. Since the contribution of the charge transfer resistance at the working electrode on the current limitation turned out to be negligible, another measure identified to maximize geometric current is to decrease the catalyst coated area on the gas diffusion layer. These measures allow further development of the GDE technique to perform measurements at current densities in the MEA mass transport limitation regime and thus enable reasonable comparison of GDE and MEA data at high current densities in future. The findings presented in this work on the maximization of the current density are not limited to the particular setup we utilized, but can be transferred to any gas diffusion electrode setup for other electro-catalyzed reactions.

CRediT authorship contribution statement

Nicolai Schmitt: Conceptualization, Methodology, Investigation, Visualization, Formal analysis, Writing – original draft. **Mareike Schmidt:** Investigation, Writing – review & editing. **Jonathan E. Mueller:** Project administration, Writing – review & editing. **Lasse Schmidt:** Project administration, Writing – review & editing. **Bastian J. M. Etzold:** Supervision, Project administration, Funding acquisition, Writing – review & editing.

Declaration of Competing Interest

The authors declare that they have no known competing financial interests or personal relationships that could have appeared to influence the work reported in this paper.

Data availability

The data will be published in an open access repository. The Link is given in the Supporting Information.

Acknowledgements

This work was supported financially by the Volkswagen AG. The results, opinions and conclusions expressed in this publication are not necessarily those of Volkswagen Aktiengesellschaft.

Appendix A. Supplementary material

Supplementary data to this article can be found online at https://doi.org/10.1016/j.elecom.2022.107362.

References

[1] A. Kovač, M. Paranos, D. Marciuš, Int. J. Hydrogen Energy 46 (2021) 10016–10035.
[2] A. Alaswad, A. Omran, J.R. Sodre, T. Wilberforce, G. Pignatelli, M. Dassisti, A. Baroutaji, A.G. Olabi, Energies 14 (2021) 144.
[3] Y. Wang, D.F.R. Diaz, K.S. Chen, Z. Wang, X.C. Adroher, Mater. Today 32 (2020) 178–203.
[4] M.K. Debe, Nature 486 (2012) 43–51.
[5] B. Han, C.E. Carlton, A. Kongkanand, R.S. Kukreja, B.R. Theobald, L. Gan, R. O'Malley, P. Strasser, F.T. Wagner, Y. Shao-Horn, Energy Environ. Sci. 8 (2015) 258–266.
[6] A. Ly, T. Asset, P. Atanassov, J. Power Sources 478 (2020), 228516.
[7] I.E.L. Stephens, J. Rossmeisl, I. Chorkendorff, Science 354 (2016) 1378–1379.
[8] A.R. Kucernak, E. Toyoda, Electrochem. Commun. 10 (2008) 1728–1731.
[9] K. Shinozaki, J.W. Zack, S. Pylypenko, B.S. Pivovar, S.S. Kocha, J. Electrochem. Soc. 162 (2015) F1384.
[10] K. Shinozaki, J.W. Zack, R.M. Richards, B.S. Pivovar, S.S. Kocha, J. Electrochem. Soc. 162 (2015) F1144.
[11] T.J. Schmidt, H.A. Gasteiger, G.D. Stäb, P.M. Urban, D.M. Kolb, R.J. Behm, J. Electrochem. Soc. 145 (1998) 2354–2358.
[12] H.A. Gasteiger, S.S. Kocha, B. Sompalli, F.T. Wagner, Appl. Catal. B 56 (2005) 9–35.
[13] W. Chen, Q. Xiang, T. Peng, C. Song, W. Shang, T. Deng, J. Wu, Iscience 23 (2020), 101532.
[14] K. Ehelebe, D. Seeberger, M.T.Y. Paul, S. Thiele, K.J.J. Mayrhofer, S. Cherevko, J. Electrochem. Soc. 166 (2019) F1259.
[15] M. Inaba, A.W. Jensen, G.W. Sievers, M. Escudero-Escribano, A. Zana, M. Arenz, Energy Environ. Sci. 11 (2018) 988–994.
[16] B.A. Pinaud, A. Bonakdarpour, L. Daniel, J. Sharman, D.P. Wilkinson, J. Electrochem. Soc. 164 (2017) F321.
[17] G.K.H. Wiberg, M. Fleige, M. Arenz, Rev. Sci. Instrum. 86 (2015) 24102.
[18] C. Zalitis, A. Kucernak, X. Lin, J. Sharman, ACS Catal. 10 (2020) 4361–4376.
[19] C.M. Zalitis, D. Kramer, A.R. Kucernak, PCCP 15 (2013) 4329–4340.
[20] A. Hrnjić, F. Ruiz-Zepeda, M. Gaberšček, M. Bele, L. Suhadolnik, N. Hodnik, P. Jovanovič, J. Electrochem. Soc. 167 (2020), 166501.
[21] S. Martens, L. Asen, G. Ercolano, F. Dionigi, C. Zalitis, A. Hawkins, A.M. Bonastre, L. Seidl, A.C. Knoll, J. Sharman, J. Power Sources 392 (2018) 274–284.
[22] R.L. Jalan, B.F. Gomes, T. Kottakat, C. Roth, Journal of Physics: Materials 4 (2021) 44004.
[23] O. Antoine, Y. Bultel, R. Durand, P. Ozil, Electrochim. Acta 43 (1998) 3681–3691.
[24] Y.-X. Chen, M.-F. Li, L.-W. Liao, J. Xu, S. Ye, Electrochem. Commun. 11 (2009) 1434–1436.
[25] L. Giorgi, E. Antolini, A. Pozio, E. Passalacqua, Electrochim. Acta 43 (1998) 3675–3680.
[26] N. Jia, R.B. Martin, Z. Qi, M.C. Lefebvre, P.G. Pickup, Electrochim. Acta 46 (2001) 2863–2869.
[27] T. Navessin, S. Holdcroft, Q. Wang, D. Song, Z. Liu, M. Eikerling, J. Horsfall, K. V. Lovell, J. Electroanal. Chem. 567 (2004) 111–122.
[28] K. Ehelebe, N. Schmitt, G. Sievers, A.W. Jensen, A. Hrnjić, P. Collantes Jiménez, P. Kaiser, M. Geuß, Y.-P. Ku, P. Jovanovič, ACS Energy Lett. 7 (2022) 816–826.
[29] N. Schmitt, M. Schmidt, G. Hübner, B.J.M. Etzold, J. Power Sources 539 (2022), 231530.
[30] S. Nösberger, J. Du, J. Quinson, E. Berner, A. Zana, G.K.H. Wiberg, M. Arenz, Electrochem. Sci. Adv. (2021), e2100190.
[31] L. Liao, J. Zhu, X. Bian, L. Zhu, M.D. Scanlon, H.H. Girault, B. Liu, Adv. Funct. Mater. 23 (2013) 5326–5333.
[32] A.W. Colburn, K.J. Levey, D. O'Hare, J.V. Macpherson, PCCP 23 (2021) 8100–8117.
[33] J.C. Myland, K.B. Oldham, Anal. Chem. 72 (2000) 3972–3980.
[34] L.H. Brickwedde, J. Res. Natl. Inst. Stan 42 (1949) 309–329.
[35] F. Barbir, H. Xu, H. Gorgun, Meet. Abstr. MA2005-01 (2006) 1522. https://doi.org/10.1149/ma2005-01/41/1522.

Supporting information

How to maximize geometric current density in testing of fuel cell catalysts by using gas diffusion electrode half-cell setups

Nicolai Schmitt[1], Mareike Schmidt[1], Jonathan E. Mueller[2], Lasse Schmidt[2], Bastian J.M. Etzold[1,]*

[1]Technische Universität Darmstadt, Ernst-Berl-Institute for Technical Chemistry and Macromolecular Science, Alarich-Weiss-Straße 8, 64287 Darmstadt

[2]Volkswagen AG, 38436 Wolfsburg, Germany

[*]Corresponding author: Prof. Bastian J.M. Etzold

Tel.: +49 (6151) 1629983. Fax: +49(6151) 1629982.

Email: bastian.etzold@tu-darmstadt.de

All data presented in the main article and in the supporting information is available from an open access repository:

DOIs:

Figure 1: https://doi.org/10.48328/tudatalib-944

Figure 2: https://doi.org/10.48328/tudatalib-945

Figure 3: https://doi.org/10.48328/tudatalib-946

Figure S4: https://doi.org/10.48328/tudatalib-947

Figure S5: https://doi.org/10.48328/tudatalib-948

Figure S7: https://doi.org/10.48328/tudatalib-949

Figure S8: https://doi.org/10.48328/tudatalib-950

Figure S9: https://doi.org/10.48328/tudatalib-951

Figure S10: https://doi.org/10.48328/tudatalib-952

How the compliance voltage is limiting the maximum achievable current in GDE half-cell measurements

In order to understand the origin of the limitation introduced by the compliance voltage, a basic understanding of the measurement principle of a Potentiostat is required, which will be provided below. The GDE half-cell in this work and in general most electrochemical cell setups are operated in three electrode configuration. Herein, current flows between counter electrode (CE) and working electrode (WE), while the potential difference is measured between the reference electrode (RE) and the sense electrode (SE), which is directly connected to the WE. Operation of the Potentiostat is possible in *potentiostatic mode* and in *galvanostatic mode*. In potentiostatic mode, the voltage between CE and WE is accurately controlled to achieve a certain potential difference between WE and RE, which is specified beforehand by the user. In galvanostatic mode, the user defines a current, which is then controlled between CE and WE. In both modes the potential difference between RE and WE and the current flowing between CE and WE are monitored throughout the experiment. In order to force current to flow through the electrochemical cell, the CE must be connected to the output of an electronic source, which is called Control Amplifier (CA). The voltage applied by the CA to the CE is equal to the potential difference between CE and WE, mentioned before, and is usually not measured during Potentiostat operation. This voltage is limited to a maximum value due to the compliance voltage of the instrument [1].

In order to introduce how the compliance voltage is limiting the maximum achievable current in GDE half-cell measurements, a general scheme introducing resistive elements that cause voltage losses in a 3-electrode setup is shown in Figure S1.

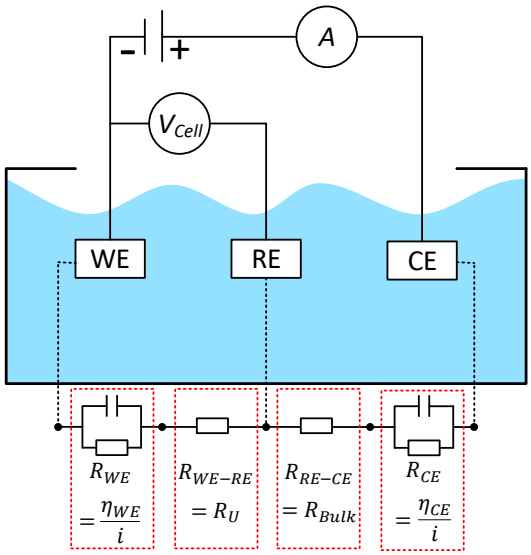

Figure S1: Resistive elements in the 3-electrode setup and resulting voltage losses.

Resistive elements in a 3-electrode cell can generally be distinguished in faradaic and ohmic resistances. Faradaic resistances (R_{WE} and R_{CE}) , which occur at both working and counter electrode, describe voltage losses at the electrode/electrolyte interface and are linked to the electrode kinetics. In our GDE half-cell, a catalyst coated gas diffusion layer (GDE) acts as WE and catalyzes the oxygen reduction reaction (ORR), that consumes electrons. These electrons have to be provided by the counter reaction at the Pt wire CE, which is the oxygen evolution reaction (OER). The standard potential of both reactions E_{Eq} is 1.23 V at standard conditions [2]. In order to draw a certain current density j from the electrochemical cell, following the Butler-Volmer equation [3] (Equation 1) negative overpotentials η (E<1.23 V) must be applied at the WE and positive overpotentials (E>1.23 V) must be applied at the CE. Thus, kinetic voltage losses at both electrodes contribute to a limitation of the maximum current density.

$$j = j_0 \cdot \left\{ exp\left[\frac{\alpha_{a,i} z F \eta_i}{RT}\right] - exp\left[\frac{\alpha_{c,i} z F \eta_i}{RT}\right] \right\} \qquad with\ \eta = E - E_{Eq};\ i = \mathrm{WE/CE} \qquad \text{Equation 1}$$

Ohmic losses ($R_{\mathrm{WE-RE}}$ and $R_{\mathrm{RE-CE}}$) are mainly linked to the solution resistance of the cell. While the value of $R_{\mathrm{RE-CE}}$, also known as the bulk solution resistance is usually not considered in electrochemical measurements, $R_{\mathrm{WE-RE}}$ describes the uncompensated resistance between working and reference electrode and is essential to be known and to be compensated during electrochemical evaluation.

Being aware of the different sources of voltage losses allows to link these to the maximum achievable current of our cell. The relation between the voltage difference between CE and WE (V_{total}) and the

cell current (i_{driven}) is given in Equation 2 and shows that a higher V_{total} results in a higher current flowing. Thus, the maximum current of the cell is achieved if V_{total} equals the compliance voltage ($V_{\mathrm{compliance}}$, see Equation 3).

$$V_{\mathrm{total}} = i_{\mathrm{driven}} \cdot R_{\mathrm{total}} = i_{\mathrm{driven}} \cdot (R_{\mathrm{WE}} + R_{\mathrm{WE-RE}} + R_{\mathrm{RE-CE}} + R_{\mathrm{CE}}) \quad \text{Equation 2}$$

$$i_{\mathrm{driven,max}} = \frac{V_{\mathrm{compliance}}}{R_{\mathrm{WE}} + R_{\mathrm{WE-RE}} + R_{\mathrm{RE-CE}} + R_{\mathrm{CE}}} \quad \text{Equation 3}$$

Experimental

Formulation of catalyst ink and electrode preparation

For catalyst ink preparation 4 mg of Pt/C 50 % catalyst (Elyst Pt50 0550, Umicore) were mixed together with deionized water (<1.1 µS cm^{-1}, VWR chemicals), ultrapure ethanol and ionomer (Aquivion® D98-25BS, Sigma-Aldrich) in an Eppendorf tube and finely dispersed with the use of an ultrasonic processor (Hielscher, UP200St). The total volume of ethanol and water was set to a value of 4.85 mL. The ionomer/carbon ratio was held at 0.5 g g^{-1} and the volume percentage of ethanol in the catalyst ink was set to a value of 45 %. For application of the catalyst on the GDL the prepared catalyst ink was further diluted and, finally, a volume of the resulting catalyst ink corresponding to a theoretical loading of 100 μg_{Pt} cm^{-2} was pipetted onto the GDL (Freudenberg H14C9), which is fixed in an alumina body preheated to 125 °C on a heating plate. The coated area is restricted by a PTFE mask, that is mounted onto the alumina body and having a round hole of varying diameter. In the present work PTFE masks resulting in catalyst coated areas of 0.196, 0.5, 0.785 cm^{-2} and 3 cm^2 were utilized.

Automated GDE half-cell setup for the electrochemical characterization

Inspired by the work of Topalov et al. [4], the GDE setup utilized in this study is automatically controlled with the use of magnetic valves and mass flow controllers, that are all controlled simultaneously (including the Potentiostat) by using a single self-developed LabVIEW-based software application. This not only allows us to save human resources by eliminating the need of user interaction throughout the entire experimental sequence, but can also increase the reproducibility of the execution of identical repeating experiments compared with manual execution and the danger of human errors and differences in time handling that accompany it.

As the measurement cell, a commercially available half-cell (FlexCell® PTFE, Gaskatel GmbH) was utilized at room temperature using 2 M perchloric acid (ROTIPURAN®Ultra 70 %, Carl-Roth), that was diluted with ultrapure water, serving as the electrolyte. Details on the specifications of the cell setup and on assembly of the cell are given in our recent publication [5]. A scheme of the cell is shown in Figure S2 and Figure S3.

The experimental setup controlled in LabVIEW can be divided into two major components: the Potentiostat and the gas system. An Ivium Octostat 5000 Potentiostat was used that is connected via ethernet; the control of the Potentiostat functionality and the data acquisition was performed using the Ivium remdriver labview interfacing. The in-house-built gas system contained commercial mass flow controllers for control of the gas flow rates (EL-Flow Select, Bronkhorst) and magnetic valves (type 6011, Bürkert) for selection of the gases. The control of the magnetic valves was performed using a digital module (NI-9476, National Instruments), that is mounted into a DAQ chassis with USB connection (cDAQ-9174, National Instruments). The two mass flow controllers for gas and electrolyte chamber, respectively, are connected via a FlowBUS network and accessible over a RS-232 converter unit. A schematic representation of the hardware components and their interface is given in Figure S2.

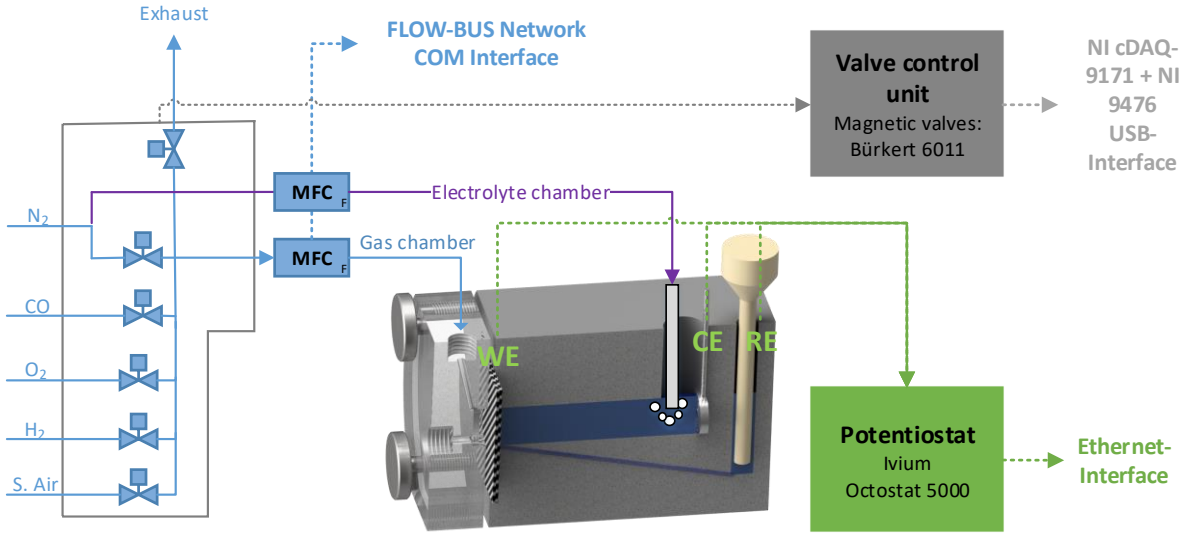

Figure S2: Schematic representations of the hardware components in the automated GDE half-cell setup and their communication interface.

The electrolyte can be purged with N_2, while the gas compartment can individually be purged with either N_2, O_2 (99.999 %, Air Liquide), CO (99.999 %, Air Liquide), H_2 (99.999 %, Air Liquide) or synthetic air (20.5 % O_2 in N_2, Air Liquide). Additionally, the gas line for the gas chamber contains a magnetic valve for venting during changes of the selected gas to avoid contamination. For monitoring of the electrolyte temperature during the ongoing measurements, a type K thermocouple was introduced through the cover of the electrolyte chamber close to the working electrode and the temperature profile was recorded by using a data logger (TC08, picolog Technology). Additionally, for temperature dependent measurements, the electrolyte was heated by using PTC heating elements. For control of the temperature, the suppliers PTC heating elements delivered with the half-cell were adapted to 240 V input voltage and controlled with a JULABO LC5-E temperature controller.

Electrochemical characterization using the GDE half-cell

The electrochemical active surface area (ECSA) was determined by integrating the hydrogen desorption area (H_{UPD}) of the CVs in N_2-atmosphere at a scan rate 100 mV s^{-1}, carried out after 200 activation cycles between 0.05 and 1.2 V vs. RHE at 500 mV s^{-1}. Additionally, CO-Stripping was carried out at a scan rate of 20 mV s^{-1} for determination of the ECSA. For ORR activity evaluation a galvanostatic step protocol is utilized, which was given in our recent publication [5] and is summarized in Table S1 in the supporting information. For constructing the ORR polarization curves, the last 3 s of each current step were used, considering only the anodic sweep. The uncompensated resistance (iR drop) in the utilized GDE setup was determined using electrochemical impedance spectroscopy (EIS) and was used for post-correction of all measured potentials. For each experiment at least two samples have been tested. Additionally, current interrupt was utilized as alternative iR correction technique by using a Current Interrupt module 5A from Ivium technologies. Therefore, the current was held at the desired value where the iR drop should be measured and was then interrupt for an interval of 1 ms with a step time of 0.01 ms while recording the resulting voltage. The cell resistance was calculated from the difference between the cell voltage before and after the current interrupt, divided by the current. During the course of the measurement, the electrolyte chamber is constantly purged with 50 mL min^{-1} N_2, while the gas flow to the gas chamber is adapted for the respective method. Additionally, CV cycling was carried out at a scan rate of 200 mV s^{-1} in oxygen atmosphere, to identify limiting currents.

Table S1: Protocol for the electrochemical characterization.

	Step	Method	Parameter	
1	Determination of iR drop	EIS galvanostatic	Gas flow	N_2 (~300 mL min^{-1})
			EIS frequency range	10000-1 Hz
			EIS amplitude	0.05 A
			Current	0 mA
2	Electrochemical cleaning	Cyclic voltammetry (CV)	Gas flow	N_2 (~300 mL min^{-1})
			Potential limits	0.05 – 1.2 V
			Scan rate	500 mV s^{-1}
			Number of cycles	~200 (until CV constant)
3	ECSA (N_2)	CV	Gas flow	N_2 (~300 mL min^{-1})
			Potential limits	0.05 – 1.2 V
			Scan rate	100 mV s^{-1}
			Number of cycles	3
4	Formation of CO-monolayer	Chronoamperometry (CA)	Gas flow	First 2 min: CO (~200 mL min^{-1})
				Remaining time: N_2 (~500 mL min^{-1})
			Potential	0.1 V
			Time	60 min
5	ECSA (CO)	CV	Gas flow	N_2 (~300 mL min^{-1})
				0.1 – 1.0 V

			Potential limits Scan rate Number of cycles	20 mV s^{-1} 3
6	ORR (O_2)	Galvanostatic staircase	Gas flow Pt-reduction step Current steps* (holding time)	O_2 (~200 mL min^{-1}) 0.1 V for 300 s in N_2 (~300 mL min^{-1}) OCV (600s); -0.04 mA; -0.08 mA (90 s); -0.20 mA; -0.40 mA (60 s); -0.80 mA; -2.00 mA; -4.00 mA; -8.00 mA (30 s) -20 mA; -40 mA; -80 mA; -200 mA; -400 mA; -800 mA; -1200 mA (5 s) →in negative and positive direction
7	ORR (Synthetic air)			See 6

*for catalyst spot sizes different from 0.785 cm^2 the applied currents were adapted

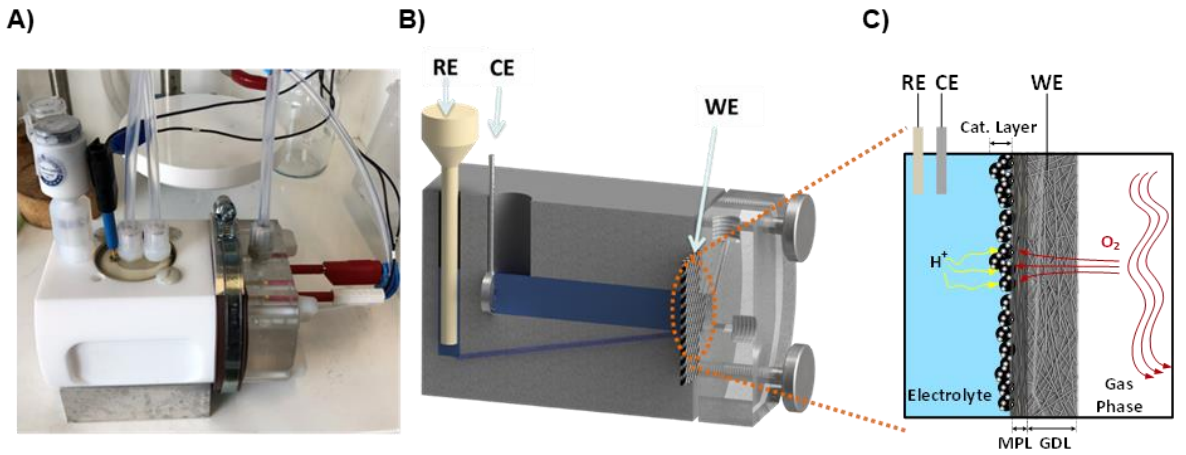

Figure S3: A) Photograph of the assembled half-cell gas diffusion electrode setup. B) Cross-section of the cell showing the position of working (WE), counter (CE) and reference electrode (RE) and the connection of the reference electrode via a luggin-capillary. C) Function principle of the characterization technique. Gas flow is provided from the backside of the GDL, while the catalyst coated microporous layer (MPL) side is in contact with the electrolyte, providing protons for the ongoing reaction.

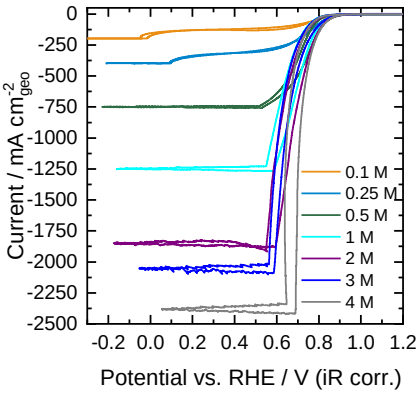

Figure S4: Influence of the electrolyte concentration on CV curves in O_2, relating to a $HClO_4$-concentration-dependent limiting current. Measurements were carried out with GDEs with a loading of 100 μg_{Pt} cm^{-2} and a catalyst-coated area of 0.785 cm^2. The size of the Pt wire CE is 2.6 cm^2. Reproduced with permission from [5].

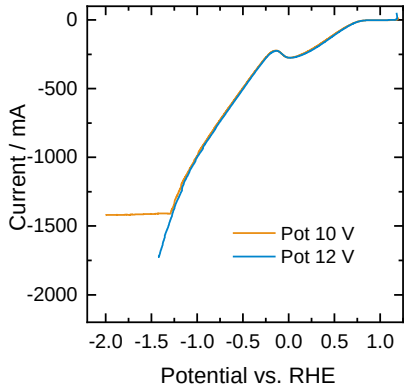

Figure S5: LSV curves recorded in ambient air with two Potentiostats with a differing compliance voltage of 10 V and 12 V, respectively. *Measurements were carried out on GDEs with a Pt loading of 100 µg cm^{-2} and a catalyst-coated area of 0.5 cm^2 in 2 M $HClO_4$. shows that the Potentiostat with the higher compliance voltage of 12 V allows a higher maximum current to flow through the cell. An interesting feature when comparing the curves recorded with the different Potentiostats is that the maximum current in the measurement with the Potentiostat with the lower compliance voltage is given as a plateau, while the Potentiostat with higher compliance voltage is stopping to record current once the compliance voltage is reached.*

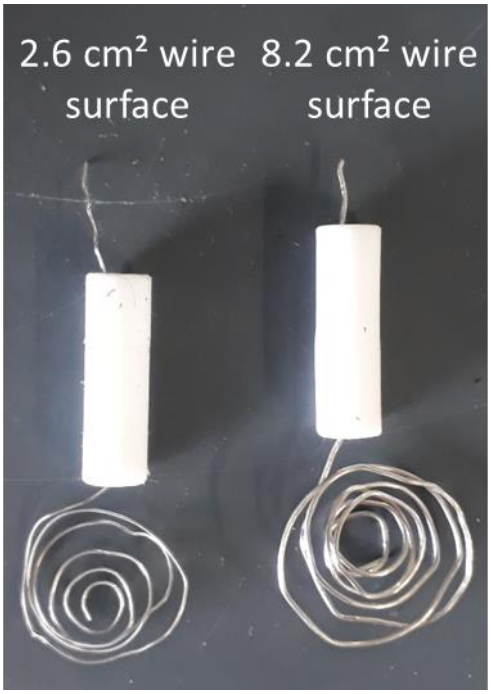

Figure S6: Photograph of the two Pt wire counter electrodes with varying size utilized in this work. The surface area was calculated from the wire diameter d and the length L with equation: Surface area $A = \pi \cdot d \cdot L$.

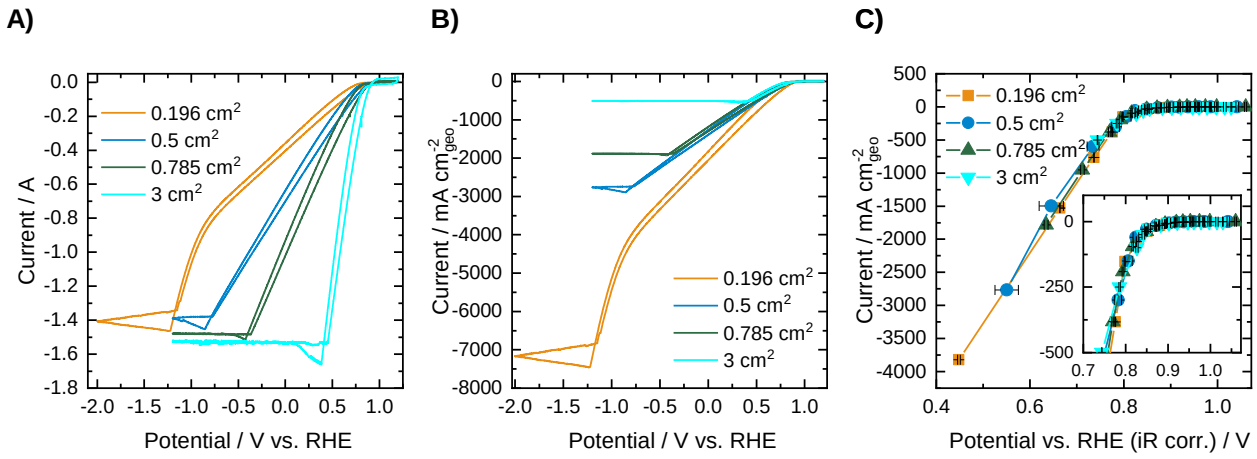

Figure S7: Effect of the size of the catalyst-coated electrode area on CV curves recorded in an O_2 atmosphere: A) absolute current, B) geometric current density. C) Resulting polarization curves given as geometric current density for the different areas in an O_2 atmosphere. Measurements were carried out on GDEs with a Pt loading of 100 µg cm^{-2}.

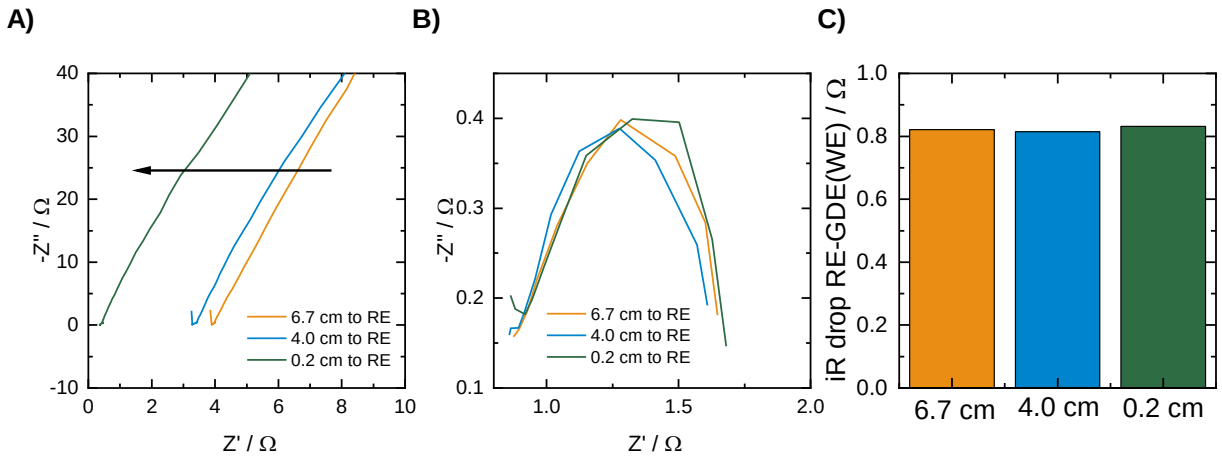

Figure S8: A) Influence of the position of the counter electrode on EIS curves recorded with the Pt wire CE as working electrode and the GDE as counter electrode @OCV. B) Influence of the position of the counter electrode on EIS curves recorded with the GDE as working electrode @-250 mA cm^{-2}_{geo} in oxygen atmosphere. C) iR drop between RE and GDE determined out of the EIS spectra shown in C).

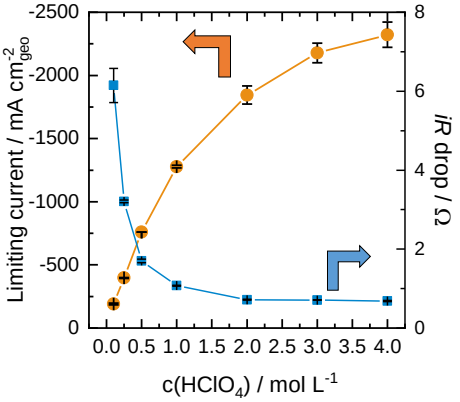

Figure S9: Limiting current observed in O_2-atmosphere and iR drop depending on the perchloric acid concentration. Measurements were carried out with GDEs with a loading of 100 μg_{Pt} cm^{-2} and a catalyst coated area of 0.785 cm^2. The size of the Pt wire CE is 2.6 cm^2.

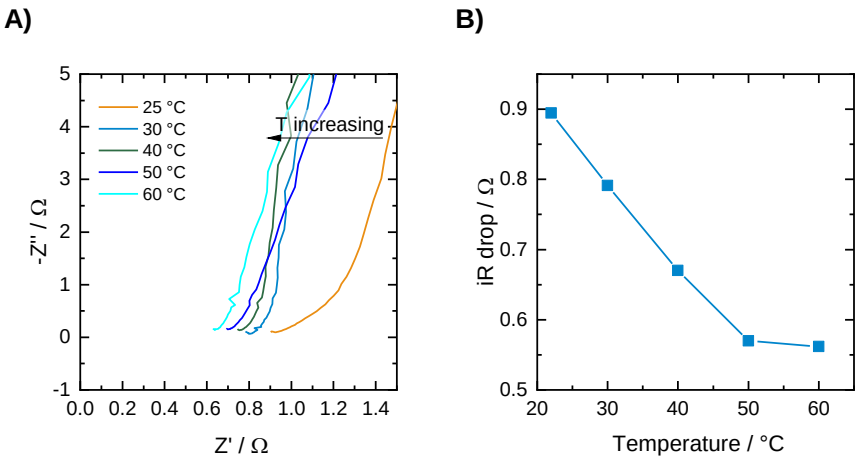

Figure S10: : A) Influence of the electrolyte temperature on EIS curves recorded @OCV. B) iR drop determined by fitting the EIS spectra shown in A).

References

[1] A.A.N. EC08, Metrohm Autolab. BV (2011) 1–3.

[2] C. Song, J. Zhang, in: PEM fuel cell electrocatalysts and catalyst layers, Springer, 2008, pp. 89–134.

[3] J. Newman, E. Thomas-Alyea, K. Electrochemical systems, John Wiley & Sons: New York, 2004.

[4] A.A. Topalov, I. Katsounaros, J.C. Meier, S.O. Klemm, K.J.J. Mayrhofer, Review of Scientific Instruments 82 (2011) 114103.

[5] N. Schmitt, M. Schmidt, G. Hübner, B.J.M. Etzold, Journal of Power Sources 539 (2022) 231530.

4.3. Which insights can gas diffusion electrode half-cell experiments give into activity trends and transport phenomena of membrane electrode assemblies?

Authors: Nicolai Schmitt, Mareike Schmidt, Jonathan E. Mueller, Lasse Schmidt, Michael Trabold, Katharina Jeschonek, Bastian J.M. Etzold

Journal: Energy Advances

Publisher: Royal Society of Chemistry

Date: 04 May 2023

DOI: https://doi.org/10.1039/D3YA00055A

Reprinted under the terms of the Creative Commons Attribution 3.0 Unported Licence.
https://creativecommons.org/licenses/by/3.0/

Energy Advances

ROYAL SOCIETY OF CHEMISTRY

PAPER

View Article Online
View Journal | View Issue

Check for updates

Cite this: *Energy Adv.*, 2023, 2, 854

Which insights can gas diffusion electrode half-cell experiments give into activity trends and transport phenomena of membrane electrode assemblies?†

Nicolai Schmitt, [a] Mareike Schmidt,[a] Jonathan E. Mueller, [b] Lasse Schmidt,[b] Michael Trabold,[a] Katharina Jeschonek[a] and Bastian J. M. Etzold *[a]

Gas diffusion electrode (GDE) half-cell setups were recently presented as a powerful tool to characterize oxygen reduction reaction (ORR) catalyst layers at fuel cell relevant potentials and current densities. In order to pave the way for a broad-based application of the technique, it is essential to assess the comparability of the GDE half-cell technique and real membrane electrode assembly (MEA) measurements. In order to face this concern, we investigate the transferability of trends from GDE half-cell experiments, in which the catalyst layer directly faces the liquid electrolyte, to MEA experiments with (i) an ionic liquid modified and unmodified Pt/C catalyst and (ii) Pt/C catalysts with and without nitrogen modified carbon support at different ionomer to carbon ratios. We show that GDE half-cell experiments can be used to reliably predict trends in catalytic activity for catalyst layers in real MEAs that are related to differences in oxygen mass transport. However, differences in catalytic activity being related to proton accessibility cannot be captured completely due to the differing interphase solid catalyst/liquid electrolyte in GDE testing and solid catalyst/solid electrolyte in MEA testing. In order to account for this, it may be necessary to introduce an ionomer between the catalyst layer and the liquid electrolyte during GDE evaluation, which would, however, dramatically increase the effort required to perform measurements. On the other hand, GDE testing with the catalyst layer being in direct contact with the liquid electrolyte is nevertheless of interest, because it allows for the study of oxygen mass transport properties at application-oriented current densities independent of other transport phenomena.

Received 31st January 2023,
Accepted 1st May 2023

DOI: 10.1039/d3ya00055a

rsc.li/energy-advances

Open Access Article. Published on 04 May 2023. Downloaded on 11/9/2023 4:50:48 PM.
This article is licensed under a Creative Commons Attribution 3.0 Unported Licence.

1. Introduction

Fuel cells converting the chemical energy stored in fuels into electricity are predicted to find increasing application as next-generation power devices due to their high efficiency combined with low emissions. Polymer electrolyte fuel cells (PEMFCs) in particular have received major attention in fuel cell research and development and are currently being commercialized or further developed for many stationary, portable and transportation power applications.[1] Furthermore, the optimization of PEMFCs focusses mainly on reducing their cost by maximizing power at minimal precious metal (Pt) content or by avoiding Pt-based materials altogether, and on improvement of the energy conversion efficiency, which is still low compared with batteries. The main focus, therefore, lies on development of improved catalysts layers for the sluggish cathodic oxygen reduction reaction (ORR).[2,3] A major obstacle is that catalysts, which are highly active in laboratory-scale test do not automatically maintain their performance when embedded within catalyst layers under industrially relevant conditions. Thus, there are many examples of catalysts which are highly active in fundamental rotating disk electrode (RDE) measurements; however, very few of these have been successfully implemented in membrane electrode assemblies (MEA) operating under industrial relevant conditions.[4–6]

A major reason for the differing performance in RDE and MEA testing is the limited mass transport in RDE experiments resulting in low maximum current densities (max. 6 mA cm_{geo}^{-2} at 1600 rpm in RDE *vs.* up to 3000 mA cm_{geo}^{-2} in MEA) and the narrow potential range where catalyst kinetics can be investigated as a result. Additionally, RDE uses a smooth glassy carbon surface with low catalyst loadings (up to 20 μg_{Pt} cm^{-2}) resulting in much thinner catalyst layers compared with MEA testing, where higher catalyst

[a] *Technical University of Darmstadt, Department of Chemistry, Ernst-Berl-Institut für Technische und Makromolekulare Chemie, 64287 Darmstadt, Germany. E-mail: bastian.etzold@tu-darmstadt.de*
[b] *Volkswagen AG, 38436, Wolfsburg, Germany*

† Electronic supplementary information (ESI) available. See DOI: https://doi.org/10.1039/d3ya00055a

© 2023 The Author(s). Published by the Royal Society of Chemistry

Open Access Article. Published on 04 May 2023. Downloaded on 11/9/2023 4:50:48 PM.
This article is licensed under a Creative Commons Attribution 3.0 Unported Licence.

loadings (up to 500 μg_{Pt} cm^{-2}) on larger gas permeable electrodes are utilized.[7–9] Furthermore, in MEA measurements the catalyst layer is in contact with an ionomer membrane, which serves as a solid electrolyte, and with Nafion®, whose addition to the catalyst layer is essential to guarantee sufficient proton transport. In contrast, in RDE evaluation the catalyst is surrounded by liquid electrolyte ensuring good proton transport and Nafion® is mainly added to stabilize the catalyst ink dispersion during electrode preparation, so that a homogenous coating is formed.[10,11] Last, but not least, RDE testing is carried out under dynamic potentiostat operation using cyclic voltammetry (CV), while MEA testing is carried out under stationary conditions using potential or current control.[12,13]

In order to improve the significance of the activity data collected in fundamental research, several approaches for evaluating PEMFC catalysts under conditions that avoid mass transport limitations have been introduced.[14–19] Gas diffusions electrode (GDE) half-cells offer a highly promising approach, which avoids mass transport limitations and fulfills the criteria necessary for wide applicability in standard research.[14,15,20,21] Mass transport limitations obtained in RDE studies are avoided by distributing the reactant gas directly to the catalyst *via* a gas diffusion layer (GDL). Most recently, an Inter-lab comparison demonstrated that GDE testing with various, slightly differing setups can deliver data that is both reliable and comparable if standardized measurement protocols are followed.[22] While these GDE setups were so far mostly utilized at room temperature and limited to ambient pressure, a setup was recently presented, which allows measurements at temperatures up to 120 °C and pressures of up to 4 bar.[23]

What is still under debate, is how GDE measurements differ in detail from MEA measurements and what possible limitations the technique has. Despite the temperature difference (mostly room temperature in GDE testing, 80 °C in MEA testing), one important issue is whether GDE half-cell characterization is carried out with or without an ionomer membrane between the catalyst surface and the liquid electrolyte. So far both variants have been utilized in GDE testing and no standard procedure exists, that was agreed on.[14,15,24–26] Utilizing a solid electrolyte results in an environment that is much more complex and heterogeneous than the environment in aqueous electrolyte cells. Therefore, comparing both systems can introduce uncertainty regarding interfacial phenomena, reactant solubility, differences in local and bulk pH and transport phenomena such as removal of product water.[27] Recently, Ehelebe *et al.* have shown that degradation of the catalyst layer in long-term durability tests characterizing Pt dissolution is significantly different when the catalyst layer and liquid electrolyte are separated by a membrane.[28] As a consequence, employing a membrane as a solid electrolyte in GDE measurements will better mimic the environment in real membrane electrode assemblies. However, in contrast to MEA measurements, it is technically difficult to compress the ionomer membrane and the GDL in liquid half-cells, and thus ensure optimum proton accessibility at the catalyst surface. Furthermore, the production method of the CL and membrane interface plays a critical role, and the resulting interfacial boundary strongly influences the performance at high current densities. Thus, fast, reliable catalyst testing at high current densities is not feasible because the layer/membrane contacting needs to be optimized for each new catalyst, an effort which requires extensive MEA testing. Additionally, measurements employing ionomer membranes require elevated temperatures to provide sufficient proton mobility, which means one must account for water management within the membrane and regulate the humidity of the gases.[15] Taken together these differences highlight the dramatic increase in technical complexity and experimental effort that is required to utilize an ionomer membrane as solid electrolyte in GDE experiments. Therefore, it should first be clarified, what GDE half-cell measurements without ionomer membranes provide and especially, how well-suited they are for predicting trends in catalyst activity at high current densities.

In order to address this concern, we compare GDE data collected at room temperature without utilization of an ionomer membrane (direct contact of the catalyst layer to the liquid electrolyte) with MEA data collected at 80 °C. As a test cases we evaluate two catalyst modifications that are the subject of current scientific discussion in both GDE and MEA setups. The catalyst modifications of interest are: (i) an ionic liquid modified and unmodified Pt/C catalyst and (ii) Pt/C catalyst with and without nitrogen modified carbon support at different ionomer to carbon (I/C) ratios.

The state of the art on both modifications is briefly summarized as follows.

Modifying a Pt/C catalyst with Ionic liquids (ILs) allows us to manipulate the microenvironment of the active site, liquid electrolyte and gaseous reactant. The concept of modifying a solid catalyst with ionic liquid was first presented in 2007 by Kernchen *et al.* for a heterogeneous catalyzed gas phase reactions and the term "SCILL" (supported catalyst with ionic liquid layer) was invented for this kind of catalyst modification.[29] Snyder *et al.* were the first to bring IL modifications to electrocatalysis and used a similar approach to improve the ORR activity of a PtNi/C catalyst in fundamental RDE studies.[30] These promising results were later validated by Etzold *et al.*, who applied the SCILL concepts to carbon supported Pt and Pt-alloy catalysts, utilizing many different kinds of ILs. However, these studies also showed that the amount of IL needs to be balanced very accurately, since excess IL added can result in mass transport limitations, most likely caused by their influence on oxygen diffusivity, and even be observed during low current density RDE testing.[31–34] So far, the extraordinary effect of ILs obtained in these RDE studies could rarely be transferred to high current density MEA testing and there are few examples for successful implementation of IL-modified Pt/C catalysts into real MEA applications.[35–37] Therefore, this material was chosen as a first example to assess the capability of GDE testing to predict and to distinguish catalyst layer activity trends in the low and the high current density regime.

N-doping of the Pt/C carbon support has been proposed to improve the ionomer-catalyst interaction in PEMFC catalyst

Open Access Article. Published on 04 May 2023. Downloaded on 11/9/2023 4:50:48 PM. This article is licensed under a Creative Commons Attribution 3.0 Unported Licence.

layers by introducing nitrogen groups, which develop coulombic interactions with $-SO_3^-$ groups in the ionomer, resulting in more homogeneous ionomer distribution over the catalyst layer.[38–41] According to this amine groups introduced on the carbon surface can react with sulfonic acid groups of the ionomer resulting in positively charged $-NH_3^+$ groups leading to strong coulombic attraction between carbon support and ionomer side chains.[42,43] Orfanidi *et al.* and Ott *et al.* used ammonolysis of Vulcan XC 72R and Ketjenblack EC-300J carbon support, respectively, to apply this concept.[39,40] In both studies improved performance in MEA testing was observed and was attributed to improved ionomer distribution after N-doping, resulting in improved proton accessibility to the Pt active sites, and also to the formation of highly accessible pores, optimizing oxygen mass transport. While it is known that adding sufficient amount of ionomer added to the catalyst layer is crucial to ensure sufficient proton conductivity in MEAs, this may be different for GDE testing, since the catalyst layer is in direct contact with the liquid electrolyte. It is not known so far, whether this can result in important differences in catalyst evaluation between the two techniques. In order to further elucidate the effect of N-doping on the ionomer interaction, a variation of the I/C ratio on both unmodified and N-doped Pt/C will be carried out in the present work.

2. Experimental

2.1 Synthesis of ionic liquid modified Pt/C catalyst

IL modified samples were prepared by coating Pt/C catalyst (HiSPEC®3000, 20 wt% Pt) with the ionic liquid [BMIM][beti]. In a typical synthesis procedure 30 mg of catalyst were mixed with 10 mL of isopropyl alcohol containing a certain amount of the IL in a round bottom flask. The mixture was stirred for 30 min at room temperature followed by 30 min of ultrasonication. Then the solvent was slowly removed from the solids by rotary evaporation under low vacuum (120 mbar, 40 °C). After total removal of isopropyl alcohol, the pressure was then further decreased to 10 mbar to ensure full intrusion of IL into the catalyst pores. Varying amounts of IL in isopropyl alcohol solution were used to achieve proportions of IL in the final catalyst of 5, 15 and 20 wt%, respectively.

2.2 Nitrogen modification of carbon support

N modification was carried out by using a procedure outlined in literature.[44] Therefore, 350 mg of carbon (Ketjenblack® EC300-J) was introduced into a 250 mL three-neck flask together with 12.7 mL of acetic anhydride (99%, Acros Organics). The mixture was placed in an ice bath and 5.6 mL of nitric acid (65 wt%, Acros Organics) was slowly added while stirring. The resulting mixture was stirred on ice for another 5 hours and then for 19 hours at room temperature. Afterwards, the solids were filtered and washed with distilled water until pH neutrality and then dried in a vacuum oven at 70 °C for 12 h. Finally, in order to reduce the amount of acidic oxygen-containing groups, the modified carbon was subjected to a thermal treatment in a tubular furnace (Gero F-A-40-200/13) in N_2-atmosphere at a temperature of 800 °C for 2 hours, resulting in the final N-modified carbon support.

The carbon support was analyzed before and after N modification with N_2 Physisorption and elemental analysis. Details can be found in the ESI.†

2.3 Deposition of Pt on carbon supports

Deposition of platinum on Ketjenblack® EC300-J and on the N-doped carbon was carried out *via* wet impregnation aiming for a theoretical loading of 40 wt% Pt on carbon. Therefore, 140 mg of Chloroplatinic acid hexahydrate (99.9%, abcr Chemie) was dissolved in 1 mL of Ethanol and then mixed thoroughly with 100 mg of the respective carbon support. In order to remove the solvent, the sample was thereafter dried at 60 °C in a vacuum oven for 12 h.

After impregnation of the carbon support with the precursor solution, a gas phase reduction was carried out in a horizontal tubular furnace (Gero F-A-40-200/13). To do this the impregnated sample was transferred into a ceramic bowl (50 × 35 × 12 mm) and positioned in the isothermal zone of the furnace. Afterwards, the sample was heated to 250 °C in a nitrogen gas flow of 10 LN h^{-1} with a heating ramp of 2.5 K min^{-1}. For reduction of the Pt precursor, the temperature was held for three hours in a mixed gas stream of 7 LN h^{-1} N_2 and 3 LN h^{-1} H_2. Finally, the furnace was cooled down to room temperature under a gas flow of 10 LN h^{-1} N_2 and the resulting Pt/C catalyst was collected and weighed.

The synthesized Pt/C catalysts were analyzed regarding their Pt content *via* ICP-OES. Details can be found in the ESI.†

2.4 RDE characterization

RDE characterization was carried out on all ionic liquid modified samples and the unmodified HiSPEC®3000 catalyst. The RDE measurements were performed on a Ivium Multichannel Potentiostat (Octostat 5000), which is controlled by IviumSoft software. As a reference electrode, a leak-free double-junction Ag/AgCl electrode (Aldrich) was used. A Pt wire (PINE) served as counter electrode. All potentials reported in this work were calibrated against a reversible hydrogen electrode (RHE) using hydrogen evolution-oxidation reaction on a Pt electrode. For each catalyst sample, two RDE tips were prepared and tested for reproducibility purposes, in order to give the standard deviation between two individual measurements. Further details on the RDE measurements are summarized in the ESI.†

2.5 GDE characterization

GDE evaluation was carried out in an automated setup and using a commercial GDE half-cell (Flexcell® PTFE, Gaskatel GmbH) operated at room temperature in 2 M $HClO_4$ as electrolyte. For GDE preparation the respective catalyst was deposited on the gas diffusion media (Sigracet 25 BC, SGL Carbon) by using a drop-casting approach, resulting in a catalyst loading of 100 μg_{Pt} cm^{-2}. Detailed information on the coating technique and the measurement procedure is given in our recent publications[26,45] and in the ESI.† For the investigation of

 © 2023 The Author(s). Published by the Royal Society of Chemistry

Open Access Article. Published on 04 May 2023. Downloaded on 11/9/2023 4:50:48 PM.
This article is licensed under a Creative Commons Attribution 3.0 Unported Licence.

HiSPEC® 3000 catalyst and the IL modified samples, the I/C ratio was set to 0.5. For the Pt/Ketjenblack catalyst and the N-modified samples, varying I/C ratios of 0.1, 0.5 and 1.7 were investigated. For each catalyst sample, two GDEs were prepared and tested for reproducibility purposes.

2.6 MEA characterization

For MEA fabrication, GDE cathodes with a size of 5 cm^2 were prepared by spray coating using a robot assisted ultrasound nozzle spraying station that includes a CNC table (High-Z S-400, CNC step), an ultrasonic atomizer spray nozzle (Sonozap, Sonaer Ultrasonics) and a syringe pump for catalyst ink feeding. The catalyst ink composition is identical to the one used for half-cell experiments, but contains a higher concentration of solids (8 mg catalyst per 5 mL of solution). During spray coating, the gas diffusion layers (Sigracet 25 BC, SGL Carbon) were heated to 125 °C on a heating plate and the ink feed rate and spraying time were adapted to aim catalyst loadings of 200 μg_{Pt} cm^{-2} on the cathode. After spray coating, the obtained cathode GDEs were weighed to determine the exact catalyst loading and were then hot-pressed together with Nafion™ NR211 membrane (thickness = 25 μm) and a commercial Pt/C GDE (0.2 mg_{Pt} cm^{-2}, 20% Pt on Vulcan, FuelCellsEtc) as anode at a temperature of 125 °C and a pressure in relation to the electrode area of 96 bar (LaboPress P200S-VAK, Vogt Labormaschinen GmbH), to obtain the final membrane electrode assemblies. Fuel cell experiments were carried out at 80 °C and a relative humidity (RH) of 17 and 100%, respectively, without backpressure on a Scribner Model 850e (Scribner Associates) under power-optimized conditions with H_2 (0.2 L min^{-1}) and O_2 (0.2 L min^{-1}). The MEAs were pre-treated with a break-in procedure consisting of repetitive potential steps at OCV, 0.3 V and 0.6 V respectively until a stable fuel cell performance was observed. The polarization data was measured galvanostatically from OCV to a total maximum current of 15 A with 10 measurement points per decade. For iR-correction, the cell resistance at every recorded polarization data point was measured automatically by the test station *via* current interrupt. For MEA characterization of HiSPEC® 3000 catalyst and the IL modified samples, the I/C ratio was set to 0.5. For the Pt/Ketjenblack catalyst and the N-modified samples, varying I/C ratios of 0.1, 0.5 and 1.7 were investigated. For each catalyst sample, two MEAs were prepared and tested for reproducibility purposes.

3. Results

3.1 ORR performance of IL-modified Pt/C in RDE, GDE and MEA

We first performed a comparative study of the influence of modifying a commercial Pt/C catalyst (HiSPEC®3000, 20 wt% Pt) with varying amounts of the ionic liquid [BMIM][beti] in RDE, GDE and MEA. Fig. 1 compares ORR activity of the different catalyst materials obtained in RDE, GDE (both measured at room temperature) and MEA (80 °C, 100%RH) experiments. The corresponding ORR polarization curves for the RDE and the GDE measurements can be found in Fig. S1 in the ESI.†

As can be seen in Fig. 1A, the mass specific activity extracted from the RDE polarization curves increases with increasing amount of ionic liquid both at potentials of 0.90 and 0.95 V *vs.* RHE. This indicates a strong activity-boosting effect of the IL on the intrinsic ORR activity of the Pt/C catalyst and is well in line with earlier RDE studies.[30–36,46,47] Fig. 1B shows ORR activity data obtained for the different IL modified samples in the GDE half-cell setup and presents the measured ORR potential at different geometric current densities of −5, −50 and −1500 mA cm_{geo}^{-2}. The results indicate that at −5 and −50 mA cm_{geo}^{-2}, the ORR potential increases with increasing amount of IL added to the Pt/C catalyst. Thus, similarly to the RDE results, an activity boosting effect of the IL is obtained in the low current density regime in the GDE setup. In the high

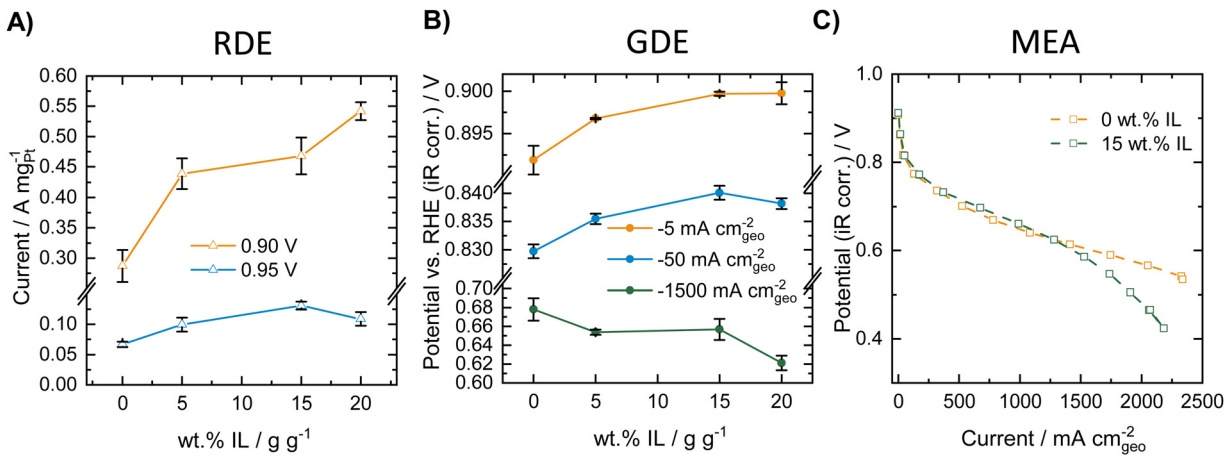

Fig. 1 ORR activity of Pt/C catalyst modified with [BMIM][beti]. (A) Mass specific ORR activity, depending on the amount of IL obtained in RDE measurements at room temperature in oxygen saturated 0.1 M $HClO_4$ and 1600 rpm at a catalyst loading of 20 μg_{Pt} cm^{-2}. (B) ORR potentials at different current densities depending on the amount of IL obtained in GDE measurements at room temperature in oxygen atmosphere in 2 M $HClO_4$ at a catalyst loading of 100 μg_{Pt} cm^{-2}. (C) ORR polarization curve of unmodified Pt/C and Pt/C modified with 15 wt% of IL measured in a MEA at 80 °C and 100%RH in oxygen atmosphere (1 atm) at a catalyst loading of 100 μg_{Pt} cm^{-2}.

Open Access Article. Published on 04 May 2023. Downloaded on 11/9/2023 4:50:48 PM.
This article is licensed under a Creative Commons Attribution 3.0 Unported Licence.

current density regime, however, a reverse trend is visible and the measured potential decreases with increasing amount of IL added, indicating a decreasing ORR activity. MEA polarization curves were recorded for the unmodified catalyst and the 15 wt% IL modified sample. Fig. 1C shows the polarization curves obtained in oxygen atmosphere at 80 °C and 100%RH. As can be seen, at low and intermediate current densities, a slight increase in ORR activity is obtained after IL-modification. However, in the high current density regime a worsening of the performance is obtained after IL modification and the corresponding curve shows a strong loss of activity at high current densities. Thus, in the case of IL-modified Pt/C catalyst, similar trends can be observed in GDE and in MEA measurements. The GDE half-cell experiments could therefore very well describe the behavior of the catalysts in the different current regimes, while only considering the RDE data would result in erroneous conclusions. GDE and MEA experiments were also carried out in synthetic air (20% O_2 in N_2), which is presented in Fig. S2 (ESI†). Herein, identical trends could be observed compared to the measurements in pure oxygen and both setups show an increase in activity at low and intermediate current densities, while in the high current density regime, the IL modification introduces mass transport limitations.

3.2 ORR performance of N-modified Pt/C in GDE and MEA at different ionomer to carbon ratio

In the second example for comparison of ORR activity data collected in GDE and in MEA measurements, a self-synthesized Pt/C catalyst with and without nitrogen modification of the Ketjenblack carbon support was investigated. Elemental analysis of the carbon support before and after the nitrogen modification revealed successful N-doping with a N content of 0.23 at% (see Table S4, ESI†). Physisorption analysis shows that the modification treatment also results in a slight increase in the surface area as determined by application of both a BET analysis and a QSDFT model, as well as a minor increase in the specific pore volume (see Table S3, ESI†).

After deposition of Pt on the untreated and on the N-doped carbon support, the resulting Pt/C and Pt/N-C catalysts were analyzed both in the GDE half-cell and in MEA measurements. Thereby, different I/C ratios of 0.1, 0.5 and 1.7 were investigated for the respective catalyst sample. GDE evaluation was carried out at room temperature in oxygen atmosphere, MEA evaluation was carried out at 80 °C both at 17 and 100%RH in oxygen atmosphere. For direct comparison of GDE and MEA data, the GDE data was corrected for the differing reaction conditions (temperature + partial pressure of oxygen reactant). To do this a kinetic and a thermodynamic correction of the GDE data was carried out following[14] (for details see ESI†). Furthermore, from the obtained polarization curves, the mass specific activity was calculated, since the catalyst loading varied slightly between the different measurements (see Table S5, ESI†). Fig. 2 shows the resulting mass specific ORR polarization curves of the N-doped and undoped catalysts in the GDE half-cell after correcting the data and in the MEA at 100%RH. GDE polarization curves before and after correction of the data, as well as MEA polarization curves showing the geometric current density are presented in Fig. S3 and S4 (ESI†).

Fig. 2A shows the obtained polarization curves with and without N-modification at an I/C ratio of 0.1. The results indicate a slight improvement of the polarization curve obtained in the MEA after N-modification in the low and intermediate mass specific current regime, and similar activity compared to the unmodified catalyst at high mass specific currents. The GDE half-cell experiments generally deliver very similar mass specific activity curves compared to MEA testing after the applied correction, although the correction can only be seen as rough estimation, since it does not cover any mass transport and MEA effects such as hydrogen crossover and resistance of the ionomer membrane. Furthermore, differences in local pH due to the differing environment solid catalyst/solid ionomer in MEA and solid catalyst/liquid electrolyte in GDE testing are not considered. A detailed look at the GDE results for an I/C ratio of 0.1, however, indicates a reverse trend

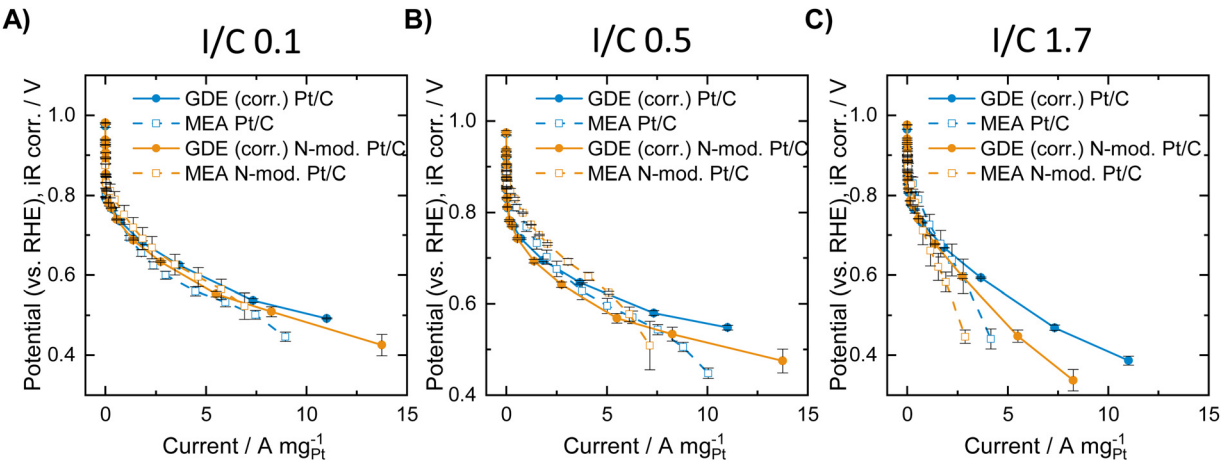

Fig. 2 Mass specific ORR polarization curves of the unmodified and N-doped Pt/C catalysts obtained in MEA measurements at 80 °C and 100%RH in oxygen atmosphere (1 atm) and in the GDE half-cell (data collected at room temperature in 2 M $HClO_4$ in oxygen atmosphere and thereafter thermodynamically and kinetically corrected for MEA conditions). (A) I/C ratio = 0.1 (B) I/C ratio = 0.5 (C) I/C ratio = 1.7.

© 2023 The Author(s). Published by the Royal Society of Chemistry

Open Access Article. Published on 04 May 2023. Downloaded on 11/9/2023 4:50:48 PM.
This article is licensed under a Creative Commons Attribution 3.0 Unported Licence.

compared with MEA testing with the unmodified catalyst exhibiting better performance over the entire current range. The results obtained for an I/C ratio of 0.5 in Fig. 2B reveal identical trends with an improvement after N-modification in the MEA and a worsening of the performance in the GDE. Direct comparison of the curves generally reveals the following: in the ohmic regime, MEA activity is better compared to GDE activity, while in the mass-transport limiting regime higher activity is obtained in the GDE half-cell. This is well in line with results earlier presented by Ehelebe *et al.*[14] for a commercial Pt/C catalyst. Fig. 2C shows the obtained mass specific polarization curves at an I/C ratio of 1.7. In this case GDE and MEA data shows the same trend with a better performance of the unmodified catalyst in the high mass specific current regime. For further analysis of the obtained data, voltage losses were determined when lowering or increasing the I/C ratio compared to an I/C ratio of 0.5. Therefore, for the respective unmodified or N-doped material, the polarization curves obtained at an I/C ratio of 0.1 and 1.7, respectively, were subtracted from the ones obtained at I/C 0.5. The resulting voltage loss curves are presented in Fig. 3.

Fig. 3A shows that a lowering of the I/C ratio results in significant activity losses in the MEA in the low current regime. These losses are not visible in the GDE half-cell, where at low mass specific currents no performance loss compared to an I/C ratio of 0.5 is obtained for both unmodified and N-doped catalyst. In Fig. 3B the obtained potential losses after increasing the I/C ratio to 1.7 is shown. In this case no activity losses are obtained for the materials in both GDE and MEA in the low current regime. At higher currents, however, strong activity losses and identical trends are observed in both cell types, while the absolute numbers differ between GDE and MEA. These activity losses might be attributed to increased oxygen mass transport limitations at higher currents for excess ionomer content and the resulting diffusion barrier through the thick ionomer film.[48]

MEA mesaurements carried out under dry conditions at 17%RH with both unmodified and N-doped Pt/C are presented in Fig. S5 and S6 (ESI†). In this case N-doping results in a dramatic increase in performance for all I/C ratios. Since proton transport is limiting under dry conditions for non optimized ionomer coverage,[49] this lets us assume that N modification of the carbon support could strongly improve dry proton accessibility of the Pt particles in the catalyst, as was previously shown by Ott *et al.*[40]

3.3 Which insights can gas diffusion electrode half-cell experiments give into activity trends and transport phenomena of membrane electrode assemblies?

The two model materials investigated in this study present the following outcome: in the case of IL-modified and unmodified Pt/C catalyst identical trends are observed in GDE and in MEA, with an increase in activity after IL modification at low and intermediate current densities and a lower activity compared to the pristine catalyst in the high current density regime. In the case of Pt/C catalyst with and without N-doped carbon support identical trends are observed at an I/C ratio of 1.7, with a decrease in activity after N-doping in the high current density regime. For lower I/C ratio of 0.1 and 0.5, however, only MEA evaluation showed an improvement after N-doping, while a reverse trend is observed in the GDE half-cell. Based on these observations, we subsequently want to consider the circumstances, under which GDE half-cell experiments with the catalyst layer in direct contact with the liquid electrolyte, can correctly predict trends for real MEAs. To do this, we now analyze each case, to determine which transport mechanism (proton accessibility or oxygen mass transport) limits the MEA performance of unmodified catalyst compared to modified catalyst, or *vice versa*.

In the case of the ionic liquid modified catalyst, the activity boosting effect observed in RDE studies was mostly attributed to higher oxygen solubility in the IL compared to the liquid electrolyte and suppressed adsorption of non-reactive oxygenated

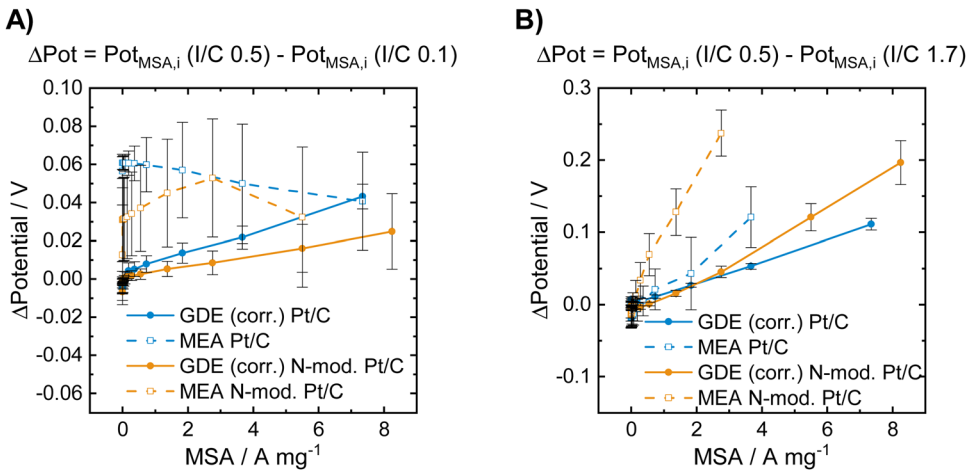

Fig. 3 Voltage losses obtained for the unmodified and for the N-doped Pt/C catalysts in GDE and in MEA characterization at low and high I/C ratio compared to an I/C ratio of 0.5. The data presented in (A) was obtained by subtracting the polarization curve of the respective catalyst in the respective cell type shown in Fig. 2B by the one shown in Fig. 2A. The data presented in (B) was obtained by subtracting the polarization curve of the respective catalyst in the respective cell type shown in Fig. 2B by the one shown in Fig. 2C.

© 2023 The Author(s). Published by the Royal Society of Chemistry

Open Access Article. Published on 04 May 2023. Downloaded on 11/9/2023 4:50:48 PM.
This article is licensed under a Creative Commons Attribution 3.0 Unported Licence.

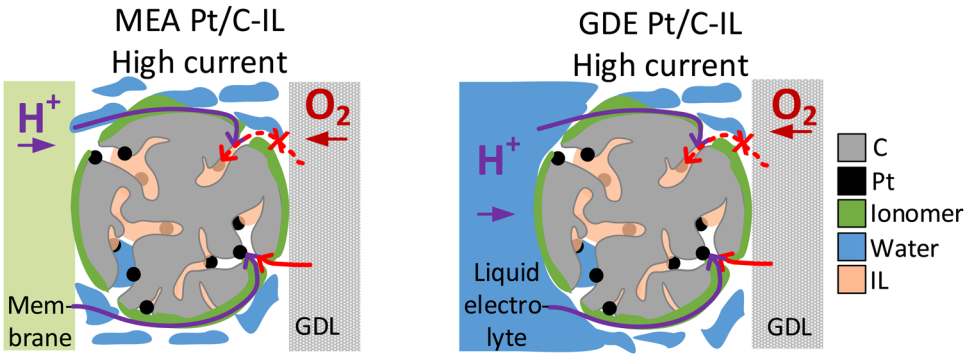

Fig. 4 Schematic illustration of oxygen transport being affected by the ionic liquid modification of Pt/C in the high current density regime in MEA (left) and GDE (right).

species.[30,32,33,50] Recent studies, however, point out that the improved proton conductivity in the catalyst layer after IL modification due to the higher ionic conductivity of ILs compared to water or liquid electrolyte is responsible for improved ORR kinetics.[37,51,52] According to this, ILs fill micropores and smaller mesopores of high surface area carbons, which are not accessible by the ionomer due to size exclusion effects, and can thus improve proton accessibility to Pt active sites within these pores.[37,53] Based on this, we exclude the hypothesis that the decrease in MEA performance of IL-modified Pt/C compared to unmodified Pt/C in the mass transport limiting regime is attributed to proton transport limitations of the IL-modified catalyst. More likely, pores filled with IL can affect oxygen transport to the Pt active sites within these pores, resulting in oxygen transport limitations at high current densities, where oxygen consumption is at a high level (see Fig. 4). This behavior would correspond well to the GDE half-cell measurement.

In the case of N-doped Pt/C catalyst, we see an improvement in the MEA performance after N modification for I/C ratios of 0.1 and 0.5, which is pronounced in the low and intermediate current regime. Ott *et al.*[40] have shown for the same carbon support and a similar nitrogen modification procedure that at an I/C ratio of 0.66, N-doping results in a significant improvement of the dry proton accessibility due to more homogenous ionomer coverage. Thus, for the unmodified catalyst, the lower performance we observed might be related to inhomogeneous distribution of ionomer and result from uncovered Pt active sites on the carbon surface (see Fig. S7, ESI†) that suffer from proton transport losses. This is also supported by the fact, that the activity boosting effect introduced by N-doping is much more pronounced under dry conditions. These trends in activity linked to proton accessibility cannot be covered in GDE half-cell measurements with the catalyst layer being surrounded by liquid electrolyte. This also becomes obvious looking at the results in Fig. 3A, which show voltage losses at an I/C ratio of 0.1 compared to an I/C ratio of 0.5. In the low current regime, these voltage losses are pronounced in the MEA measurements, while no losses are observed during GDE evaluation. Thus, the liquid electrolyte surrounding the catalyst in the GDE half-cell can also ensure good proton accessibility for unideal ionomer coverage (see Fig. 5). This phenomenon is also well known in RDE evaluation, where measurements without ionomer are standard to avoid poisoning of the Pt surface by ionomer.[54,55] Additionally, similar phenomena were also recently described by Lin *et al.* using a floating electrode (FE) setup.[57] The FE technique generally follows the same principle as the herein presented GDE approach with the catalyst being in contact with the liquid electrolyte and the gaseous reactant being delivered through a porous hydrophobic gas diffusion media, but uses much thinner catalyst layers (catalyst loading <10 μg_{Pt} cm^{-2}) and a different substrate (Au coated polymer

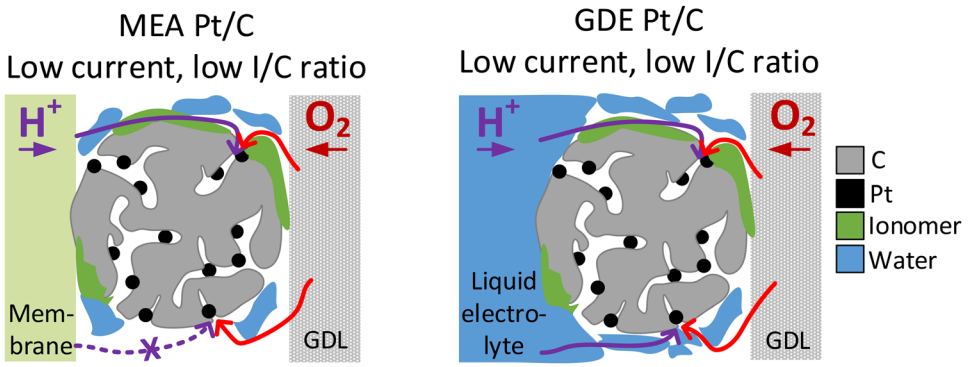

Fig. 5 Comparison of proton accessibility of Pt active sites in MEA catalyst layers (left) and GDE catalyst layers (right) at low current densities and for low I/C ratio and/or unideal ionomer coverage.

© 2023 The Author(s). Published by the Royal Society of Chemistry

Open Access Article. Published on 04 May 2023. Downloaded on 11/9/2023 4:50:48 PM.
This article is licensed under a Creative Commons Attribution 3.0 Unported Licence.

membranes with hydrophobic coating).[18] Lin *et al.* have compared commercial Pt/C catalyst at different I/C ratio and also without addition of any ionomer. It could be shown that the ionomer free catalyst layer exhibits similar activity compared to an I/C ratio of 1 at lower overpotential and even higher activity in the high current density regime, while the maximum geometric current densities were lower compared to this study (<300 mA cm_{geo}^{-2} *vs.* 2500 mA cm_{geo}^{-2}). In our study, in difference, improved performance in the high current density regime was found at an I/C ratio of 0.5 compared to 0.1. This might be linked to the much thicker catalyst layers utilized in this study compared to the FE approach. While for the ultrathin catalyst layers utilized in FE, also at a higher reaction rate good proton accessibility might be guaranteed by the surrounding electrolyte, in the thicker catalyst layers utilized in GDE, the ionomer might play a bigger role for proton transport and thus give a more realistic picture of trends for real MEAs.

The presented observations, however, also imply that the catalyst layer is always flooded with electrolyte to a certain extent during GDE evaluation and raises the question whether this will affect oxygen transport. Indeed, we see better performance in the MEA compared with the GDE in Fig. 2 for all catalyst samples in the ohmic current regime. This observation could be linked to slower oxygen mass transport in the GDE due to partial flooding of the catalyst layer by the electrolyte. At even higher current densities this behavior is no longer observed and the GDE performance becomes better compared with the MEA performance for all investigated materials. This is connected with another interesting phenomenon: in MEA experiments it is well known that flooding the gas diffusion layer on the cathode side hinders gas transport and is thus responsible for the observed limiting current density.[56] In contrast, in GDE experiments the water produced does not need to be transported through the cathodic gas diffusion electrode but will more likely dilute the aqueous acidic electrolyte instead. This is also supported by the fact, that no flooding of the GDLs is visually observed during GDE testing. This might explain how flooding the channels in the gas diffusion layer is prevented and the resulting improved performance of GDE over MEA in the mass transport limiting current regime (see Fig. 6). Besides differences in water removal pathways, this behaviour might also be linked to the differing measurement times in both GDE and MEA. For MEA polarization curves, the holding time per point was 60 s and a higher number of measurement points was applied in the high current density regime compared to GDE. In GDE, the number of high current density measurement points, as well as the holding time at these points (5 s) was kept low to prevent heating of the electrolyte. Thus, the amount of excess water produced in the MEA is also much higher, which could also result in excess flooding compared to the GDE. Similar behaviour and conclusions were recently also presented by Jackson *et al.* comparing MEA data of Pt/C with measurements carried out in a FE setup with ultrathin catalyst layers.[59] Interestingly, in this study this behaviour in the MEA mass-transport limitation regime is thus also observed for much thicker catalyst layers compared to the FE and close to industrial application. The study by Jackson *et al.* generally has seen an improved performance of FE over MEA in the whole current regime, and does not show the behaviour seen in this study in the ohmic regime with a superior performance of MEA over GDE. This difference observed between GDE and FE is most likely linked to the differences in the catalyst layer thickness and partial flooding of the thicker catalyst layer in the GDE, as discussed above.

For the N-doped Pt/C catalyst at an I/C ratio of 1.7, worse performance in the high current density regime and a stronger break-in of the polarization curve compared with the unmodified material was observed during MEA evaluation. Since the previous results indicated an improved proton accessibility after N-modification, these performance losses will be linked to increased oxygen transport losses for the N-doped catalyst, which are well described by GDE testing. Ott *et al.*[58] showed that N modification not only influences the ionomer-carbon support interaction, but can also alter the pore structure of the carbon support. Thus, the harsh conditions during the nitric acid treatment performed in this study may have resulted in a detrimental change in the pore structure within the carbon support. This is not visible under dry conditions and in the case of low ionomer content, where proton transport losses are dominating for the unmodified catalyst. However, at an I/C ratio of 0.5 (in the high current density regime) and 1.7 under wet conditions, where proton transport is sufficient for both unmodified and N-doped catalyst, it becomes evident. This could also explain why the GDE experiments, which guarantee

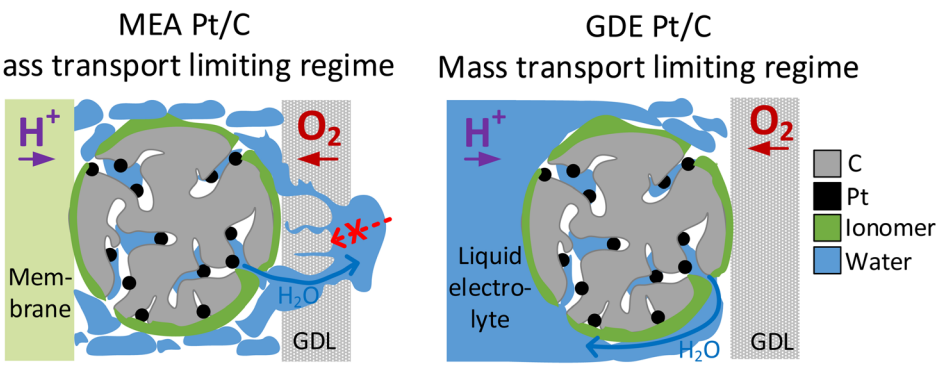

Fig. 6 Comparison of water transport in the mass transport limiting regime in MEA catalyst layers (left) and GDE catalyst layers (right).

Open Access Article. Published on 04 May 2023. Downloaded on 11/9/2023 4:50:48 PM.
This article is licensed under a Creative Commons Attribution 3.0 Unported Licence.

good proton accessibility due to the surrounding liquid electrolyte, display a decrease in performance after N-doping in the ohmic regime, independent of the I/C ratio.

4. Conclusion

In this study we systematically compared ORR data collected in GDE half-cell experiments, where the catalyst layer directly faces the liquid electrolyte, and in real membrane electrode assemblies. The investigated materials were (i) an ionic liquid modified and unmodified Pt/C catalyst and (ii) Pt/C catalyst on unmodified and nitrogen modified carbon supports at various ionomer to carbon ratios. In the case of the IL modified Pt/C catalyst it could be shown that oxygen mass transport is negatively affected by the IL in the high current density regime in MEA experiments, resulting in pronounced mass transport limitations compared to the unmodified catalyst. This behavior was well described in the GDE experiment, where correct trends in MEA activity could be predicted for the respective current regime. In the case of the N-doped Pt/C catalyst, MEA characterization displayed an improvement after N modification under dry conditions and in the case of low ionomer content, where proton transport losses are dominant for the unmodified catalyst. However, at higher I/C ratio and under wet conditions, where proton transport is sufficient for both unmodified and N-doped catalyst, worse performance after N modification is observed in the high current density regime. During GDE evaluation only the latter phenomenon could be captured and the unmodified catalyst showed a superior performance over the N-doped material at any I/C ratio in the ohmic and in the mass transport limiting regime.

In conclusion, our results show that GDE half-cell experiments with the catalyst layer in direct contact with the liquid electrolyte are a reliable proxy to describe trends for real MEAs under high current densities in case of differences in catalytic activity being linked to oxygen mass transport. In particular, GDE testing is superior in this regard compared to the wide-spread RDE technique, which cannot capture the high-current density regime and can therefore give misleading results. However, for a reliable description of all transport phenomena in real fuel cells (*e.g.* proton accessibility of Pt active sites and water transport within the gas diffusion layer), introduction of an ionomer membrane between catalyst layer and liquid electrolyte might be necessary during GDE evaluation. On the other hand, our results also indicate that GDE measurements without the utilization of an ionomer membrane allow for the study of oxygen mass transport properties independent of other transport phenomena, which is typically not possible in a MEA setup. This valuable information will help guide future applications of the GDE technique for the evaluation of fuel cell electrocatalysts.

Author contributions

N. Schmitt: writing – original draft, writing – review & editing, conceptualization, visualization, methodology, investigation M. Schmidt + M. Trabold + K. Jeschonek: writing – review & editing, investigation J. Mueller + L. Schmidt: writing – review & editing, project administration, conceptualization; B. Etzold: writing – review & editing, supervision, conceptualization, funding acquisition.

Conflicts of interest

There are no conflicts of interest to declare.

Acknowledgements

This work was supported financially by the Volkswagen AG. The results, opinions and conclusions expressed in this publication are not necessarily those of Volkswagen Aktiengesellschaft.

References

1 Y. Wang, Y. Pang, H. Xu, A. Martinez and K. S. Chen, *Energy Environ. Sci.*, 2022, **15**, 2288–2328.
2 Y. Wang, D. F. R. Diaz, K. S. Chen, Z. Wang and X. C. Adroher, *Mater. Today*, 2020, **32**, 178–203.
3 A. Alaswad, A. Omran, J. R. Sodre, T. Wilberforce, G. Pignatelli, M. Dassisti, A. Baroutaji and A. G. Olabi, *Energies*, 2020, **14**, 144.
4 B. Han, C. E. Carlton, A. Kongkanand, R. S. Kukreja, B. R. Theobald and L. Gan, *Energy Environ. Sci.*, 2015, **8**, 258–266.
5 I. E. L. Stephens, J. Rossmeisl and I. Chorkendorff, *Science*, 2016, **354**, 1378–1379.
6 A. Ly, T. Asset and P. Atanassov, *J. Power Sources*, 2020, **478**, 228516.
7 M. K. Debe, *Nature*, 2012, **486**, 43–51.
8 T. J. Schmidt, H. A. Gasteiger, G. D. Stäb, P. M. Urban, D. M. Kolb and R. J. Behm, *J. Electrochem. Soc.*, 1998, **145**, 2354.
9 H. A. Gasteiger and S. G. Yan, *J. Power Sources*, 2004, **127**, 162–171.
10 K. Shinozaki, J. W. Zack, S. Pylypenko, B. S. Pivovar and S. S. Kocha, *J. Electrochem. Soc.*, 2015, **162**, F1384.
11 Y. Garsany, I. L. Singer and K. E. Swider-Lyons, *J. Electroanal. Chem.*, 2011, **662**, 396–406.
12 H. A. Gasteiger, S. S. Kocha, B. Sompalli and F. T. Wagner, *Appl. Catal., B*, 2005, **56**, 9–35.
13 Y. Garsany, J. Ge, J. St-Pierre, R. Rocheleau and K. E. Swider-Lyons, *J. Electrochem. Soc.*, 2014, **161**, F628.
14 K. Ehelebe, D. Seeberger, M. T. Y. Paul, S. Thiele, K. J. J. Mayrhofer and S. Cherevko, *J. Electrochem. Soc.*, 2019, **166**, F1259.
15 M. Inaba, A. W. Jensen, G. W. Sievers, M. Escudero-Escribano, A. Zana and M. Arenz, *Energy Environ. Sci.*, 2018, **11**, 988–994.
16 B. A. Pinaud, A. Bonakdarpour, L. Daniel, J. Sharman and D. P. Wilkinson, *J. Electrochem. Soc.*, 2017, **164**, F321–F327, DOI: **10.1149/2.0891704jes**.

© 2023 The Author(s). Published by the Royal Society of Chemistry

Open Access Article. Published on 04 May 2023. Downloaded on 11/9/2023 4:50:48 PM.
This article is licensed under a Creative Commons Attribution 3.0 Unported Licence.

17 C. Zalitis, A. Kucernak, X. Lin and J. Sharman, *ACS Catalysis*, 2020, **10**, 4361–4376.
18 C. M. Zalitis, D. Kramer and A. R. Kucernak, *Phys. Chem. Chem. Phys.*, 2013, **15**, 4329–4340, DOI: 10.1039/C3CP44431G.
19 G. K. H. Wiberg, M. Fleige and M. Arenz, *Rev. Sci. Instrum.*, 2015, **86**, 24102.
20 J. Schröder, J. Quinson, J. K. Mathiesen, J. J. K. Kirkensgaard, S. Alinejad, V. A. Mints and M. Arenz, *J. Electrochem. Soc.*, 2020, **167**, 134515.
21 S. Alinejad, M. Inaba, J. Schröder, J. Du, J. Quinson, A. Zana and M. Arenz, *J. Phys.: Energy*, 2020, **2**, 24003.
22 K. Ehelebe, N. Schmitt, G. Sievers, A. W. Jensen, A. Hrnjić, P. Collantes Jiménez, P. Kaiser, M. Geuß, Y.-P. Ku and P. Jovanovič, *ACS Energy Lett.*, 2022, **7**, 816–826.
23 G. K. H. Wiberg, S. Nösberger and M. Arenz, *Curr. Opin. Electrochem.*, 2022, 101129.
24 S. Nösberger, J. Du, J. Quinson, E. Berner, A. Zana, G. K. H. Wiberg and M. Arenz, *Electrochem. Sci. Adv.*, 2021, e2100190.
25 A. Hrnjić, F. Ruiz-Zepeda, M. Gaberšček, M. Bele, L. Suhadolnik, N. Hodnik and P. Jovanovič, *J. Electrochem. Soc.*, 2020, **167**, 166501.
26 N. Schmitt, M. Schmidt, G. Hübner and B. J. M. Etzold, *J. Power Sources*, 2022, **539**, 231530.
27 J. G. Petrovick, G. C. Anderson, D. I. Kushner, N. Danilovic and A. Z. Weber, *J. Electrochem. Soc.*, 2021, **168**, 56517.
28 K. Ehelebe, J. Knöppel, M. Bierling, B. Mayerhöfer, T. Böhm, N. Kulyk, S. Thiele, K. J. J. Mayrhofer and S. Cherevko, *Angew. Chem.*, 2021, **133**, 8964–8970.
29 U. Kernchen, B. Etzold, W. Korth and A. Jess, *Chem. Eng. Technol.*, 2007, **30**, 985–994.
30 J. Snyder, T. Fujita, M. W. Chen and J. Erlebacher, *Nat. Mater.*, 2010, **9**, 904–907.
31 G.-R. Zhang, M. Munoz and B. J. M. Etzold, *ACS Appl. Mater. Interfaces*, 2015, **7**, 3562–3570, DOI: 10.1021/am5074003.
32 G.-R. Zhang, T. Wolker, D. J. S. Sandbeck, M. Munoz, K. J. J. Mayrhofer, S. Cherevko and B. J. M. Etzold, *ACS Catalysis*, 2018, **8**, 8244–8254.
33 G.-R. Zhang, M. Munoz and B. J. M. Etzold, *Angew. Chem., Int. Ed.*, 2016, **55**, 2257–2261.
34 M. George, G.-R. Zhang, N. Schmitt, K. Brunnengräber, D. J. S. Sandbeck, K. J. J. Mayrhofer, S. Cherevko and B. J. M. Etzold, *ACS Catalysis*, 2019, **9**, 8682–8692.
35 J. Snyder, K. Livi and J. Erlebacher, *Adv. Funct. Mater.*, 2013, **23**, 5494–5501.
36 H. Zhang, J. Liang, B. Xia, Y. Li and S. Du, *Front. Chem. Sci. Eng.*, 2019, **13**, 695–701.
37 A. Avid, J. L. Ochoa, Y. Huang, Y. Liu, P. Atanassov and I. V. Zenyuk, *Nat. Commun.*, 2022, **13**, 1–13.
38 R. Arrigo, M. Hävecker, S. Wrabetz, R. Blume, M. Lerch, J. McGregor, E. P. J. Parrott, J. A. Zeitler, L. F. Gladden and A. Knop-Gericke, *J. Am. Chem. Soc.*, 2010, **132**, 9616–9630.
39 A. Orfanidi, P. Madkikar, H. A. El-Sayed, G. S. Harzer, T. Kratky and H. A. Gasteiger, *J. Electrochem. Soc.*, 2017, **164**, F418.
40 S. Ott, A. Orfanidi, H. Schmies, B. Anke, H. N. Nong, J. Hübner, U. Gernert, M. Gliech, M. Lerch and P. Strasser, *Nat. Mater.*, 2020, **19**, 77–85.
41 H. Schmies, E. Hornberger, B. Anke, T. Jurzinsky, H. N. Nong, F. Dionigi, S. Kühl, J. Drnec, M. Lerch and C. Cremers, *Chem. Mater.*, 2018, **30**, 7287–7295.
42 L.-X. Sun and T. Okada, *J. Membr. Sci.*, 2001, **183**, 213–221.
43 K. Miyazaki, N. Sugimura, K. Kawakita, T. Abe, K. Nishio, H. Nakanishi, M. Matsuoka and Z. Ogumi, *J. Electrochem. Soc.*, 2010, **157**, A1153, DOI: 10.1149/1.3483105.
44 A. Weiß, M. Munoz, A. Haas, F. Rietzler, H.-P. Steinrück, M. Haumann, P. Wasserscheid and B. J. M. Etzold, *ACS Catalysis*, 2016, **6**, 2280–2286.
45 N. Schmitt, M. Schmidt, J. E. Mueller, L. Schmidt and B. J. M. Etzold, *Electrochem. Commun.*, 2022, **141**, 107362.
46 G.-R. Zhang and B. J. M. Etzold, *Adv. Funct. Mater.*, 2021, **31**, 2010977.
47 G.-R. Zhang and B. J. M. Etzold, *J. Energy Chem.*, 2016, **25**, 199–207.
48 R. Alink, R. Singh, P. Schneider, K. Christmann, J. Schall, R. Keding and N. Zamel, *Molecules*, 2020, **25**, 1523.
49 Y. Liu, M. W. Murphy, D. R. Baker, W. Gu, C. Ji, J. Jorne and H. A. Gasteiger, *J. Electrochem. Soc.*, 2009, **156**, B970, DOI: 10.1149/1.3143965.
50 H. Liu, Y. Liu and J. Li, *Phys. Chem. Chem. Phys.*, 2010, **12**, 1685–1697.
51 K. Huang, T. Song, O. Morales-Collazo, H. Jia and J. F. Brennecke, *J. Electrochem. Soc.*, 2017, **164**, F1448.
52 X. Yan, F. Zhang, H. Zhang, H. Tang, M. Pan and P. Fang, *ACS Appl. Mater. Interfaces*, 2019, **11**, 6111–6117.
53 T. Soboleva, X. Zhao, K. Malek, Z. Xie, T. Navessin and S. Holdcroft, *ACS Appl. Mater. Interfaces*, 2010, **2**, 375–384.
54 A. Ohma, K. Fushinobu and K. Okazaki, *Electrochim. Acta*, 2010, **55**, 8829–8838.
55 K. Shinozaki, Y. Morimoto, B. S. Pivovar and S. S. Kocha, *J. Power Sources*, 2016, **325**, 745–751.
56 R. Anderson, M. Blanco, X. Bi and D. P. Wilkinson, *Int. J. Hydrogen Energy*, 2012, **37**, 16093–16103.
57 X. Lin, C. M. Zalitis, J. Sharman and A. Kucernak, *ACS Appl. Mater. Interfaces*, 2020, **12**, 47467–47481, DOI: 10.1021/acsami.0c12718.
58 S. Ott, F. Du, M. L. Luna, T. A. Dao, S. Selve, B. R. Cuenya, A. Orfanidi and P. Strasser, *Appl. Catal., B*, 2022, **306**, 121118.
59 C. Jackson, X. Lin, P. B. J. Levecque and A. R. J. Kucernak, *ACS Catal.*, 2022, **12**, 200–211, DOI: 10.1021/acscatal.1c03908.

© 2023 The Author(s). Published by the Royal Society of Chemistry

Electronic Supplementary Material (ESI) for Energy Advances.
This journal is © The Royal Society of Chemistry 2023

Supporting information

Which insights can gas diffusion electrode half-cell experiments give into activity trends and transport phenomena of membrane electrode assemblies?

Nicolai Schmitt[1], Mareike Schmidt[1], Jonathan E. Mueller[2], Lasse Schmidt[2], Michael Trabold[1], Katharina Jeschonek[1], Bastian J.M. Etzold[1,]*

[1]Technical University of Darmstadt, Department of Chemistry, Ernst-Berl-Institut für Technische und Makromolekulare Chemie, 64287 Darmstadt, Germany

[2] Volkswagen AG, 38436, Wolfsburg, Germany

[*]Corresponding author, E-Mail: bastian.etzold@tu-darmstadt.de

All data presented in the main article and in the supporting information is available from an open access repository:

DOIs:

Figure 1	https://doi.org/10.48328/tudatalib-1046
Figure 2	https://doi.org/10.48328/tudatalib-1047
Figure 3	https://doi.org/10.48328/tudatalib-1048
Figure S1	https://doi.org/10.48328/tudatalib-1049
Figure S2	https://doi.org/10.48328/tudatalib-1050
Figure S3	https://doi.org/10.48328/tudatalib-1051
Figure S4	https://doi.org/10.48328/tudatalib-1052
Figure S5	https://doi.org/10.48328/tudatalib-1053
Figure S6	https://doi.org/10.48328/tudatalib-1054

RDE measurements

RDE measurements were carried out on a Octostat5000 Multichannel Potentiostat by Ivium Technologies and controlled by IviumSoft software. A leak-free double-junction Ag/AgCl electrode (Aldrich) was used as reference electrode and a Pt wire (PINE) as counter electrode. All potentials shown in this work were calibrated against reversible hydrogen electrode (RHE) using hydrogen evolution-oxidation reaction on a Pt electrode. A glassy carbon rotating disk electrode (GC-RDE, 5 mm diameter, PINE) was used as working electrode. Before every measurement the RDE was cleaned by ultrasonication in ethanol, acetone and ultrapure water. In order to coat the RDE with catalyst at first a catalyst ink was prepared. Therefore, the catalyst powder was placed in an eppendorf tube together with 5 wt-% Nafion® solution and an ethanol/water-mixture as solvent. The amount of Nafion® solution was adapted to achieve an ionomer-to-carbon ratio (I/C ratio) of 0.5. The amount of solvent was chosen to achieve a Pt concentration in the catalyst ink of 0.393 mg mL^{-1}. The catalyst was finely dispersed in the solvent by ultrasonic treatment using an ultrasonic processor (Hielscher, UP200St). Afterwards 10 µL of the homogeneous catalyst ink were pipetted on the RDE to achieve a Pt loading on the electrode of 20 µg cm^{-2}. In order to ensure a uniform catalyst layer on the RDE the catalyst ink was dried under rotation at 700 rpm. The electrochemical measurements were conducted at room temperature in N_2-saturated 0.1 M $HClO_4$ solution. For determination of the electrochemically active surface area (ECSA), the catalyst was first electrochemically cleaned via potential cycling between 0.05 and 1.2 V (vs. RHE) at 500 mV s^{-1} for at least 200 cycles until the hydrogen adsorption/desorption signal was stable. Thereafter, CV curves in N_2-saturated 0.1 M HClO4 in a potential range between 0.05 and 1.2 V (vs. RHE) at 20 mV s^{-1} were measured and the charges associated with the hydrogen desorption signals were used to calculate the final ECSA, assuming 210 µC cm^{-2} for calibrating the desorption charge of a monolayer of hydrogen on a Pt surface.

For the determination of the catalyst activity for the ORR the electrolyte was saturated with O_2 for at least 20 min and O_2 bubbling was maintained during the measurement. Then 3 cycles were recorded under rotation of the RDE with 1600 rpm in a potential range of 1.05 - 0.05 V vs. RHE with a scan rate of 20 mV s^{-1}. The ORR activity was determined out of the resulting polarization curves regarding the anodic sweep of the third cycle. Therefore, the measured current was baseline corrected by a current recorded previously with the same settings in N_2 atmosphere. For the determination of the ORR activity the mass-transport corrected kinetic current $j_{kinetic}$ was calculated by using the *Koutecky-Levich* equation:

$$\frac{1}{j} = \frac{1}{j_{kinetic}} + \frac{1}{j_{diffusion}} \qquad \text{Equation 1}$$

where j is the baseline corrected experimentally measured current and $j_{diffusion}$ is the diffusion limited current. The kinetic current was calculated at 0.90 and 0.95 V vs. RHE. The calculated values were then normalized to the Pt mass, to obtain the mass specific activity (MSA).

GDE measurements

Catalyst coating of gas diffusion layers

For GDE evaluation, at first gas diffusion electrodes were prepared by catalyst coating of Sigracet 25 BC gas diffusion media. For catalyst ink preparation 4 mg of the respective catalyst sample were mixed together with deionized water (<1.1 µS cm^{-1}, VWR chemicals), ultrapure ethanol and ionomer (Aquivion® D98-25BS, Sigma-Aldrich) in an Eppendorf tube and finely dispersed with the use of an ultrasonic processor (Hielscher, UP200St). The total volume of ethanol and water was chosen to achieve a Pt concentration in the catalyst ink of 0.393 mg mL^{-1}. The ionomer/carbon ratio was held at 0.5 g g^{-1} and the volume percentage of ethanol in the catalyst ink was set to a value of 45 %. For application of the catalyst on the GDL the prepared catalyst ink was further diluted with an ethanol/ water (45 % EtOH) in the ratio 1:1 and, finally, a volume of the resulting catalyst ink corresponding to a theoretical loading of 100 μg_{Pt} cm^{-2} was pipetted onto the GDL, which is fixed in an alumina body preheated to 125 °C on a heating plate. The coated area is restricted by a PTFE mask, that is mounted onto the alumina body and having a round hole of varying diameter. In the present work PTFE masks resulting in catalyst coated areas of 0.785 cm^2 for the IL modified samples and 0.5 cm^2 for the N-doped catalysts were utilized.

Electrochemical protocol for GDE evaluation

GDE measurements were carried out in an automated setup, that is controlled using a single self-developed LabVIEW-based software application. As the measurement cell, a commercially available half-cell (FlexCell® PTFE, Gaskatel GmbH) was utilized at room temperature using 2 M perchloric acid (ROTIPURAN®Ultra 70 %, Carl-Roth), that was diluted with ultrapure water, serving as the electrolyte.

The electrochemical active surface area (ECSA) was determined by integrating the hydrogen desorption area (H_{UPD}) of the CVs in N_2-atmosphere at a scan rate 100 mV s^{-1}, carried out after 200 activation cycles between 0.05 and 1.2 V vs. RHE at 500 mV s^{-1}. Additionally, CO-Stripping was carried out at a scan rate of 20 mV s^{-1} for determination of the ECSA. For ORR activity evaluation a galvanostatic step protocol is utilized, which is summarized in Table S1. For constructing the ORR polarization curves, the last 3 s of each current step were used, considering only the anodic sweep. The uncompensated resistance (iR drop) in the utilized GDE setup was determined using electrochemical impedance spectroscopy (EIS) and was used for post-correction of all measured potentials. In order to avoid any overcorrection of the iR drop due to heating of the electrolyte, for the

two highest measured current densities, the iR drop was determined separately during the course of the polarization curve measurement via EIS and used for post-correction of the potentials measured at these currents. All lower currents were corrected by using a uniform value determined at the beginning of the electrochemical evaluation (Step 1 in Table S1). For each experiment at least two samples have been tested. During the course of the measurement, the electrolyte chamber is constantly purged with 50 mL min^{-1} N_2, while the gas flow to the gas chamber is adapted for the respective method.

Table S1: Protocol for the electrochemical characterization for 0.785 cm^2 catalyst spot size.

Step		Method	Parameter	
1	Determination of iR drop	EIS galvanostatic	Gas flow	N_2 (~300 mL min^{-1})
			EIS frequency range	10000-1 Hz
			EIS amplitude	0.05 A
			Current	0 mA
2	Electrochemical cleaning	Cyclic voltammetry (CV)	Gas flow	N_2 (~300 mL min^{-1})
			Potential limits	0.05 – 1.2 V
			Scan rate	500 mV s^{-1}
			Number of cycles	~200 (until CV constant)
3	ECSA (N_2)	CV	Gas flow	N_2 (~300 mL min^{-1})
			Potential limits	0.05 – 1.2 V
			Scan rate	100 mV s^{-1}
			Number of cycles	3
4	Formation of CO-monolayer	Chronoamperometry (CA)	Gas flow	First 2 min: CO (~200 mL min^{-1}) Remaining time: N_2 (~500 mL min^{-1})
			Potential	0.1 V
			Time	60 min
5	ECSA (CO)	CV	Gas flow	N_2 (~300 mL min^{-1})
			Potential limits	0.1 – 1.0 V
			Scan rate	20 mV s^{-1}
			Number of cycles	3
6	ORR (O_2)	Galvanostatic staircase	Gas flow	O_2 (~200 mL min^{-1})
			Pt-reduction step	0.1 V for 300 s in N_2 (~300 mL min^{-1})
			Current steps* (holding time)	OCV (600 s); -0.04 mA; -0.08 mA (90 s); -0.20 mA; -0.40 mA (60 s); -0.80 mA; -2.00 mA; -4.00 mA; -8.00 mA (30 s) -20 mA; -40 mA; -80 mA; -200 mA; -400 mA; -800 mA; -1200 mA (5 s) →in negative and positive direction
7	ORR (Synthetic air)			See 6

*for 0.5 cm^2 catalyst spot size, the applied currents were adapted to reach identical geometric current densities compared to 0.785 cm^2 catalyst spot size. Additionally, a measurement point at a current density of -2500 mA cm^{-2}_{geo} was added.

Thermodynamic and kinetic correction of GDE data for comparison with MEA data

In order to compare GDE and MEA results for the N-modified samples, the GDE data was corrected for the differing reaction conditions (temperature + partial pressure of oxygen reactant). Therefore, following [1], a kinetic and a thermodynamic correction of the GDE data was carried out. Thermodynamic correction was carried out using Nernst equation, whereby the influence of oxygen partial pressure and temperature on the Redox potential can be taken into account (see equation 2+3). For this comparison only MEA data collected at 100 %RH in oxygen atmosphere and GDE data measured in oxygen atmosphere was considered.

$$E(a_i, T) = E^0(T) - \frac{RT}{zF}\ln\left(\frac{a_{H2O}}{a_{H2}a_{O2}{}^{0.5}}\right) = E^0(T) + \Delta E^{conc}(a_i, T) \qquad \text{Equation 2}$$

With

$$E^0(T) = E^0(T^0) + \frac{\Delta s^0(T^0)}{zF}(T - T^0)$$

$$T^0 = 298.15\ K \rightarrow E^0(T^0) = 1.229\ V; z = 2, F = 96485\frac{C}{mol}; R = 8{,}314\ \frac{J}{K\ mol}$$

$$\Delta s^0(T^0) = s^0_{H2O} - s^0_{H2} + 0.5\ s^0_{O2} = -163.3\frac{J}{K\ mol}$$

$$a_{H2O} = 1; a_{\frac{o2}{H2}} = \frac{p_{system} - p_{H2O}(T_{Humidifier})}{p^0};\ p^0 = 1.013\ bar$$

$$MEA{:}T = 80°C, p_{H2O} = 0.476\ bar \quad GDE{:}T = 20°C, p_{H2O} = 0.023\ bar\ (asssuming\ 100\ \%RH)$$

$$E_{GDE,\,corr} = E_{GDE} + \left[E(a_{MEA}, T_{MEA}) - E(a_{GDE}, T_{GDE})\right] = E_{GDE} - 65\ mV \qquad \text{Equation 3}$$

For kinetic correction, the concentration effect on the kinetics is taken into account following equation 4:

$$j_{GDE,\,corr} = j_{GDE}\frac{p_{O2,\,MEA}}{p_{O2,\,GDE}} = 0.54\ j_{GDE} \qquad \text{Equation 4}$$

Inductively coupled plasma optical emission spectrometry

Inductively coupled plasma optical emission spectroscopy (ICP-OES, Perkin Elmer Optima 2000DV) was used to determine the platinum loading on the prepared N-doped and undoped Pt/KB catalyst samples. From each sample approximately 5 mg was taken and weighed into a vial. The vials were heated up in a muffle oven (Nabertherm® N7) to a temperature of 800 °C. The temperature was kept for four hours to eliminate the entire carbon from the catalyst. After cooling down, 5 mL of fresh aqua regia were added to the remaining residue. Afterwards, the samples were let stand for five days for full dissolution of platinum and then diluted with deionized water to a total volume of 50 mL. These samples were finally used for ICP-OES analysis.

Table S2: Pt content of the synthesized Pt/C catalysts with and without N-doped carbon support determined via ICP-OES.

Sample	Pt-content / $wt.\%$
Pt/C	30
N-mod Pt/C	38

Nitrogen Physisorption

Nitrogen physisorption was used to determine the specific surface area and the pore volume of the N-doped and undoped Ketjenblack carbon support. For all measurements the measuring device Quadrasorb evo (Quantachrome Instruments) was used.

Therefore, around 30 mg of the respective carbon support were measured into the glass tubes and then degassed in vacuum. For degassing, the samples were heated to 200 °C with a heating ramp of 2.5 K min^{-1} and held at this temperature for 15 h. After cooling down, the samples were transferred to the sample room, evacuated and cooled down to 77 K with liquid nitrogen. The adsorption and desorption isotherms were recorded in a range of $10^{-5} \leq p/p_0 \leq 0.995$ with p_0 as the saturation pressure and p as gas pressure. The BET method was applied to evaluate the overall surface area by using a multipoint fit in the range of $0.04 \leq p/p_0 \leq 0.2$. Additionally, a DFT model was applied for determination of the specific surface area and for determination of the specific pore volume. The evaluation is carried out by using the software VersaWin.

Sample	BET surface area / $m^2 g^{-1}$	QSDFT surface area / $m^2 g^{-1}$	QSDFT specific pore volume / $cm^2 g^{-1}$
KB EC300-J	774	744	1.404
N-mod KB	792	760	1.445

Table S3: Results of the physisorption analysis of the unmodified and the N-doped Ketjenblack carbon support.

Elementary analysis

Elementary analysis was used to analyze the content of nitrogen, hydrogen and carbon of the N-doped and undoped Ketjenblack carbon support. The oxygen content was further calculated from the remaining difference after combustion of the sample. The measurements were carried out on the measuring device VarioEL III CHN (Company Elementar).

Table S4: Results of the elemental analysis of the unmodified and the N-doped Ketjenblack carbon support.

Sample	C / $at\%$	N / $at\%$	H / $at\%$	O / $at\%$
KB EC300-J	98.92 $\pm$ 0.01	-	-	1.08
N-mod KB	98.21 $\pm$ 0.01	0.23 $\pm$ 0.01	0.36 $\pm$ 0.00	1.18

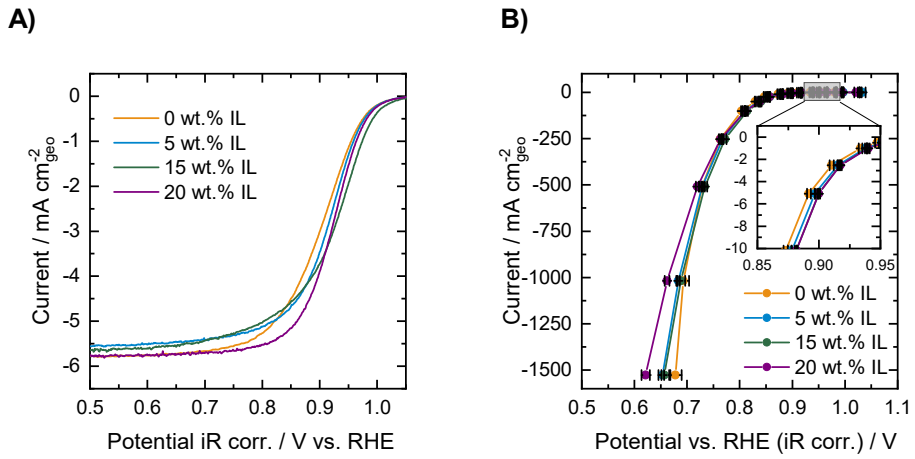

Figure S1: ORR activity of Pt/C catalyst modified with [BMIM][beti]. A) ORR polarization curves obtained in RDE measurements at room temperature in oxygen saturated 0.1 M $HClO_4$ and 1600 rpm at a catalyst loading of 20 μg_{Pt} cm^{-2}. B) ORR polarization curves obtained in GDE measurements at room temperature in oxygen atmosphere in 2 M $HClO_4$ at a catalyst loading of 100 μg_{Pt} cm^{-2}.

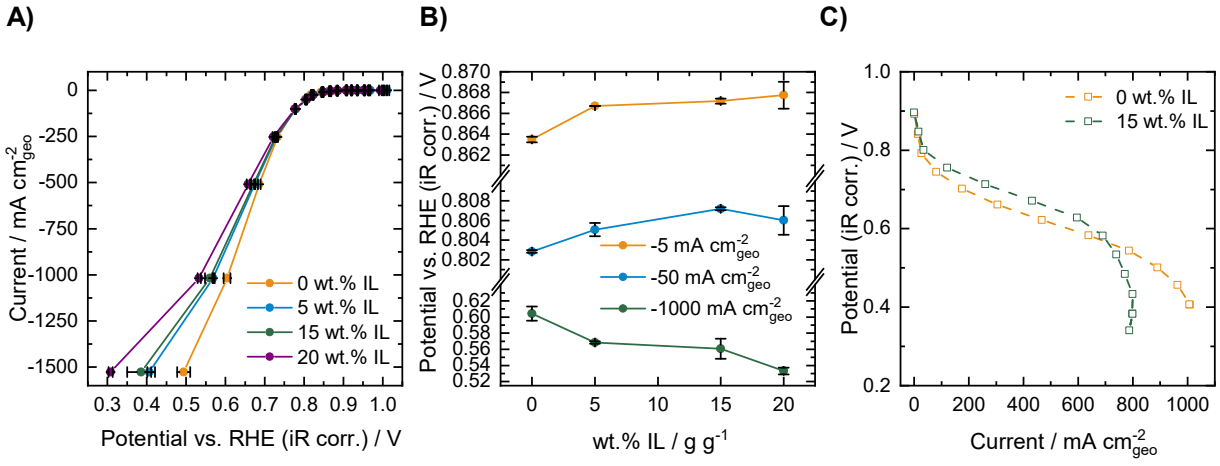

Figure S2: ORR activity of Pt/C catalyst modified with [BMIM][beti] in synthetic air. A) ORR polarization curves obtained in GDE measurements at room temperature in synthetic air in 2 M $HClO_4$ at a catalyst loading of 100 μg_{Pt} cm^{-2}. B) ORR potentials at different current densities depending on the amount of IL obtained in GDE measurements. C) ORR polarization curve of

unmodified Pt/C and Pt/C modified with 15 wt.% of IL measured in a MEA at 80 °C, and 100%RH synthetic air (1 atm) at a catalyst loading of 100 μg_{Pt} cm^{-2}.

Table S5: Pt loadings of the gas diffusion layers coated with the synthesized Pt/C catalysts with and without N-doped carbon support and analyzed in GDE half-cell and in MEA measurements.

Sample	GDE half-cell loading / μg_{Pt} cm^{-2}	MEA cathode loading / μg_{Pt} cm^{-2}
Pt/C I/C 0.1 #1	75	172
Pt/C I/C 0.1 #2	75	163
N mod. Pt/C I/C 0.1 #1	99	215
N mod. Pt/C I/C 0.1 #2	99	219
Pt/C I/C 0.5 #1	75	194
Pt/C I/C 0.5 #2	75	204
N mod. Pt/C I/C 0.5 #1	101	253
N mod. Pt/C I/C 0.5 #2	101	237
Pt/C I/C 1.7 #1	75	187
Pt/C I/C 1.7 #2	75	173
N mod. Pt/C I/C 1.7 #1	102	270
N mod. Pt/C I/C 1.7 #2	102	250

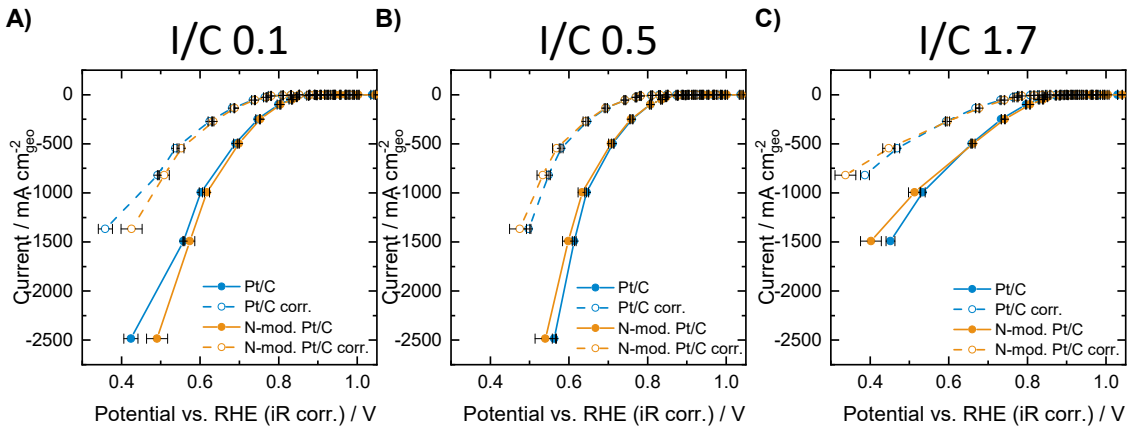

Figure S3: ORR polarization curves of the unmodified and N-doped Pt/C catalysts obtained in the GDE half-cell (data collected at room temperature in 2 M $HClO_4$ in oxygen atmosphere) before and after thermodynamic and kinetic correction for MEA conditions (80 °C, 100 %RH). A) I/C ratio = 0.1 B) I/C ratio = 0.5 C) I/C ratio = 1.7.

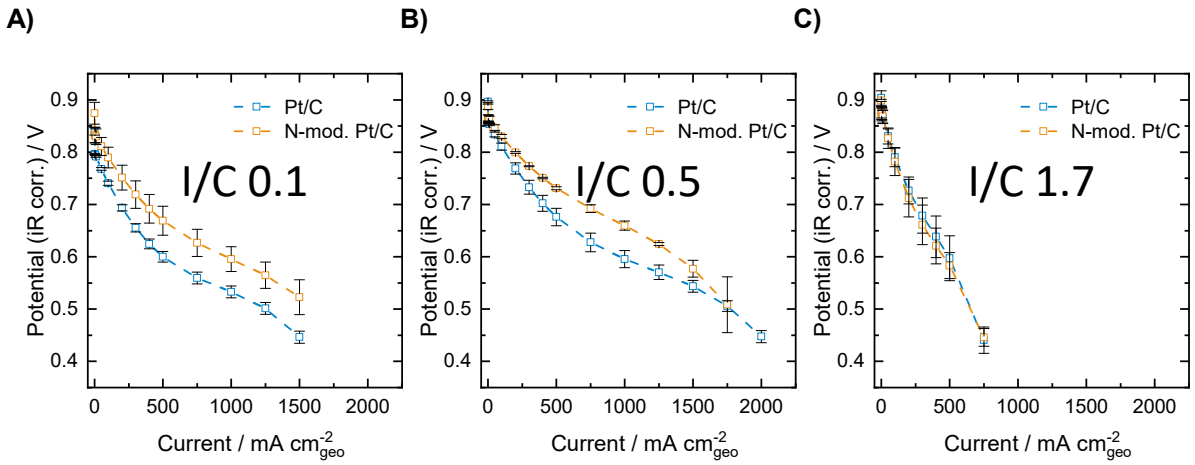

Figure S4: ORR polarization curves of the unmodified and N-doped Pt/C catalysts obtained in MEA measurements at 80 °C and 100 %RH in oxygen atmosphere (1 atm) A) I/C ratio = 0.1 B) I/C ratio = 0.5 C) I/C ratio = 1.7.

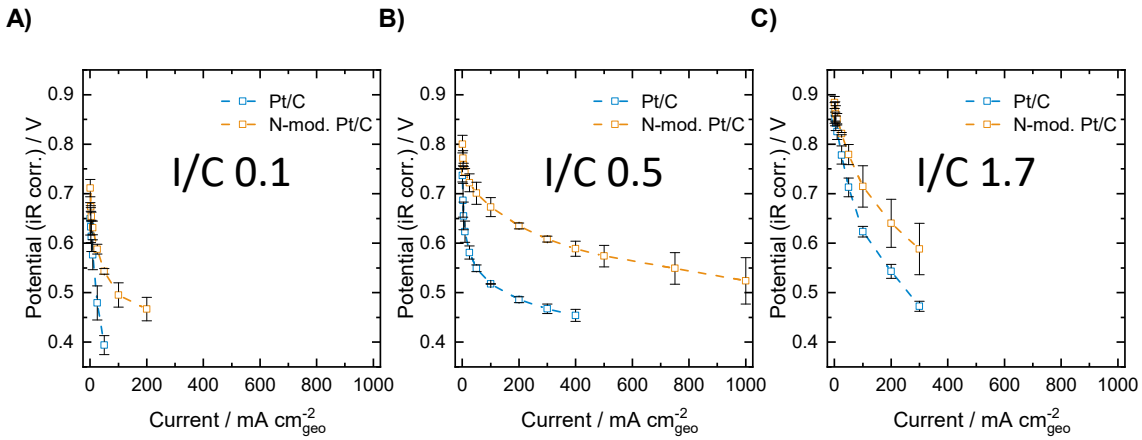

Figure S5: ORR polarization curves of the unmodified and N-doped Pt/C catalysts obtained in MEA measurements at 80 °C and 17 %RH in oxygen atmosphere (1 atm) A) I/C ratio = 0.1 B) I/C ratio = 0.5 C) I/C ratio = 1.7.

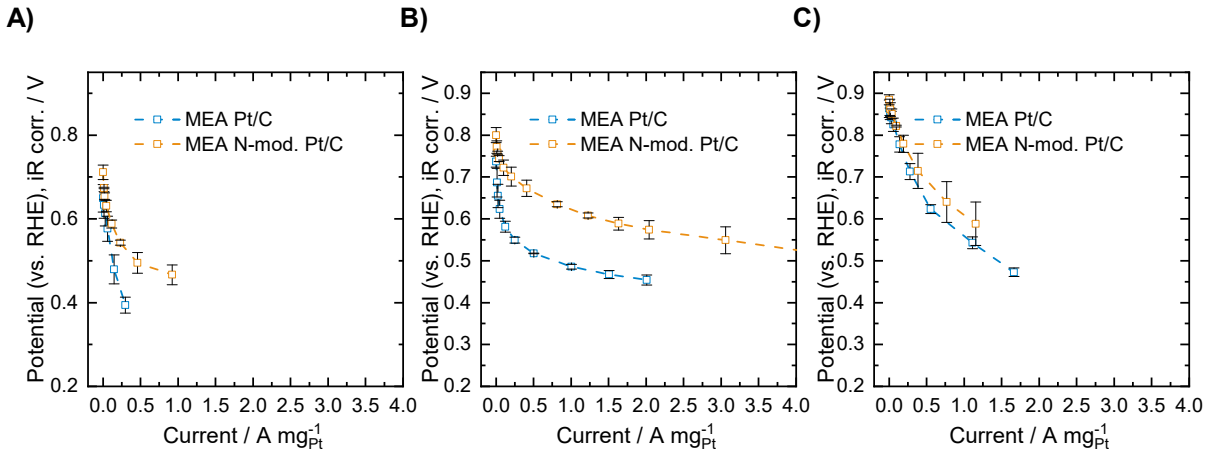

Figure S6: Mass specific ORR polarization curves of the unmodified and N-doped Pt/C catalysts obtained in MEA measurements at 80 °C and 17 %RH in oxygen atmosphere (1 atm) A) I/C ratio = 0.1 B) I/C ratio = 0.5 C) I/C ratio = 1.7.

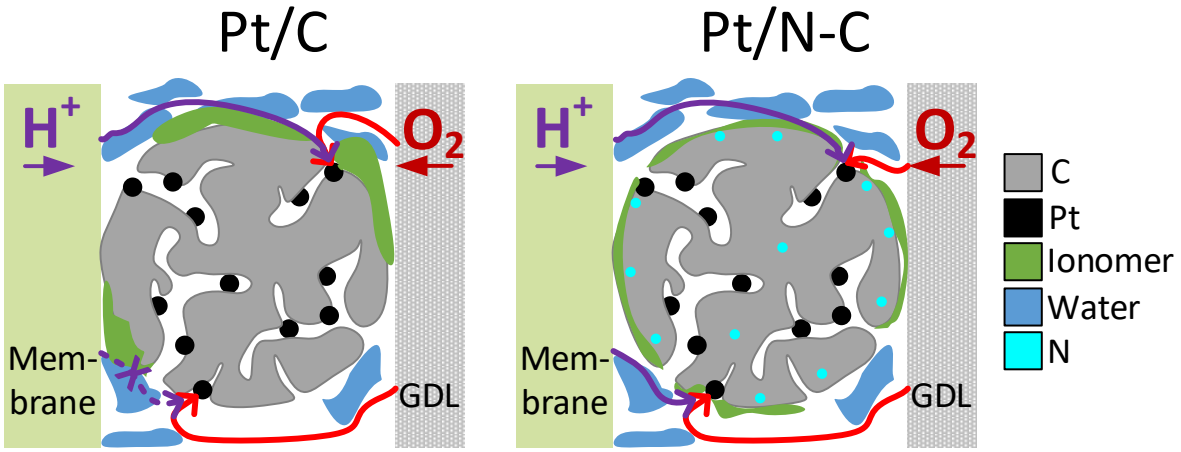

Figure S7: Schematic illustration of oxygen and proton transport pathways being affected by N-doping of Pt/C for low I/C ratio in MEA measurements.

References

[1] K. Ehelebe, D. Seeberger, M.T.Y. Paul, S. Thiele, K.J.J. Mayrhofer, S. Cherevko, Journal of the Electrochemical Society 166 (2019) F1259.

5. Summary and outlook

The aim of this thesis was to figure out if gas diffusion electrode (GDE) half-cell testing allows to overcome the limited significance of fundamental rotating disk electrode (RDE) testing in predicting activity of PEMFC catalysts towards the oxygen reduction reaction (ORR). In detail, the thesis addressed the questions, how reproducible high current density GDE half-cell testing can be carried out and which insights can be gained through the GDE approach. Achievements within this thesis can be summarized as follows:

A commercially available half-cell GDE setup could be established for fast and highly reproducible testing of ORR catalysts in realistic catalyst layers and with application-oriented catalyst loadings in fuel cell relevant current and potential regimes. Thereby, best practice advice could be derived regarding preparation of gas diffusion electrodes, measurement of the electrochemical active surface area and measurement of ORR polarization curves. Hereby, optimization of GDE preparation focused on maximizing the 3-phase boundary during GDE application by fine-tuning the procedure and the catalyst ink composition during catalyst coating on the gas diffusion layer (GDL) substrate. Also, different GDL types were compared to each other. Regarding ORR polarization curve measurement, it could be shown that a protocol based on galvanic steps with minimized holding time at the higher current densities allows to avoid undesirable heating of the electrolyte during evaluation and ensures reliability and reproducibility of the collected data. Thereby it was feasible to analyze catalyst loadings up to 0.4 mg cm^{-2}_{Pt} without severe mass transport limitations. Also, the significance of iR correction of the polarization curves during GDE evaluation was considered. Therefore, the two techniques current interrupt (CI) and electrochemical impedance spectroscopy (EIS) were compared to each other for determination of the uncompensated resistance (iR drop) within the electrochemical setup. Based on these findings a protocol utilizing EIS was proposed with the iR drop being determined separately for every single high current density measurement point. These measures allow to avoid overcorrection of the measured ORR potentials during GDE evaluation.

Furthermore, an important step was to further develop the GDE setup in order to avoid limitations of the maximum current density, that can be reached. Therefore, measures including minimizing the distance of the electrodes to each other, utilizing a higher surface area counter electrode, minimizing the catalyst coated area at the working electrode and increasing the perchloric acid electrolyte concentration were proposed. While earlier publications on GDE testing were limited to maximum current densities around 2000 mA cm^{-2}_{geo}, thus not giving access to the full MEA current regime, application of the mentioned measures allowed to measure ORR activity up to around 4000 mA $cm^{-2}_{geo.}$ The measures even allowed to reach current densities as high as 10500 mA cm^{-2}_{geo}. However, it must be noted that at thus high current densities, which are also not reached in MEAs, the measured faradaic current is sum of both ORR and hydrogen evolution reaction (HER) taking place.

In the last part of the thesis, two model catalyst systems were comparatively analyzed in the half-cell GDE setup and in a single-cell MEA. The two catalyst systems were an ionic liquid (IL) modified and unmodified Pt/C catalyst, as well as Pt/C catalysts with and without nitrogen modified carbon support at different ionomer to carbon (I/C) ratios. For the IL modified catalyst, it could be shown that mass transport limitations arise from the IL modification in the high current density MEA regime, linked to a negative influence of the IL on oxygen diffusion. This behavior could be well described in the GDE half-cell, thus pointing out that GDE half-cells are superior compared to RDE testing in description of oxygen mass transport phenomena in realistic catalyst layers. For the second model catalyst, it was observed that N modification of the carbon support can significantly improve the MEA performance of the catalyst, especially at low I/C ratio in combination with dry conditions under low humidity. These improvements, being linked to optimized proton accessibility after N modification, could not be recognized within GDE half-cell testing with the catalyst layer in direct contact with the liquid electrolyte. Thus, similar to the situation in RDE testing, where the catalyst layer is flooded by the acidic electrolyte providing protons, GDE testing in this configuration is not optimal to give a full description of all transport phenomena in real fuel cells. Especially the complex interaction of catalyst and ionomer, which is key to a high performing MEA, can only be studied with limited significance. In order to overcome the observed limitations, it is suggested that introduction of an ionomer membrane between catalyst layer and electrolyte is necessary to simulate the exact catalyst environment in real MEAs. Future research needs to figure out, whether this is feasible without dramatically increasing the measurement effort during GDE evaluation and thus, without losing the benefit of simple and fast catalyst testing. Therefore, similarly to MEA testing, eventually gas humidity and temperature control would be required and also compression of GDE and ionomer membrane would first need to be established. Furthermore, identical to MEA testing, time–consuming optimization of the catalyst layer/membrane contact could be required for every new catalyst.

Based on these findings, this work highlights the promising potential of GDE half-cells for testing of ORR catalysts and helps guide future application of the technique in PEMFC catalyst research. A great benefit of three-electrode half-cell GDE testing coupled to external analytics is that it allows to study highly interesting phenomena in realistic catalyst layers under application-oriented conditions, which were not accessible so far with MEA testing alone. Near-future research needs to figure out, if GDE half-cell testing can also be used as wide-spread tool for fast, simple and reliable screening of novel ORR catalyst and thus become a standard tool in PEMFC research. Furthermore, application of GDE half-cell testing must not be limited to study catalysts for the ORR alone, but can also be used for catalyst layer optimization for other reactions, such as water electrolysis, electrochemical CO_2 reduction and organic electrosynthesis. Therefore, it could become an indispensable tool in the vibrant field of electrochemical reaction engineering, that will play a key role towards a sustainable future.

Abbreviations and symbols

Abbreviations

AFC	Alkaline fuel cell
Aq.	Aqueous
BEV	Battery electric vehicle
BP	Bipolar plate
CCM	Catalyst coated membrane
CCS	Catalyst coated substrate
CI	Current interrupt
CL	Catalyst layer
DFT	Density functional theory
DMFC	Direct methanol fuel cell
EIS	Electrochemical impedance spectroscopy
FE	Floating electrode
FCEV	Fuel cell electric vehicle
GDE	Gas diffusion electrode
GDL	Gas diffusion layer
GHG	Greenhouse gas
HER	Hydrogen evolution reaction
HOR	Hydrogen oxidation reaction
I/C	Ionomer to carbon
ICP	Inductively coupled plasma
IL	Ionic liquid
IL-TEM	Identical location transmission electron microscopy
MCFC	Molten carbonate fuel cell
MEA	Membrane electrode assembly
MPL	Microporous layer
MS	Mass spectrometry
ORR	Oxygen reduction reaction
PAFC	Phosphoric acid fuel cell
PAN	Polyacrylonitrile
PEM	Proton exchange membrane
PEMFC	Polymer electrolyte membrane fuel cell
PGM	Platin group metal

RDE	Rotating disk electrode
RHE	Reversible hydrogen electrode
SOFC	Solid oxide fuel cell

Symbols

c	Molar concentration	mol L^{-1}
F_{in}	Energy content of fuel input	J
ΔG	Gibbs free energy	J
ΔH	Enthalpy	J
E	Voltage	V
ECSA	Electrochemically Active Surface Area	$m^2 g_{Pt}^{-1}$
F	Faraday constant	96485 C mol^{-1}
j	Current	A
M	Molecular weight	g mol^{-1}
n	Molar amount	mol
Q	Amount of electric charge	A s^{-1}
rpm	Revolutions per minute	s^{-1}
t	Time	s

Literature

[1] U. Nations, What Is Climate Change? | United Nations, 2023, https://www.un.org/en/climatechange/what-is-climate-change, accessed 24 April 2023.

[2] IPCC, "Summary for policymakers" in Climate Change 2022: Impacts, Adaptation, and Vulnerability, Cambridge University Press. In Press Cambridge, 2022.

[3] K. Abbass, M.Z. Qasim, H. Song, M. Murshed, H. Mahmood, I. Younis, Environmental Science and Pollution Research 29 (2022) 42539–42559.

[4] Global Monitoring Laboratory - Carbon Cycle Greenhouse Gases, 2023, https://gml.noaa.gov/ccgg/trends/mlo.html, accessed 24 April 2023.

[5] AR6 Synthesis Report: Climate Change 2023, 2023, https://www.ipcc.ch/report/ar6/syr/, accessed 24 April 2023.

[6] Paris agreement, HeinOnline, 2015.

[7] Hannah Ritchie, Max Roser, Pablo Rosado, Our World in Data (2020).

[8] J. Tian, L. Yu, R. Xue, S. Zhuang, Y. Shan, Applied energy 307 (2022) 118205.

[9] T. Capurso, M. Stefanizzi, M. Torresi, S.M. Camporeale, Energy Conversion and Management 251 (2022) 114898.

[10] L. Pingkuo, H. Xue, International Journal of Hydrogen Energy 47 (2022) 9485–9503.

[11] M. Dvoynikov, G. Buslaev, A. Kunshin, D. Sidorov, A. Kraslawski, M. Budovskaya, Resources 10 (2021) 3. https://doi.org/10.3390/resources10010003.

[12] A.I. Osman, N. Mehta, A.M. Elgarahy, M. Hefny, A. Al-Hinai, A.H. Al-Muhtaseb, D.W. Rooney, Environmental Chemistry Letters (2022) 1–36.

[13] Hydrogen, 2023, https://www.irena.org/Energy-Transition/Technology/Hydrogen, accessed 24 April 2023.

[14] Renewable Electrolysis, 2023, https://www.nrel.gov/hydrogen/renewable-electrolysis.html, accessed 25 April 2023.

[15] Y. Wang, D.F.R. Diaz, K.S. Chen, Z. Wang, X.C. Adroher, Materials today 32 (2020) 178–203.

[16] L. Fan, H. Deng, Y. Zhang, Q. Du, D.Y.C. Leung, Y. Wang, K. Jiao, Energy & Environmental Science (2023).

[17] T. Yoshida, K. Kojima, The Electrochemical Society Interface 24 (2015) 45.

[18] S. Herwartz, J. Pagenkopf, C. Streuling, International Journal of Hydrogen Energy 46 (2021) 29597–29615.

[19] P. Britz, N. Zartenar, Fuel Cells 4 (2004) 269–275.

[20] R.L. Borup, A. Kusoglu, K.C. Neyerlin, R. Mukundan, R.K. Ahluwalia, D.A. Cullen, K.L. More, A.Z. Weber, D.J. Myers, Current Opinion in Electrochemistry 21 (2020) 192–200.

[21] A. Alaswad, A. Omran, J.R. Sodre, T. Wilberforce, G. Pignatelli, M. Dassisti, A. Baroutaji, A.G. Olabi, Energies 14 (2020) 144.

[22] B. Han, C.E. Carlton, A. Kongkanand, R.S. Kukreja, B.R. Theobald, L. Gan, R. O'Malley, P. Strasser, F.T. Wagner, Y. Shao-Horn, Energy & Environmental Science 8 (2015) 258–266.

[23] A. Ly, T. Asset, P. Atanassov, Journal of Power Sources 478 (2020) 228516.

[24] I.E.L. Stephens, J. Rossmeisl, I. Chorkendorff, Science 354 (2016) 1378–1379.

[25] F. Barbir, PEM fuel cells: theory and practice, Academic press, 2012.

[26] Energy.gov, Comparison of Fuel Cell Technologies, 2023, https://www.energy.gov/eere/fuelcells/comparison-fuel-cell-technologies, accessed 25 April 2023.

[27] S. Mekhilef, R. Saidur, A. Safari, Renewable and Sustainable Energy Reviews 16 (2012) 981–989.

[28] R. O'hayre, S.-W. Cha, W. Colella, F.B. Prinz, Fuel cell fundamentals, John Wiley & Sons, 2016.

[29] Y. Wang, B. Seo, B. Wang, N. Zamel, K. Jiao, X.C. Adroher, Energy and AI 1 (2020) 100014.

[30] Mohrdieck, World Electric Vehicle Journal 3 (2009) 209–213.

[31] C. Palmer, Engineering 11 (2022) 9–11.
[32] D.A. Cullen, K.C. Neyerlin, R.K. Ahluwalia, R. Mukundan, K.L. More, R.L. Borup, A.Z. Weber, D.J. Myers, A. Kusoglu, Nature energy 6 (2021) 462–474.
[33] electrive.com, Hydrogen fuel cell aircraft – what for and when? - electrive.com, 2023, https://www.electrive.com/2022/08/26/hydrogen-fuel-cell-aircraft-what-for-and-when/, accessed 25 April 2023.
[34] DLRARTICLE DLR Portal, Fuel cells reduce ship emissions, 2023, https://www.dlr.de/content/en/articles/news/2021/02/20210518_nautilus-project.html, accessed 25 April 2023.
[35] S.K. Dash, S. Chakraborty, M. Roccotelli, U.K. Sahu, Sustainability 14 (2022) 8285.
[36] Viessmann.
[37] M.K. Debe, Nature 486 (2012) 43–51.
[38] Hyundai Motor Deutschland GmbH, Hyundai Nexo Technische Daten, https://www.hyundai.news/newsroom/dam/de/Pressemappen/Nexo/hyundai-nexo-sep2018-technische-daten.pdf, accessed 25 April 2023.
[39] Gasdiffusionsschichten für Polymerelektrolytbrennstoffzellen, 2023, https://www.sglcarbon.com/loesungen/anwendung/polymer-elektrolyt-membran-brennstoffzellen-pemfc/#, accessed 25 April 2023.
[40] Y. Song, C. Zhang, C.-Y. Ling, M. Han, R.-Y. Yong, D. Sun, J. Chen, International Journal of Hydrogen Energy 45 (2020) 29832–29847.
[41] Y. Yang, X. Zhou, B. Li, C. Zhang, International Journal of Hydrogen Energy 46 (2021) 4259–4282.
[42] Q. Chen, Z. Niu, H. Li, K. Jiao, Y. Wang, International Journal of Hydrogen Energy 46 (2021) 8640–8671.
[43] A.-C. Dupuis, Progress in Materials Science 56 (2011) 289–327.
[44] Nafionmembran, Chemours Nafion, Protonenaustauschmembran, 2023, https://www.nafion.de/products/sulfonic-membranes, accessed 8 May 2023.
[45] M. Chen, C. Zhao, F. Sun, J. Fan, H. Li, H. Wang, ETransportation 5 (2020) 100075.
[46] A.V. Da Rosa, J.C. Ordóñez, Fundamentals of renewable energy processes, Academic press, 2021.
[47] F. Barbir, T. Gomez, International Journal of Hydrogen Energy 22 (1997) 1027–1037.
[48] Z. Li, Z. Zheng, L. Xu, X. Lu, BMC Energy 1 (2019) 1–23.
[49] J.K. Nørskov, J. Rossmeisl, A. Logadottir, L. Lindqvist, J.R. Kitchin, T. Bligaard, H. Jonsson, The Journal of Physical Chemistry B 108 (2004) 17886–17892.
[50] J. Zhang, PEM fuel cell electrocatalysts and catalyst layers: fundamentals and applications, Springer Science & Business Media, 2008.
[51] H.S. Wroblowa, G. Razumney, Journal of Electroanalytical Chemistry and Interfacial Electrochemistry 69 (1976) 195–201.
[52] X. Yang, Y. Zeng, W. Alnoush, Y. Hou, D. Higgins, G. Wu, Advanced Materials 34 (2022) 2107954.
[53] R. Christensen, H.A. Hansen, C.F. Dickens, J.K. Nørskov, T. Vegge, The Journal of Physical Chemistry C 120 (2016) 24910–24916.
[54] Z.-F. Huang, J. Song, S. Dou, X. Li, J. Wang, X. Wang, Matter 1 (2019) 1494–1518.
[55] J.K. Nørskov, F. Abild-Pedersen, F. Studt, T. Bligaard, Proceedings of the National Academy of Sciences 108 (2011) 937–943.
[56] B. Hammer, J.K. Nørskov, Surface science 343 (1995) 211–220.
[57] V.R. Stamenkovic, B. Fowler, B.S. Mun, G. Wang, P.N. Ross, C.A. Lucas, N.M. Markovic, Science 315 (2007) 493–497.
[58] Z. Peng, H. Yang, Nano today 4 (2009) 143–164.
[59] M. Min, J. Cho, K. Cho, H. Kim, Electrochimica Acta 45 (2000) 4211–4217.
[60] A. Kulkarni, S. Siahrostami, A. Patel, J.K. Nørskov, Chemical Reviews 118 (2018) 2302–2312.

[61] K. Jayasayee, J.R. van Veen, T.G. Manivasagam, S. Celebi, E.J.M. Hensen, F.A. de Bruijn, Applied Catalysis B: Environmental 111 (2012) 515–526.
[62] S. Deshpande, J.R. Kitchin, V. Viswanathan, Acs Catalysis 6 (2016) 5251–5259.
[63] C. Fu, C. Liu, T. Li, X. Zhang, F. Wang, J. Yang, Y. Jiang, P. Cui, H. Li, Computational Materials Science 170 (2019) 109202.
[64] L. Gan, C. Cui, M. Heggen, F. Dionigi, S. Rudi, P. Strasser, Science 346 (2014) 1502–1506.
[65] X. Huang, Z. Zhao, L. Cao, Y. Chen, E. Zhu, Z. Lin, M. Li, A. Yan, A. Zettl, Y.M. Wang, Science 348 (2015) 1230–1234.
[66] X. Huang, Z. Zhao, Y. Chen, E. Zhu, M. Li, X. Duan, Y. Huang, Energy & Environmental Science 7 (2014) 2957–2962.
[67] Z. Zhao, M. Feng, J. Zhou, Z. Liu, M. Li, Z. Fan, O. Tsen, J. Miao, X. Duan, Y. Huang, Chemical Communications 52 (2016) 11215–11218.
[68] L. Liu, E. Pippel, Angewandte Chemie International Edition 50 (2011) 2729–2733.
[69] X. Zhang, H. Li, J. Yang, Y. Lei, C. Wang, J. Wang, Y. Tang, Z. Mao, RSC advances 11 (2021) 13316–13328.
[70] M. Shao, Q. Chang, J.-P. Dodelet, R. Chenitz, Chemical Reviews 116 (2016) 3594–3657.
[71] C. Zhang, X. Shen, Y. Pan, Z. Peng, Frontiers in Energy 11 (2017) 268–285.
[72] M. Shao, A. Peles, K. Shoemaker, Nano letters 11 (2011) 3714–3719.
[73] Y. Takasu, N. Ohashi, X.-G. Zhang, Y. Murakami, H. Minagawa, S. Sato, K. Yahikozawa, Electrochimica Acta 41 (1996) 2595–2600.
[74] S.M. Alia, G. Zhang, D. Kisailus, D. Li, S. Gu, K. Jensen, Y. Yan, Advanced Functional Materials 20 (2010) 3742–3746.
[75] S. Fu, C. Zhu, J. Song, M.H. Engelhard, H. Xia, D. Du, Y. Lin, ACS applied materials & interfaces 8 (2016) 35213–35218.
[76] D.S. He, D. He, J. Wang, Y. Lin, P. Yin, X. Hong, Y. Wu, Y. Li, Journal of the American Chemical Society 138 (2016) 1494–1497.
[77] L. Zhang, L.T. Roling, X. Wang, M. Vara, M. Chi, J. Liu, S.-I. Choi, J. Park, J.A. Herron, Z. Xie, Science 349 (2015) 412–416.
[78] S.L. Candelaria, Y. Shao, W. Zhou, X. Li, J. Xiao, J.-G. Zhang, Y. Wang, J. Liu, J. Li, G. Cao, Nano energy 1 (2012) 195–220.
[79] T.J. Schmidt, H.A. Gasteiger, G.D. Stäb, P.M. Urban, D.M. Kolb, R.J. Behm, Journal of the Electrochemical Society 145 (1998) 2354.
[80] E. Antolini, Applied Catalysis B: Environmental 88 (2009) 1–24.
[81] ICBA, Resources from ICBA — ICBA, 2023, https://www.carbon-black.org/resources-from-icba, accessed 9 May 2023.
[82] S. Sharma, B.G. Pollet, Journal of Power Sources 208 (2012) 96–119.
[83] B. Xie, Y. Zhang, R. Zhang, Journal of Materials Chemistry A 5 (2017) 17544–17548.
[84] J. Zhu, G. He, Z. Tian, L. Liang, P.K. Shen, Electrochimica Acta 194 (2016) 276–282.
[85] Y. Sun, S. Polani, F. Luo, S. Ott, P. Strasser, F. Dionigi, Nature communications 12 (2021) 5984.
[86] Z.W. Seh, J. Kibsgaard, C.F. Dickens, I.B. Chorkendorff, J.K. Nørskov, T.F. Jaramillo, Science 355 (2017) eaad4998.
[87] S. Shahgaldi, J. Hamelin, Carbon 94 (2015) 705–728.
[88] T.T. van Ho, C.-J. Pan, J. Rick, W.-N. Su, B.-J. Hwang, Journal of the American Chemical Society 133 (2011) 11716–11724.
[89] Y. Liu, W.E. Mustain, Journal of the American Chemical Society 135 (2013) 530–533.
[90] K. Ehelebe, T. Ashraf, S. Hager, D. Seeberger, S. Thiele, S. Cherevko, Electrochemistry communications 116 (2020) 106761.
[91] Y. Wang, J. Li, Z. Wei, Journal of Materials Chemistry A 6 (2018) 8194–8209.
[92] L. Yang, J. Shui, L. Du, Y. Shao, J. Liu, L. Dai, Z. Hu, Advanced Materials 31 (2019) 1804799.

[93] Z. Wu, M. Song, J. Wang, X. Liu, Catalysts 8 (2018) 196.
[94] C. Tang, Q. Zhang, Advanced Materials 29 (2017) 1604103.
[95] D. Banham, S. Ye, ACS Energy Letters 2 (2017) 629–638.
[96] K. Ehelebe, N. Schmitt, G. Sievers, A.W. Jensen, A. Hrnjić, P. Collantes Jiménez, P. Kaiser, M. Geuß, Y.-P. Ku, P. Jovanovič, Benchmarking fuel cell electrocatalysts using gas diffusion electrodes: Inter-lab comparison and best practices, ACS Publications, 2022.
[97] T. Lazaridis, B.M. Stühmeier, H.A. Gasteiger, H.A. El-Sayed, Nature Catalysis 5 (2022) 363–373.
[98] S. Martens, L. Asen, G. Ercolano, F. Dionigi, C. Zalitis, A. Hawkins, A.M. Bonastre, L. Seidl, A.C. Knoll, J. Sharman, Journal of Power Sources 392 (2018) 274–284.
[99] A.J. Bard, L.R. Faulkner, H.S. White, Electrochemical methods: fundamentals and applications, John Wiley & Sons, 2022.
[100] U.A. Paulus, T.J. Schmidt, H.A. Gasteiger, R.J. Behm, Journal of Electroanalytical Chemistry 495 (2001) 134–145.
[101] P. Kurzweil, Brennstoffzellentechnik, Springer, 2013.
[102] S.S. Kocha, Handbook of fuel cells (2010).
[103] V. Yarlagadda, S.E. McKinney, C.L. Keary, L. Thompson, B. Zulevi, A. Kongkanand, Journal of the Electrochemical Society 164 (2017) F845.
[104] N. Garland, T. Benjamin, J. Kopasz, ECS Transactions 11 (2007) 923.
[105] M. Inaba, J. Quinson, J.R. Bucher, M. Arenz, Journal of Visualized Experiments: JoVE (2018).
[106] S.S. Kocha, K. Shinozaki, J.W. Zack, D.J. Myers, N.N. Kariuki, T. Nowicki, V. Stamenkovic, Y. Kang, D. Li, D. Papageorgopoulos, Electrocatalysis 8 (2017) 366–374.
[107] Y. Garsany, J. Ge, J. St-Pierre, R. Rocheleau, K.E. Swider-Lyons, Journal of the Electrochemical Society 161 (2014) F628.
[108] J. Zhang, J. Wu, H. Zhang, J. Zhang, PEM fuel cell testing and diagnosis, Newnes, 2013.
[109] Z. Xing, K. Shi, X. Hu, X. Feng, Journal of Energy Chemistry 66 (2022) 45–51.
[110] Y. Garsany, I.L. Singer, K.E. Swider-Lyons, Journal of Electroanalytical Chemistry 662 (2011) 396–406.
[111] Y. Garsany, J. Ge, J. St-Pierre, R. Rocheleau, K. Swider-Lyons, ECS Transactions 58 (2013) 3.
[112] C. Zalitis, A. Kucernak, X. Lin, J. Sharman, Acs Catalysis 10 (2020) 4361–4376.
[113] K. Shinozaki, J.W. Zack, R.M. Richards, B.S. Pivovar, S.S. Kocha, Journal of the Electrochemical Society 162 (2015) F1144.
[114] K. Shinozaki, J.W. Zack, S. Pylypenko, B.S. Pivovar, S.S. Kocha, Journal of the Electrochemical Society 162 (2015) F1384.
[115] J. Fan, M. Chen, Z. Zhao, Z. Zhang, S. Ye, S. Xu, H. Wang, H. Li, Nature energy 6 (2021) 475–486.
[116] H.-E. Kim, J. Kwon, H. Lee, Chemical Science 13 (2022) 6782–6795.
[117] A. Kobayashi, T. Fujii, C. Harada, E. Yasumoto, K. Takeda, K. Kakinuma, M. Uchida, ACS Applied Energy Materials 4 (2021) 2307–2317.
[118] V. Yarlagadda, M.K. Carpenter, T.E. Moylan, R.S. Kukreja, R. Koestner, W. Gu, L. Thompson, A. Kongkanand, ACS Energy Letters 3 (2018) 618–621.
[119] J.P. Owejan, J.E. Owejan, W. Gu, Journal of the Electrochemical Society 160 (2013) F824.
[120] Y.-C. Park, H. Tokiwa, K. Kakinuma, M. Watanabe, M. Uchida, Journal of Power Sources 315 (2016) 179–191.
[121] R. Alink, R. Singh, P. Schneider, K. Christmann, J. Schall, R. Keding, N. Zamel, Molecules 25 (2020) 1523.
[122] Y. Liu, M.W. Murphy, D.R. Baker, W. Gu, C. Ji, J. Jorne, H.A. Gasteiger, Journal of the Electrochemical Society 156 (2009) B970.
[123] A. Orfanidi, P.J. Rheinländer, N. Schulte, H.A. Gasteiger, Journal of the Electrochemical Society 165 (2018) F1254-F1263.
[124] S. Ott, A. Orfanidi, H. Schmies, B. Anke, H.N. Nong, J. Hübner, U. Gernert, M. Gliech, M. Lerch, P. Strasser, Nature materials 19 (2020) 77–85.

[125] N. Ramaswamy, S. Kumaraguru, R. Koestner, T. Fuller, W. Gu, N. Kariuki, D. Myers, P.J. Dudenas, A. Kusoglu, Journal of the Electrochemical Society 168 (2021) 24518.
[126] Y. Garsany, R.W. Atkinson, M.B. Sassin, R.M.E. Hjelm, B.D. Gould, K.E. Swider-Lyons, Journal of the Electrochemical Society 165 (2018) F381.
[127] C. Lei, D. Bessarabov, S. Ye, Z. Xie, S. Holdcroft, T. Navessin, Journal of Power Sources 196 (2011) 6168–6176.
[128] T. van Cleve, G. Wang, M. Mooney, C.F. Cetinbas, N. Kariuki, J. Park, A. Farghaly, D. Myers, K.C. Neyerlin, Journal of Power Sources 482 (2021) 228889.
[129] T. Yoshizumi, H. Kubo, M. Okumura, Development of high-performance FC stack for the new MIRAI, 2021.
[130] K. Shinozaki, Y. Morimoto, B.S. Pivovar, S.S. Kocha, Journal of Power Sources 325 (2016) 745–751.
[131] M. Escudero-Escribano, K.D. Jensen, A.W. Jensen, Current Opinion in Electrochemistry 8 (2018) 135–146.
[132] L. Zhang, C. Ma, S. Mukerjee, Journal of Electroanalytical Chemistry 568 (2004) 273–291.
[133] A. Parthasarathy, C.R. Martin, S. Srinivasan, Journal of the Electrochemical Society 138 (1991) 916.
[134] S. Mitsushima, N. Araki, N. Kamiya, K. Ota, Journal of the Electrochemical Society 149 (2002) A1370.
[135] V. Basura, P. Beattie, S. Holdcroft, Journal of Electroanalytical Chemistry 458 (1998) 1–5.
[136] A.R. Kucernak, E. Toyoda, Electrochemistry communications 10 (2008) 1728–1731.
[137] C.M. Zalitis, D. Kramer, A.R. Kucernak, Physical Chemistry Chemical Physics 15 (2013) 4329–4340.
[138] C.M. Zalitis, D. Kramer, J. Sharman, E. Wright, A.R. Kucernak, ECS Transactions 58 (2013) 39.
[139] C.M. Zalitis, J. Sharman, E. Wright, A.R. Kucernak, Electrochimica Acta 176 (2015) 763–776.
[140] M. Inaba, A.W. Jensen, G.W. Sievers, M. Escudero-Escribano, A. Zana, M. Arenz, Energy & Environmental Science 11 (2018) 988–994.
[141] A. Hrnjić, F. Ruiz-Zepeda, M. Gaberšček, M. Bele, L. Suhadolnik, N. Hodnik, P. Jovanovič, Journal of the Electrochemical Society 167 (2020) 166501.
[142] G. Zhang, A. Kucernak, Acs Catalysis 10 (2020) 9684–9693.
[143] A. Hrnjic, A.R. Kamšek, A. Pavlišič, M. Šala, M. Bele, L. Moriau, M. Gatalo, F. Ruiz-Zepeda, P. Jovanovič, N. Hodnik, Electrochimica Acta 388 (2021) 138513.
[144] K. Ehelebe, J. Knöppel, M. Bierling, B. Mayerhöfer, T. Böhm, N. Kulyk, S. Thiele, K.J.J. Mayrhofer, S. Cherevko, Angewandte Chemie 133 (2021) 8964–8970.
[145] M. Watanabe, H. Sei, P. Stonehart, Journal of Electroanalytical Chemistry and Interfacial Electrochemistry 261 (1989) 375–387.
[146] O. Antoine, Y. Bultel, R. Durand, P. Ozil, Electrochimica Acta 43 (1998) 3681–3691.
[147] O. Antoine, Y. Bultel, R. Durand, Journal of Electroanalytical Chemistry 499 (2001) 85–94.
[148] Y.-X. Chen, M.-F. Li, L.-W. Liao, J. Xu, S. Ye, Electrochemistry communications 11 (2009) 1434–1436.
[149] L. Giorgi, E. Antolini, A. Pozio, E. Passalacqua, Electrochimica Acta 43 (1998) 3675–3680.
[150] E. Antolini, L. Giorgi, A. Pozio, E. Passalacqua, Journal of Power Sources 77 (1999) 136–142.
[151] B.A. Pinaud, A. Bonakdarpour, L. Daniel, J. Sharman, D.P. Wilkinson, Journal of the Electrochemical Society 164 (2017) F321.
[152] A. Bonakdarpour, J. Kwan, B.A. Pinaud, L. Daniel, G. Afonso, D.P. Wilkinson, ECS Transactions 80 (2017) 367.
[153] G.K.H. Wiberg, M. Fleige, M. Arenz, Review of Scientific Instruments 86 (2015) 24102.
[154] K. Ehelebe, D. Seeberger, M.T.Y. Paul, S. Thiele, K.J.J. Mayrhofer, S. Cherevko, Journal of the Electrochemical Society 166 (2019) F1259-F1268.
[155] G.K.H. Wiberg, S. Nösberger, M. Arenz, Current Opinion in Electrochemistry (2022) 101129.
[156] S. Alinejad, M. Inaba, J. Schröder, J. Du, J. Quinson, A. Zana, M. Arenz, Journal of Physics: Energy 2 (2020) 24003.

[157] H. Hoffmann, M.C. Paulisch, M. Gebhard, J. Osiewacz, M. Kutter, A. Hilger, T. Arlt, N. Kardjilov, B. Ellendorff, F. Beckmann, Journal of the Electrochemical Society 169 (2022) 44508.
[158] J. Schröder, J. Quinson, J.K. Mathiesen, J.J.K. Kirkensgaard, S. Alinejad, V.A. Mints, M. Arenz, Journal of the Electrochemical Society 167 (2020) 134515.
[159] B. Hasa, M. Jouny, B.H. Ko, B. Xu, F. Jiao, Angewandte Chemie International Edition 60 (2021) 3277–3282.
[160] M.C. Paulisch, M. Gebhard, D. Franzen, A. Hilger, M. Osenberg, S. Marathe, C. Rau, B. Ellendorff, T. Turek, C. Roth, ACS Applied Energy Materials 4 (2021) 7497–7503.
[161] M. Gebhard, M. Paulisch, A. Hilger, D. Franzen, B. Ellendorff, T. Turek, I. Manke, C. Roth, Materials 12 (2019) 1275.
[162] V. Gridin, J. Du, S. Haller, P. Theis, K. Hofmann, G.K.H. Wiberg, U.I. Kramm, M. Arenz, Electrochimica Acta 444 (2023) 142012.
[163] K. Ehelebe, T. Ashraf, S. Hager, D. Seeberger, S. Thiele, S. Cherevko, Electrochemistry communications 116 (2020) 106761.
[164] Y.-P. Ku, K. Ehelebe, A. Hutzler, M. Bierling, T. Böhm, A. Zitolo, M. Vorokhta, N. Bibent, F.D. Speck, D. Seeberger, Journal of the American Chemical Society 144 (2022) 9753–9763.

Declarations

Erklärungen laut Promotionsordnung

§8 Abs. 1 lit. c der Promotionsordnung der TU Darmstadt
Ich versichere hiermit, dass die elektronische Version meiner Dissertation mit der schriftlichen Version übereinstimmt und für die Durchführung des Promotionsverfahrens vorliegt.

§8 Abs. 1 lit. d der Promotionsordnung der TU Darmstadt
Ich versichere hiermit, dass zu einem vorherigen Zeitpunkt noch keine Promotion versucht wurde und zu keinem früheren Zeitpunkt an einer in- oder ausländischen Hochschule eingereicht wurde. In diesem Fall sind nähere Angaben über Zeitpunkt, Hochschule, Dissertationsthema und Ergebnis dieses Versuchs mitzuteilen.

§9 Abs. 1 der Promotionsordnung der TU Darmstadt
Ich versichere hiermit, dass die vorliegende Dissertation selbstständig und nur unter Verwendung der angegebenen Quellen verfasst wurde.

§9 Abs. 2 der Promotionsordnung der TU Darmstadt
Die Arbeit hat bisher noch nicht zu Prüfungszwecken gedient.

Darmstadt, den …….

Nicolai Schmitt

Erklärung zum Eigenanteil an den Veröffentlichungen der kumulativen Dissertation

Im Folgenden ist aufgelistet, mit welchem Anteil ich an den Veröffentlichungen beteiligt war.

Mein Anteil an der folgenden Veröffentlichung beträgt 90 %

1] Schmitt, N., Schmidt, M., Hübner, G., & Etzold, B. J.
Oxygen reduction reaction measurements on platinum electrocatalysts in gas diffusion electrode half-cells: Influence of electrode preparation, measurement protocols and common pitfalls.
Journal of Power Sources **2022**, 539, 231530.
DOI: https://doi.org/10.1016/j.jpowsour.2022.231530

Mein Anteil an der folgenden Veröffentlichung beträgt 90 %

2] Schmitt, N., Schmidt, M., Mueller, J. E., Schmidt, L., & Etzold, B. J.
How to maximize geometric current density in testing of fuel cell catalysts by using gas diffusion electrode half-cell setups.
Electrochemistry Communications **2022**, 141, 107362.
DOI: https://doi.org/10.1016/j.elecom.2022.107362

Mein Anteil an der folgenden Veröffentlichung beträgt 80 %

3] N. Schmitt, M. Schmidt, J. E. Mueller, L. Schmidt, M. Trabold, K. Jeschonek, B.J.M. Etzold
Which insights can gas diffusion electrode half-cell experiments give into activity trends and transport phenomena of membrane electrode assemblies?
Energy Adv., accepted
DOI: https://doi.org/10.1039/D3YA00055A

Datum

Nicolai Schmitt

Erklärung zur Begutachtung der Veröffentlichung

Prof. Dr.-Ing. Bastian J. M. Etzold

Referent

Prof. Dr. Jan Philipp Hofmann

Co-Referent

Prof. Dr. Karl Mayrhofer, FAU Erlangen-Nürnberg

Dritter, externer Gutachter

Weder Referent (Prof. Dr.-Ing. Bastian J. M. Etzold) noch Co-Referent*in (Prof. Dr. Jan Philipp Hofmann) und Drittgutachter (Prof. Dr. Karl Mayrhofer) der vorliegenden kumulativen Doktorarbeit waren an der Begutachtung nachstehender Veröffentlichungen beteiligt:

1] Schmitt, N., Schmidt, M., Hübner, G., & Etzold, B. J.
Oxygen reduction reaction measurements on platinum electrocatalysts in gas diffusion electrode half-cells: Influence of electrode preparation, measurement protocols and common pitfalls.
Journal of Power Sources **2022**, 539, 231530.
DOI: https://doi.org/10.1016/j.jpowsour.2022.231530

2] Schmitt, N., Schmidt, M., Mueller, J. E., Schmidt, L., & Etzold, B. J.
How to maximize geometric current density in testing of fuel cell catalysts by using gas diffusion electrode half-cell setups.
Electrochemistry Communications **2022**, 141, 107362.
DOI: https://doi.org/10.1016/j.elecom.2022.107362

3] N. Schmitt, M. Schmidt, J. E. Mueller, L. Schmidt, M. Trabold, K. Jeschonek, B.J.M. Etzold
Which insights can gas diffusion electrode half-cell experiments give into activity trends and transport phenomena of membrane electrode assemblies?
Energy Adv., accepted
DOI: https://doi.org/10.1039/D3YA00055A

Datum……..

Referent (Prof. Dr.-Ing. Bastian Etzold)	Co-Referent (Prof. Dr. Jan Philipp Hofmann)	Drittgutachter (Prof. Dr. Karl Mayrhofer)

List of publications

Parts of this thesis were published along the following research articles and conferences:

Research articles

Ehelebe, K., Schmitt, N., Sievers, G., Jensen, A. W., Hrnjic , A., Collantes Jiménez, P., ... & Cherevko, S.
Benchmarking Fuel Cell Electrocatalysts Using Gas Diffusion Electrodes: Inter-lab Comparison and Best Practices.
ACS Energy Lett. **2022**, 7, 2, 816-826.
DOI: https://doi.org/10.1021/acsenergylett.1c02659

Schmitt, N., Schmidt, M., Hübner, G., & Etzold, B. J.
Oxygen reduction reaction measurements on platinum electrocatalysts in gas diffusion electrode half-cells: Influence of electrode preparation, measurement protocols and common pitfalls.
Journal of Power Sources **2022**, 539, 231530.
DOI: https://doi.org/10.1016/j.jpowsour.2022.231530

Schmitt, N., Schmidt, M., Mueller, J. E., Schmidt, L., & Etzold, B. J.
How to maximize geometric current density in testing of fuel cell catalysts by using gas diffusion electrode half-cell setups.
Electrochemistry Communications **2022**, 141, 107362.
DOI: https://doi.org/10.1016/j.elecom.2022.107362

N. Schmitt, M. Schmidt, J. E. Mueller, L. Schmidt, M. Trabold, K. Jeschonek, B.J.M. Etzold
Which insights can gas diffusion electrode half-cell experiments give into activity trends and transport phenomena of membrane electrode assemblies?
Energy Adv., **2023**, Advance article
DOI: https://doi.org/10.1039/D3YA00055A

Talks

Schmitt, N., Etzold, B.J.M.
Best practice for accurate determination of oxygen reduction reaction (ORR) catalyst activity in gas diffusion electrode half-cells
Jahrestreffen Reaktionstechnik 2021. 10. - 12. Mai 2021; Würzburg, Germany - Online event

Schmitt, N., Etzold, B.J.M.
Best practice for accurate determination of oxygen reduction reaction (ORR) catalyst activity in gas diffusion electrode half-cells
72nd Annual Meeting of the International Society of Electrochemistry. 29. August - 3. September 2021; Hybrid Meeting - Jeju Island, Korea/Online

Schmitt, N., Schmidt M., Jeschonek K., Etzold, B.J.M.
Can gas diffusion electrode half-cell experiments predict catalyst layer activity trends of membrane electrode assemblies?
GRS fuel cells: From Fundamental Electrochemistry to Engineering Applied Materials
23. - 24. Juli 2022; Bryant University, Smithfield, RI, United States

Schmitt, N., Etzold, B.J.M.
Best practice for accurate determination of oxygen reduction reaction (ORR) catalyst activity in gas diffusion electrode half-cells
Symposium on Insights into Gas Diffusion Electrodes: From Fundamentals to Industrial Applications. 5. - 7. September 2022; Magdeburg, Germany

Poster

Schmitt, N., Zhang, G. R., Etzold, B. J.M.
Assessing catalytic activity of oxygen reduction catalysts at high current densities
Jahrestreffen Reaktionstechnik 2019 gemeinsam mit der Fachgruppe Mehrphasenströmungen. 27. - 29. Mai 2019; Würzburg, Germany

Schmitt, N., Zhang, G. R., Etzold, B. J.M.
Assessing catalytic activity of oxygen reduction catalysts at high current densities
Infotag Elektrochemische Reaktionstechnik. 15. Oktober 2019; Frankfurt am Main, Germany

Schmitt, N., Schmidt M., Jeschonek K., Etzold, B.J.M.
Can gas diffusion electrode half-cell experiments predict catalyst layer activity trends of membrane electrode assemblies?
GRC fuel cells: From Fundamental Electrochemistry to Engineering Applied Materials
24. - 29. Juli 2022; Bryant University, Smithfield, RI, United States

Schmitt, N., Schmidt M., Jeschonek K., Etzold, B.J.M.
Can gas diffusion electrode half-cell experiments predict catalyst layer activity trends of membrane electrode assemblies?
GdCh Electrochemistry 2022
27. - 30. September 2022; Berlin, Germany